

Università degli Studi di Padova

Dipartimento di Scienze Chimiche

SCUOLA DI DOTTORATO DI RICERCA IN SCIENZE MOLECOLARI

INDIRIZZO SCIENZE CHIMICHE

CICLO XXIV

**“STUDY ON STRUCTURE AND MORPHOLOGY
OF POLYMER NANOCOMPOSITES”**

Direttore della Scuola: Prof. Maurizio Casarin

Coordinatore d’indirizzo: Prof. Maurizio Casarin

Supervisore: Prof. Antonio Marigo

Dottorando: Ramesh Neppalli

January 2012

DECLARATION

I hereby declare that the thesis entitled “**STUDY ON STRUCTURE AND MORPHOLOGY OF POLYMER NANOCOMPOSITES**” submitted for Ph. D. degree to the University of Padova, Italy, has been carried under the supervision of **Prof. Antonio Marigo**. The work is original and has not been submitted in part or full by me for any degree or diploma to this or any other University.

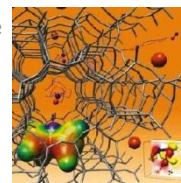
January 2012
Padova

(Ramesh Neppalli)



**UNIVERSITÀ
DEGLI STUDI
DI PADOVA**

Scuola Dottorato in Scienze
Molecolari
Via Marzolo1, I-35131
PADOVA



Phone: +39 049 827 5164

Maurizio Casarin
Professor of Inorganic Chemistry
Padova, 31 Dicembre

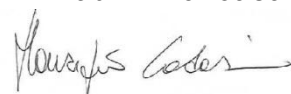
2011

Dr. Ramesh Neppalli
Dottorato in Scienze Molecolari, Indirizzo Scienze Chimiche
XXIV Ciclo

Il dr. Ramesh Neppalli ha concluso il suo percorso di formazione di terzo livello riguardante lo studio della struttura, morfologia e proprietà meccaniche di nanocomposti polimerici formati da polimeri biodegradabili mescolati con argille (Cloisite 15-A) o con fibre di nylon. Nel corso del seminario finale tenutosi in data 17/11/11 presso l'Aula Nasini del DiSC, il candidato ha esposto in maniera abbastanza chiara il lavoro svolto, illustrando in particolare la caratterizzazione della struttura cristallina attraverso misure WAXS e SAXS, e la morfologia con immagini SEM. Inoltre ha esplorato le proprietà di biodegradabilità in diversi ambienti (ads esempio: terriccio, soluzione alcalina etc.). Dopo l'esposizione al candidato sono state effettuate domande specifiche sulla relazione esistente tra le proprietà meccaniche osservate nei nanocomposti polimerici esaminati e gli studi di caratterizzazione strutturale effettuati e sui motivi che hanno condotto alla scelta dei diversi ambienti utilizzati per testarne la biodegradabilità. Il candidato ha risposto in maniera esauriente alle domande poste. Il Consiglio Direttivo della Scuola di Dottorato in Scienze Molecolari

dell'Università di Padova fa propria la valutazione della Commissione Triennale del Dr. Neppalli ed ammette il candidato all'esame finale per il conseguimento del titolo di dottore di ricerca in Scienze Molecolari, indirizzo Scienze Chimiche.

Il Direttore della Scuola
Maurizio Casarin



*Dedicated to
My Family*

*Happiness is the meaning and
Purpose of Life, the whole Aim and
End of Human existence*

– Aristotle

Wonder is the Beginning of All Science

– Aristotle

Acknowledgements

*I take this opportunity to express my gratitude to **Prof. Antonio Marigo**, my research supervisor, for his guidance, fruitful discussions, support and advices throughout the course. More importantly for the freedom he has given to me. My sincere regards and reverence are for him, forever.*

*It is my honor to acknowledge **Cassa di Risparmio Padova e Rovigo (CARIPARO)** for the financial support throughout the course.*

*I would like to thank **Prof. Maurizio Casarin**, the Director of doctoral school, for his kind support throughout the course.*

*I express my sincere thanks to the committee, **Prof. Camilla Ferrante, Prof. Vito di Noto, and Prof. Paolo Caliceti**, for their valuable suggestions during the course.*

*I am extremely grateful to **Dr. Valerio Causin** who inspired me in so many ways. He gave stimulating scientific discussions and suggestions. I truly appreciate his patience, helpfulness and encouragement in every aspect of life, during my stay at Padova. He was my mentor will remain my inspiration forever. And I am forever indebted to him.*

*I express my thanks to **Dr. Carla Marega** (for her fruitful scientific discussions throughout the course) and **Dr. Roberta Saini** (for her technical assistance throughout the course).*

*I acknowledge an appreciation that extends beyond any words for the love and support of my friends, particularly all **CARIPAROs**. I extend my deep sense of gratitude towards them. Also I wholeheartedly thank the **Indian community** who made my stay at Padova memorable and pleasant.*

*I would like to express wholehearted thanks to my Italian friends, **Maria Chiara (sici), Maria Girardin, Francesco**, who made my stay at Padova memorable and very pleasant.*

*On this occasion, I am expressing my sincere gratitude to **Dr. C. Ramesh, Prof. A. Varadarajulu, and Dr. S. R. Mallikharjuna** for their kind help, and for fruitful scientific discussions.*

Words are not enough to express my gratitude for my parents, and all other family members for all their love, and for the freedom, moral support they have given towards my choice of career and life style and their patience and sacrifice will be remained gratefully.

Though, many have not been mentioned, none is forgotten.

January 2012

Padova, Italy

Neppalli Ramesh

Table of Contents

Description	Page No.
Abstract	xiii
Glossary	xvii
List of Figures	xix
List of Tables	xxiv
Chapter 1: Introduction	1
1. Introduction	2
1.1. Fillers from Bio sources	4
1.2A. Layered Silicates	5
1.2B. Layered Double Hydroxides	8
1.3. Electrospun Nanofibers	12
1.4. Polymer Matrices	15
Chapter 2: Scope and Objectives	17
2. Scope and Objectives	18
Chapter 3: Characterization Techniques	20
3. Characterization Techniques	21
3.1. Wide Angle X-ray Diffraction (WAXD)	21
3.2. Small Angle X-ray Scattering (SAXS)	21
3.3. Scanning Electron Microscopy (SEM)	22

3.4.	Field Emission Scanning Electron Microscopy (FESEM)	22
3.5.	Infrared Spectroscopy (IR)	23
3.6.	Transmission Electron Microscopy (TEM)	23
3.7.	Differential Scanning Calorimetry (DSC)	23
3.8.	Polarized Light Optical Microscopy (PLOM)	23
3.9.	Thermogravimetric Analysis (TGA)	24
3.10.	Universal Testing Machine (UTM)	24
Chapter 4: Poly (ϵ-caprolactone) (PCL) based Nanocomposites		25
4.	Poly (ϵ -caprolactone) (PCL) based Nanocomposites	26
4.1.	Introduction	26
4.2.	Structure, Morphology, and Biodegradability of Poly (ϵ -caprolactone)-based Nanocomposites	27
4.3.	Poly (ϵ -caprolactone) filled with electrospun nylon fibers: A model for a facile composite fabrication	39
4.4.	Improvement of tensile properties and tuning of the biodegradation behavior of poly(ϵ -caprolactone) by addition of electrospun fibers	52
Chapter 5: Poly (Lactic acid) (PLA) based Composites		67
5.	Poly (Lactic acid) (PLA) based Composites	68
5.1.	The effect of different clays on the structure, morphology and the degradation behavior of Poly(lactic acid)	69
5.2.	Electrospun nylon fibers for the improvement of mechanical properties and for the control of biodegradation rate of Poly (lactide) – based composites	80
5.3.	Green Composites: PLA reinforced with Natural Fibers	97

Chapter 6: Poly (butylene succinate-co-adipate) (PBSA) based Nanocomposites	111
6. Nanofibers with multi-compositions as reinforcement for Poly (butylene - succinate-co-adipate) (PBSA): study on structure, morphology and properties	112
6.1. PBSA/PS electrospun nanofiber nanocomposites	114
6.2. PBSA/PVDF electrospun fiber nanocomposites	122
Chapter 7: Conclusions	128
Conclusions	129
References	131
List of Publication	145

Abstract

The reinforcement of polymers using fillers, whether inorganic or organic, is common in modern plastics. Polymer nanocomposites or, with a more inclusive term, polymer nanostructured materials, represent a radical alternative to these traditional filled polymer compositions. In contrast to ordinary polymer systems where reinforcement is on the order of microns, polymer nanocomposites are exemplified by discrete constituents on the order of a few nanometers. In the past decade polymer/clay nanocomposites have emerged as a new class of materials and attracted considerable interest in research and development worldwide after initial reports from the Toyota group on Nylon 6 / clay nanocomposites. Enormous amount of work has been done on preparation and characterization of polymer/organoclay nanocomposites because by this approach it is possible to impart much improved mechanical, thermal, electrical properties with respect to their macro and micro counterparts.

There are now many well-developed techniques that are used to produce conventional polymer blends and composites, and various products have been widely commercialized. There are also numerous papers, patents, books, and handbooks that introduce and discuss the development and application of various polymeric blends and composites. Over the past two decades, however, biodegradable/compatible polymers and polymers from renewable resources (PFRR) have been attracting increasing attention, primarily for two major reasons: environmental concerns, and the realization that our petroleum resources are finite. A third reason for the growing interest in polymers from renewable resources relates to adding value to agricultural products, which is economically important for many countries.

The present thesis is organized and presented in seven chapters. A brief overview of polymer nanocomposites, of the different fillers used for the preparation polymer composites, and of the different matrices used for polymer nanocomposites are discussed in the first chapter. The scope and objectives of the thesis are described in the second chapter. In the third chapter, various characterization techniques used in this work such as wide angle X-ray diffraction (WAXD), small angle X-ray scattering (SAXS), optical microscopy, scanning electron microscopy (SEM), transmission electron microscopy (TEM), Infrared spectroscopy (IR), differential scanning calorimetry (DSC), polarized light optical microscopy (PLOM), thermogravimetric analysis (TGA), etc. are described. The fourth chapter describes poly(ϵ -

caprolactone) (PCL) based nanocomposites. For this, PCL was reinforced with different kinds of nanofillers such as clay nanoparticles and different types of electrospun nanofibers. The effect of those nanofillers on PCL matrix structure, morphology, tensile mechanical properties and degradation behavior was analyzed. The fifth chapter deals with poly(lactic acid) (PLA) based composites, in which PLA was reinforced with clay nanoparticles, electrospun nanofibers and also natural fibers. We tried to study the morphology, properties, and degradation behavior of these materials, etc.

In the sixth chapter, the efficiency of particles filled electrospun nanofibers as reinforcement for poly(butylene succinate-co-adipate) (PBSA) was studied. Thus, the effect of those fibers on PBSA structure, morphology, and physical mechanical properties was elaborated. It was observed that by using this kind of nanofillers, it is possible to control the structural morphology of pristine polymer matrices and thus their mechanical properties and degradation behavior. Finally, in the seventh chapter, the general conclusions are given.

Abstract (Italian)

Il rinforzo dei polimeri con cariche, sia organiche che inorganiche, è una comune strategia nella moderna industria delle materie plastiche. I nanocompositi polimerici, o secondo una definizione più ampia i materiali polimerici nanostrutturati, rappresentano una radicale alternativa alle tradizionali formulazioni dei compositi polimerici. Al contrario dei sistemi ordinari, in cui la carica è dell'ordine di grandezza dei micron, i nanocompositi polimerici contengono costituenti discreti di dimensioni nanometriche. A partire dal lavoro del gruppo della Toyota, nello scorso decennio, i nanocompositi polimerici con argilla sono emersi come una nuova classe di materiali che ha attratto l'interesse del mondo della ricerca e sviluppo sia accademico che industriale. Da allora è stata svolta un'enorme mole di lavoro riguardo la preparazione e la caratterizzazione di questo tipo di nanocompositi perché grazie a questo approccio è possibile impartire proprietà meccaniche, termiche ed elettriche molto migliori rispetto ai più comuni micro e macrocompositi.

Oggi esistono molte tecniche sviluppate e mature per produrre compositi e blend polimerici convenzionali e sono stati posti in commercio moltissimi prodotti. Inoltre è disponibile un'ampia letteratura scientifica che introduce e discute gli sviluppi e le applicazioni di questi materiali. Negli ultimi due decenni, tuttavia, è cresciuto l'interesse per polimeri biodegradabili/biocompatibili e per polimeri da fonti rinnovabili, principalmente per due motivi: attenzione all'ambiente e la constatazione che le riserve di petrolio siano finite. Una terza ragione di interesse per i polimeri da fonti rinnovabili consiste nel valore aggiunto che tali materiali possono dare ai prodotti agricoli, un aspetto di grande interesse economico per molti paesi.

Il presente lavoro di tesi è organizzato e presentato in sette capitoli. I nanocompositi polimerici saranno brevemente introdotti, assieme ai diversi additivi ed alle diverse matrici impiegate nei nanocompositi polimerici. Lo scopo e gli obiettivi della tesi sono descritti nel secondo capitolo. Nel terzo capitolo sono descritti i metodi usati per la caratterizzazione dei materiali, come la diffrazione dei raggi X ad alto angolo, la diffusione dei raggi X a basso angolo, la microscopia ottica, la microscopia elettronica a scansione, la microscopia elettronica in trasmissione, la spettroscopia infrarossa, la calorimetria differenziale a scansione, la microscopia ottica in luce polarizzata e la termogravimetria. Il quarto capitolo

descrive i nanocompositi basati sul poli(ϵ -caprolattone) (PCL). Il PCL è stato rinforzato con diversi tipi di nanofiller come nanoparticelle di argilla e diversi tipi di nanofibre da elettrospinning. È stato analizzato l'effetto di questi nanofiller sulla struttura, sulla morfologia, sulle proprietà meccaniche e sul comportamento di degradazione del PCL. Il quinto capitolo presenta i risultati riguardanti i compositi dell'acido polilattico (PLA), nei quali il PLA è stato rinforzato con nanoparticelle di argilla, nanofibre da elettrospinning ed anche con fibre naturali. Anche in questo caso, abbiamo studiato approfonditamente struttura, morfologia e proprietà di questi materiali.

Nel sesto capitolo, è stata studiata l'efficienza di nanofibre da elettrospinning caricate da particelle inorganiche come rinforzo per una matrice di poli(butilen succinato-co-adipato) (PBSA). È stato quindi investigato l'effetto di queste fibre sulla struttura, sulla morfologia e sulle proprietà del PBSA. Si è osservato che usando questo tipo di nanofiller è possibile controllare la morfologia e la struttura delle matrici polimeriche e quindi le loro proprietà meccaniche ed il loro comportamento di degradazione.

Il settimo capitolo, infine, presenterà le conclusioni generali.

Glossary

C15A	Cloisite 15A
C30B	Cloisite 30B
CEC	Cation Exchange Capacity
CNT	Carbon Nanotubes
DSC	Differential Scanning Calorimetry
ECM	Extra Cellular Matrix
FESEM	Field Emission Scanning Electron Microscopy
FRPC	Fiber Reinforced Polymer Composites
IR	Infrared Spectroscopy
LDH	Layered Double Hydroxides
LS	Layered Silicates
MWNT	Multi Wall Carbon Nanotubes
Ny	Nylon 6
PA-6	Nylon 6
PA	Polyamide
PAN	Poly (aniline)
PBS	Poly (butylene succinate)
PBS	Phosphate Buffer Solution
PBSA	Poly (butylene succinate-co-adipate)
PC	Poly Carbonate
PCL	Poly (ϵ -caprolactone)
PET	Poly (ethylene terephthalate)

PGA	Poly (glycolic acid)
PHB	Poly (3-hydroxyl butyrate)
PLA	Poly (lactic acid) or Poly (lactide)
PLOM	Polarized Light Optical Microscopy
PLS	Polymer Layered Silicates
PMMA	Poly (methyl methacrylate)
PNC	Polymer Nanocomposites
PS	Poly (styrene)
PVC	Poly (vinyl chloride)
PVDF	Poly (vinylidene fluoride)
PVP	Poly (vinyl pyrrolidone)
SAXS	Small Angle X-ray Scattering
SEM	Scanning Electron Microscopy
Si	Silica
TEM	Transmission Electron Microscopy
TGA	Thermogravimetric Analysis
THF	Tetrahydrofuran
THG	Alkali Treated Hildegardia
TiO₂	Titanium dioxide
UTHG	Untreated Hildegardia
UTM	Universal Testing Machine
WAXD	Wide Angle X-ray Diffraction

List of Figures

Figure No.	Description	Page No.
1.1.	Schematic representation of reinforcing natural/biofibers classification	4
1.2.	Digital photographs of some natural fibers and sources of natural fibers	5
1.3.	Structure of 2:1 phyllosilicates	6
1.4.	Idealized structure of an LDH, with interlayer carbonate anions	8
1.5.	Structure of clay in nanocomposites with corresponding wide angle X-ray scattering (WAXS) and transmission electron microscopy (TEM) results	11
1.6.	Schematic diagram to show polymer nanofibers by electrospinning	13
1.7.	Left: SEM image of fibers of PA produced by melt electrospinning. Right: TEM image of fibers of PLA produced by solution electrospinning	14
1.8.	Number of scientific publications per year (2000–2010) with the keyword “electrospinning” (source: Web of Science)	15
4.2.1.	a) WAXD traces of the composites and of the neat filler in the angular region of the basal peaks of clay. b) WAXD trace of sample PCL80-1, in the angular range of the diffraction signals of the polymeric crystalline cell	28-29
4.2.2.	SAXS patterns (dotted lines) of the considered samples. Traces calculated during the fitting procedure (solid lines) are also shown	30
4.2.3.	DSC patterns for a) the first heating ramp and b) cooling ramp of the considered samples	33
4.2.4.	Tensile stress vs. strain curves of the samples of the a) PCL42 and b) PCL80 series	35
4.2.5.	Samples of the PCL42 before the biodegradation experiment and after 13 weeks in compost	36
4.2.6.	Samples of the PCL80 series before the biodegradation experiment and after 13Weeks in compost	36

4.2.7. Mass residue of the samples of the PCL42 series as a function of time	37
4.2.8. Mass residue of the samples of the PCL80 series as a function of time	37
4.3.1. Preparation procedure of the PCL/NY composites	41
4.3.2. FE-SEM micrographs of (a) the cross section of the fiber mat and (b) of a detail of the fibers	42
4.3.3. SEM micrographs of the nylon electrospun fibers at different magnifications (A) 1000x, (B) 3000x	43
4.3.4. WAXD traces of blank PCL matrix, of pure electrospun fibers and of the Composites	43
4.3.5. SAXS patterns (dotted lines) of the considered samples. Traces calculated during the fitting procedure (solid lines) are also shown	46
4.3.6. Trend of (a) the degree of crystallinity measured by WAXD and of Young's modulus, and of (b) ultimate strain and lamella thickness as a function of filler content	48
4.3.7. SEM micrographs of the cryogenic fracture surfaces of samples (a) PCL/NY3, (b) PCL/NY5, and (c) PCL/NY8	49
4.3.8. SEM micrographs at different magnification of the cryogenic fracture surface of sample PCL/NY3	50
4.3.9. SEM micrographs at different magnification of the cryogenic fracture surface of sample PCL/NY8	51
4.4.1. FESEM micrographs of a) the Ny fiber mat and of b) the PVP fiber mat	55
4.4.2. WAXD diffractograms of pristine PCL, and of the composites	56
4.4.3. SAXS patterns (solid line) of the considered samples. Traces calculated during the fitting procedure (dotted line) are also shown	58
4.4.4. SEM micrographs of the cryogenic fracture surfaces of samples a) PCLPvp, b) PCLNy and c) PCLNyPvp	59
4.4.5. High magnification SEM micrographs of the cryogenic fracture surfaces of samples a) PCLPvp, b) and c) PCLNyPvp	60
4.4.6. Mass residue of the samples as a function of time, obtained during biodegradation in soil	61

4.4.7. Mass residue of the samples as a function of time, obtained during biodegradation in buffer	61
4.4.8. SEM micrographs of the cryogenic fracture surfaces of samples PCLNyPvp (a) and (b), and PCLNy (c)	63
4.4.9. Pictures before and after degradation in buffer solution of PCL and composites	65
5.1.1. WAXD diffractograms for different clays and composites at lower angles	72
5.1.2. TEM images of PLA43B (a); PLAPERK (b); and PLAHPS (c)	74
5.1.3. WAXD diffractograms of PLA and of its composites at higher angles	75
5.1.4. Lorentzean SAXS patterns of pure PLA matrix polymer and of its composites	76
5.1.5. % of weight loss of pure PLA matrix and of its composites in PBS solution	78
5.1.6. (a) before degradation studies (b) after degradation studies	78
5.2.1. SEM micrograph of the nylon fiber mat. The inset shows the distribution of fiber diameters	83
5.2.2. WAXD diffractograms of PLA, and of its composites with different amount of filler content	84
5.2.3. SAXS patterns (solid line) of the considered samples, traces calculated during the fitting procedure (dotted line) are also shown	85
5.2.4. Polarized light optical micrographs of the spherulitic texture obtained after 20 minutes of isothermal crystallization at 100°C for a) the neat matrix and for b) sample PLANY1.5	87
5.2.5. SEM micrographs of PLANY1.5 in a region where fibers are preferentially positioned a) perpendicular and b) parallel to the fracture surface	88
5.2.6. SEM micrographs of PLANY2.5 in a region where fibers are preferentially positioned a) perpendicular and b) parallel to the fracture surface	88
5.2.7. IR spectra of the reference matrix, of the composites and of the neat nylon fibers. Part a) shows the entire spectrum, part b) shows an enlargement of the spectral region where the C=O stretching (~1640 cm ⁻¹) and the N-H bending (~1540 cm ⁻¹) bands of nylon appear	90

5.2.8. Comparison of the trend of tensile modulus (closed circles) and of the thickness of lamellae (open squares) as a function of fiber content	92
5.2.9. Comparison of the trend of stress at break (closed circles) and of the thickness of the amorphous layer between the lamellae (open squares) as a function of fiber content	92
5.2.10. Residual weight of the samples as a function of residence time in NaOH solution	93
5.2.11. Residual weight of the samples at the end of the degradation experiments, as a function of fiber content	94
5.2.12. Images of the samples before and after degradation in NaOH solution	96
5.3.1. SEM micrographs of Hildegardia fabric and PLA/Hildegardia composites; a) treated Hildegardia, b) untreated Hildegardia c) PLA3	101
5.3.2. SEM micrograph of PLA1	102
5.3.3. WAXD diffractograms of PLA and of its composites	103
5.3.4. WAXD pattern (solid line) of PLA4 sample, dotted line shows the fitting for the peaks and solid line with dots line shows fitting for amorphous region	103
5.3.5. TGA thermograms of untreated Hildegardia (UTHG) and alkali treated Hildegardia (THG)	104
5.3.6. TGA thermograms of neat PLA and of its composites with Hildegardia fabric	105
5.3.7. Tensile modulus of neat PLA and of its composites	107
5.3.8. Tensile strength at break of neat PLA and of its composites	107
5.3.9. SEM micrograph of the composite PLA3	108
5.3.10. % weight loss of the samples in NaOH solution	109
5.3.11. Images of the samples before (a), and after (b) degradation studies	109
6.1.1. WAXD diffractograms of PBSA and of its composites with PS electrospun nanofibers with TiO ₂ in fibers	116
6.1.2. DSC thermograms of neat PBSA and of its composites	118
6.1.3. SEM images of PBSA composites; a) PBSAPS, b)PBSAPS5, c) PBSAPS15, d) PBSAPS25	119

6.1.4. Tensile mechanical properties of PBSA and of its composites (a) tensile modulus (b) correlation between modulus and long period (c) tensile strength (d) elongation at break	120
6.1.5. Mass residue of the samples as a function of time, obtained during biodegradation in compost	121
6.2.1. WAXD diffractograms of PBSA and of its composites with PVDF fibers	123
6.2.2. WAXD pattern (solid line of the) of the sample PBSAPVDF3. Dotted line shows the fitting for the peaks and semi solid line shows fitting for amorphous region	124
6.2.3. SEM images of PBSA composites; a) PBSAPVDF3, b) PBSAPVDF5	125
6.2.4. Images of samples after degradation in compost for 5 months	127

List of Tables

Table No.	Description	Page No.
1.1.	List of the main applications of nanocomposite polymers	12
4.2.1.	Morphological parameters of the lamellar stacks obtained by SAXS analysis of the samples. The thickness of the crystalline (C) and amorphous layer (A), the long period (D), and the crystallinity (Φ_{SAXS}), along with their relative distributions ($\sigma_c/C = \sigma_A/A$, σ_D/D) are shown. Samples PCL10-5 and PCL42-5 are not shown, since their SAXS patterns were barely detectable and were not fittable	31
4.2.2.	Tensile properties of the samples based on the PCL80 and PCL42 matrices	34
4.2.3.	Crystallinity degree of the samples of the PCL42 and PCL80 series before and after Biodegradation	38
4.3.1.	Composition and preparation procedure of the samples	42
4.3.2.	Degree of crystallinity obtained by WAXD and morphological parameters of the lamellar stacks obtained by SAXS analysis of the samples. The thickness of the crystalline (C) and amorphous layer (A), the long period (D), and the crystallinity (Φ_{SAXS}), along with their relative distributions ($\sigma_c/C = \sigma_A/A$, σ_D/D and $\sigma_\phi/\phi_{\text{SAXS}}$), and number of lamellae (N) are shown	44
4.3.3.	Thermal data obtained in the DSC experiments. Data regarding melting of nylon are not shown, since they were constant in all the tests	45
4.3.4.	Tensile properties of the samples	47
4.4.1.	Formulation of the samples	55

4.4.2. Degree of crystallinity obtained by WAXD (Φ_{WAXD}) and morphological parameters of the lamellar stacks obtained by SAXS analysis of considered samples. The thickness of the crystalline (C) and amorphous layer (A), the long period (D), and the crystallinity (Φ_{SAXS}), along with their relative distributions ($\sigma_{\text{C}}/\text{C} = \sigma_{\text{A}}/\text{A}$ and $\sigma_{\text{D}}/\text{D}$) are shown	57
4.4.3. Tensile properties of the samples	60
4.4.4. Degree of crystallinity before and after degradation of the samples	62
5.1.1. Degree of crystallinity of all prepared samples measured by fitting WAXD traces	76
5.1.2. Isothermal crystallization kinetic studies at different temperatures	77
5.2.1. Formulation and codes of the samples	81
5.2.2. Degree of crystallinity obtained by WAXD (Φ_{WAXD}) and morphological parameters of the lamellar stacks obtained by SAXS analysis of considered samples. The thickness of the crystalline (C) and amorphous layer (A), the long period (D), and the crystallinity (Φ_{SAXS}). $\sigma_{\text{C}}/\text{C}$, $\sigma_{\text{A}}/\text{A}$, $\sigma_{\text{D}}/\text{D}$ and $\sigma_{\Phi}/\Phi_{\text{SAXS}}$ are the distributions of the aforementioned parameters and can be interpreted as the relative deviation from the average of the values of such features	84
5.2.3. Tensile mechanical properties of PLA and of its composites	90
5.3.1. Compositions and preparation procedure of the samples	100
5.3.2. Φ_{WAXD} of PLA and of its composites	104
5.3.3. Tensile mechanical properties	105
6.1.1. Formulation and codes of the samples	115
6.1.2. Degree of crystallinity obtained by WAXD (Φ_{WAXD}) and morphological parameters of the lamellar stacks obtained by SAXS analysis of considered samples. The thickness of the crystalline (C) and amorphous layer (A), the long period (D), and the crystallinity (Φ_{SAXS}), along with their relative distributions ($\sigma_{\text{C}}/\text{C}$, $\sigma_{\text{A}}/\text{A}$, $\sigma_{\text{D}}/\text{D}$ and $\sigma_{\Phi}/\Phi_{\text{SAXS}}$)	117
6.2.1. Formulation and codes of the samples	122

6.2.2. Degree of crystallinity obtained by WAXD (Φ_{WAXD}) and morphological parameters of the lamellar stacks obtained by SAXS analysis of considered samples. The thickness of the crystalline (C) and amorphous layer (A), the long period (D), and the crystallinity (Φ_{SAXS}), along with their relative distributions ($\sigma_{\text{C}}/\text{C}$, $\sigma_{\text{A}}/\text{A}$, $\sigma_{\text{D}}/\text{D}$ and $\sigma_{\Phi}/\Phi_{\text{SAXS}}$)	125
6.2.3. Tensile mechanical properties of prepared samples	126

CHAPTER 1

INTRODUCTION

1. Introduction

In our modern civilization, materials are key components. The development of mankind passed through several important epochs, like Stone Age, Bronze Age, and Iron Age and later on Steel Age (the industrial revolution). Post to World War II, the developments in industrial chemistry brought to the market many synthetic polymeric materials very close to the modern civilization, thus now we are living in Polymer Age. Polymer Science deals with the polymers, polymer blends, polymer composites, filled polymers, investigation methods and the study on control of the properties of these materials.[1]

In recent decades, especially composite materials based on polymeric materials have been an area of interest in both academics and industry as well. 'Composite' is a blend of two or more components, one of which is made up of stiff and strong material (filler), and the other one is a 'binder' or 'matrix' (polymer) which holds the filler in place. When the different components (filler and matrix) are mixed together, the resulting composite material will retain the individual (both filler and matrix) identities and both directly influence the composites final properties.[2]

Natural fibers have been playing a major role in the field of composite materials. The term natural fiber covers a broad range of vegetable, animal and mineral fibers. However, in the composite industry, it usually refers to wood fibers and agro-based bast, leaf, seed, and stem fibers. When these fibers are used in plastic composites, they can provide significant reinforcement to the new material.

Though, natural fibers are in use since several decades, interest in them is reduced with the development of synthetic fibers. The success of synthetic fibers in providing significant reinforcement to the polymer matrices with better performance pushed down the use of natural fibers in polymer composite materials.[1] Some of the most employed synthetic fibers are glass fiber, aramid, poly ethylene, graphite, boron, silicon carbide, silicon nitride, silica, alumina silica, etc.[2]

As the 21st century unfolds, the development in science and technology allowed researchers to better understand structure-property relationship in polymeric composite materials. Some important features of nanoscale materials, and the development in nano science & technology, allow researchers to use them in polymeric composite materials, which afford

unique opportunities to create novel materials with unique and useful properties. Normally, the term nano encompasses the 1-100 nm range. These novel materials promise new applications by exploiting the unique synergisms between constituents that only occur when the length scale of the morphology and the critical length associated with the fundamental physics of a given property coincide. We can consider nanoscience and nanotechnology as a revolutionary science in the multidisciplinary area combining chemistry, physics, material science, electronics and bio sciences.[3]

Polymer nanocomposites (PNC) are a novel class of composites that are particle-filled polymers in which; at least, one dimension of the dispersed particles is in the nanometer range. Polymer nanocomposites have been an area of intense industrial and academic research for the past twenty years. PNCs represent an alternative to conventional filled polymers or polymer blends— a staple of the modern plastics industry. In contrast to conventional composites, where the reinforcement is of the order of microns, PNCs are exemplified by discrete constituents of the order of a few nanometers.

Okada et.al [4] from Toyota research group was the first who prepared commercial polymer nanocomposites by solution polymerization of Caprolactam in the clay galleries. Later on, this product was marketed by UBE Industries and Bayer. Currently, these nylon 6-based nanocomposites are used to make belts for Toyota car engines and also for the production of packaging film.[3]

Depending on how many dimensions of the particles are in nanometer range, nanoparticles are mainly categorized into three types. First, when all the dimensions are in the order of nanometers, they are called isodimensional nanoparticles, such as spherical silica nanoparticles [5,6] and some nanoclusters,[7] etc. The second type, when two dimensions of the particles are in the nanometer range and the third one is larger, which usually form an elongated structure, is called nanotubes or nanowhiskers, for example carbon nanotubes,[8] and cellulose nanowhisker.[9,10] The third type of nanoparticles is characterized by only one dimension in the order of nano range. In this case the particles are present in the form of sheets one to a few nanometer thick to hundreds to thousands nanometer long, for example layered silicates (LS).

In the past two decades, a very wide range of research has been carried out to study the preparation of PNCs, their structure-property relationship, characterization of PNCs, and their end-use applications. Scientists discussed the PNCs by considering the various potential nanofillers such as carbon nanotubes (CNTs), Silica (Si), Talc, nano biofillers, and layered silicates (LS). In this chapter, we try to give a brief introduction of some filler and few examples of their reinforcement in various polymers.[3]

1.1 Fillers from Bio sources

The unstable price of petrochemicals, and very finite deposits of other mineral sources, increases the demand for sustainable fillers in polymer industry to develop strong, light and bio friendly materials. Natural fibers possess high strength and stiffness but are difficult to use in load-bearing applications by themselves because of their fibrous structure. In fiber-reinforced composites, the fibers serve as reinforcement by giving strength and stiffness to the structure while the plastic matrix serves as the adhesive to hold the fibers in place so that suitable structural components can be made. A broad classification (nonwood and wood fibers) of natural fibers is represented schematically in Figure 1.1, whereas Figure 1.2 displays images of several natural fibers with reinforcement potential.

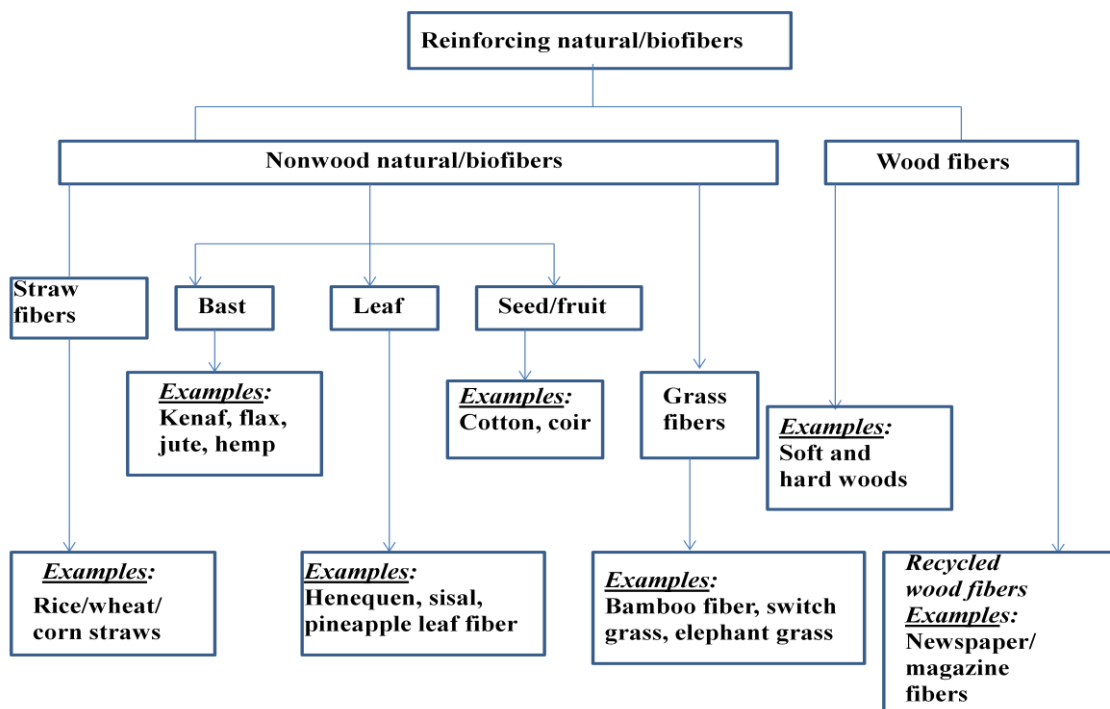


Fig.1.1. Schematic representation of reinforcing natural/biofibers classification [11]



Fig.1.2. Digital photographs of some natural fibers and sources of natural fibers [11]

Nanoscale biofillers also can be synthesized from naturally occurring fibers, such as, hemp, flax, wheat, wood fibers, and starch, and so on. Possibility of chemical treatment and modifications to these fibers allows obtaining nanoscale fibers (6-60 nm). These nanofibers are used in different polymer systems to enhance the properties.[12-16]

1.2A. Layered Silicates (LS)

Layered silicates are probably the first kind of filler which was used for the preparation of polymer-based nanocomposites. The most commonly used LS in nanocomposites belong to the structural family known as the 2:1 phyllosilicates. They are important in many areas, like automobile industry, constructions, ceramics, paper industry, cosmetic industry, bio materials, and electronic field, etc. They include natural and synthetic clays such as mica, bentonite, magadite, laponite, fluorohectorite and so on. Their crystal lattice consists of two-dimensional layers where a central octahedral sheet of alumina or magnesia is fused to two external silica tetrahedra by the tip so that the oxygen ions of the octahedral sheet also belong to the tetrahedral sheets. The layer thickness is around 1 nm and the lateral dimensions of

these layers may vary from 300 Å to several microns and even larger depending on the particular silicate. These layers organize themselves to form stacks with a regular van der Waals gap in between them called the interlayer or the gallery space. Isomorphic substitution within the layers (for example, Al^{3+} replaced by Mg^{2+} or by Fe^{2+} or Mg^{2+} replaced by Li^+ .) generates negative charges that are counterbalanced by alkali or alkaline earth cations situated in the interlayer. As the forces that hold the stacks together are relatively weak, the intercalation of small molecules between the layers becomes easier.[17] The structure of phyllosilicates is shown in [Figure 1.3](#).

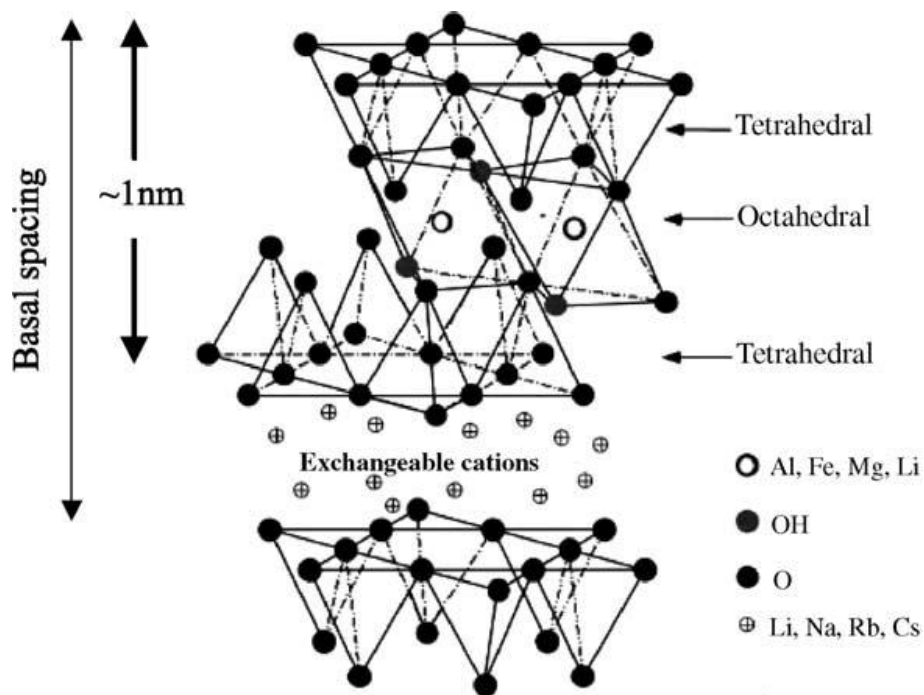


Fig.1.3. Structure of 2:1 phyllosilicates

Layered silicates are hydrophilic in nature, so when they are mixed with a polymer, obtaining very well dispersed structures is difficult. Thus, LS has to be modified into organophilic by exchanging the cations of the interlayer with organic cationic surfactants such as alkylammonium or alkylphosphonium salts. The maximum extent to which these cations can be exchanged is called Cation Exchange Capacity (CEC), and is generally expressed in mequiv/100 g. Montmorillonite, Hectorite, and Saponite are the most commonly used layered silicates. In some studies, for reducing the hydrophilicity of the clays, the hydroxyl groups at the edges of the platelets are reacted with silane coupling agents.

Nowadays, several pristine and organoclays are available commercially. Commercial organoclays include Cloisite 10A, 15A, 20A and 30B produced from Southern Clay Products (U.S.A.),[18] Bentone 107, 108, 109 and 2010 from Elementis Specialties Company,[19] Nanomer 1.30P, 1.31PS, 1.44P, 1.44PS, 1.44PT and 1.28E from Nanocor, Inc. (U.S.A.),[20] Nanofil 2, 5, 9, SE 3000 and SE 3010 from Sud-Chemie (Germany)[21] as well as Dellite 72T from Laviosa Chimica Mineraria (Italy). Synthetic fluoromica clays (Somasif ME100) are supplied to Asian customers by Co-op Chemicals, Japan. Most of these commercially available organoclays are modified with ammonium cations and few of them are with silane modification.

Amongst all the potential nanocomposite precursors, those based on clay and layered silicates have been more widely investigated probably because the starting clay materials are easily available and their intercalation chemistry has been studied for a long time.[17,22] The important characteristics pertinent to application of clay minerals in polymer nanocomposites are their rich intercalation chemistry, high strength and stiffness and higher aspect ratio of individual platelets, abundance in nature and low cost. Their unique layered structure and high intercalation capabilities allow them to be chemically modified to be compatible with polymers, which make them particularly attractive in the development of clay-based polymer nanocomposites.

Therefore, very low loading of clays is required to achieve equivalent properties compared to the conventional composites. Finally, and importantly, they are ubiquitous in nature and, therefore, inexpensive. Owing to the nanometer-size particles obtained by dispersion, these nanocomposites exhibit markedly improved mechanical, thermal, optical and physico-chemical properties when compared with the pure polymer or conventional (microscale) composites. There are several reviews and books published highlighting the major developments in this area of polymer/clay nanocomposites and which discuss various preparation techniques, the characterization and the properties that those materials can display; in addition to their potential and commercial applications.[23-38]

1.2B. Layered Double Hydroxides (LDHs)

Layered double hydroxides (LDHs), known as anionic clays, consist of a stacking of positive hydroxylated layers $[M_{1-x}^{2+} M_x^{3+} (OH)_2]^{x+}$ separated by interlayer anionic species and water molecules $[A_{x/q}^{q-} \cdot nH_2O]$, where M^{2+} is a divalent metal ion (such as Mg^{2+} , Zn^{2+}), M^{3+} is a trivalent metal ion (such as Al^{3+} , Cr^{3+}), and A is an anion with valency q (such as CO_3^{2-} , Cl^- , NO_3^-). [39] Because of their highly tunable properties and unique anion exchange properties, LDHs are considered as a new emerging class of layered materials for the preparation of polymeric nanocomposites. [39,40] These clays are used in many different fields such as poly vinyl chloride (PVC) stabilizers, medical applications, electrodes, anion exchangers, catalysts and catalyst precursors.

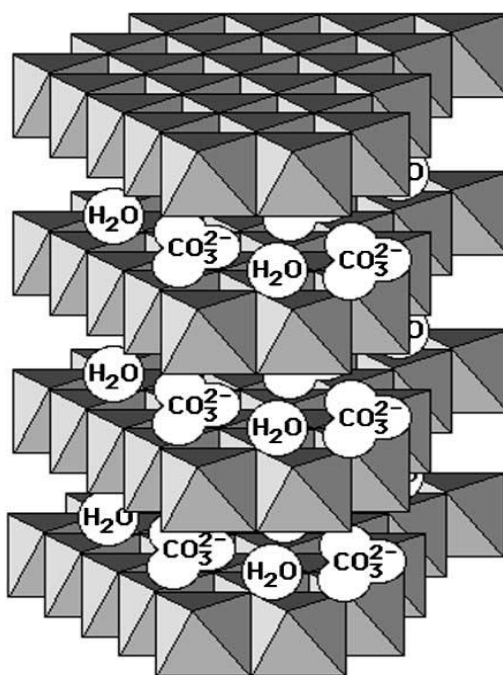


Fig.1.4. Idealized structure of an LDH, with interlayer carbonate anions [41]

Perkalite is organically modified synthetic clay based on magnesium-aluminum layered double hydroxide modified with hydrogenated fatty acid, also referred as hydrotalcite. Recently perkalite attained more interest in polymer-clay nanocomposites, because upon compounding with polymers, perkalite can be delaminated to nanoscale level, resulting in improved polymer properties such as thermo-mechanical, flame retardant, barrier and rheological properties. [42,43]

Nanocomposites preparation methods

Several strategies have been used for the preparation of polymer-layered silicate nanocomposites. They are explained briefly in the following paragraphs.

Solution mixing

When the polymer solution is mixed with a dispersion of clay, the polymer chains intercalate and displace the solvent within the interlayer of the silicate. Upon solvent removal, the intercalated structure remains, resulting in the formation of nanocomposites. The requirement of large quantities of solvents and the non-availability of many compatible polymer-clay solvent systems limits the use of this method.

In-situ intercalative polymerization

In this method, the layered silicates are swollen within the liquid monomer or a monomer solution so that the polymer formation can occur in between the intercalated sheets. Polymerization can be initiated either by heat, radiation, by the diffusion of a suitable initiator or by an organic initiator/catalyst fixed via cation exchange inside the interlayer before the swelling step.

Melt intercalation

The melt intercalation method has become the standard technique for the preparation of polymer layered silicates (PLS) - nanocomposites. This method involves annealing, statically or under shear, a mixture of polymer and organoclay above the softening point of the polymer. This method has great advantages over either *in-situ* intercalative polymerization or polymer solution intercalation. First, this method is environmentally benign due to the absence of organic solvents. Second, it is compatible with current industrial process such as extrusion and injection molding.

The enhancement of the mechanical properties depends on the interaction of the polymer chains on the clay platelet surface. This is mainly affected by the amount of clay loading and the extent of dispersion so as to allow maximum platelet surface available to interact.

Therefore, the key issue in the design of polymer–clay nanocomposites is to monitor the dispersion of clay platelets on a nanometer scale in a polymer matrix. Accordingly, it is necessary to understand the interaction between the clay surface and the intercalants to prepare the desired morphology of (exfoliated) clay–polymer nanocomposites. In other words, understanding the structure of organoclays and the interaction of surfactant–clay is of crucial importance to the design, fabrication and characterization of nanocomposites.

Nanocomposites can be classified in to three types depending on the structure and arrangement of the clay in the polymer matrix. They are (a) intercalated nanocomposites, in which the polymer chains are inserted in the interlayer gallery and the interlayer distance increases, resulting in a well ordered multi-layer morphology built up with alternating polymeric and inorganic layers (b) flocculated nanocomposites which are similar to intercalated nanocomposites wherein the clay platelet sizes have been increased by flocculation due to hydroxylated edge-edge interaction and (c) exfoliated or delaminated nanocomposites, where the individual clay layers are separated and uniformly distributed in a continuous polymer matrix.

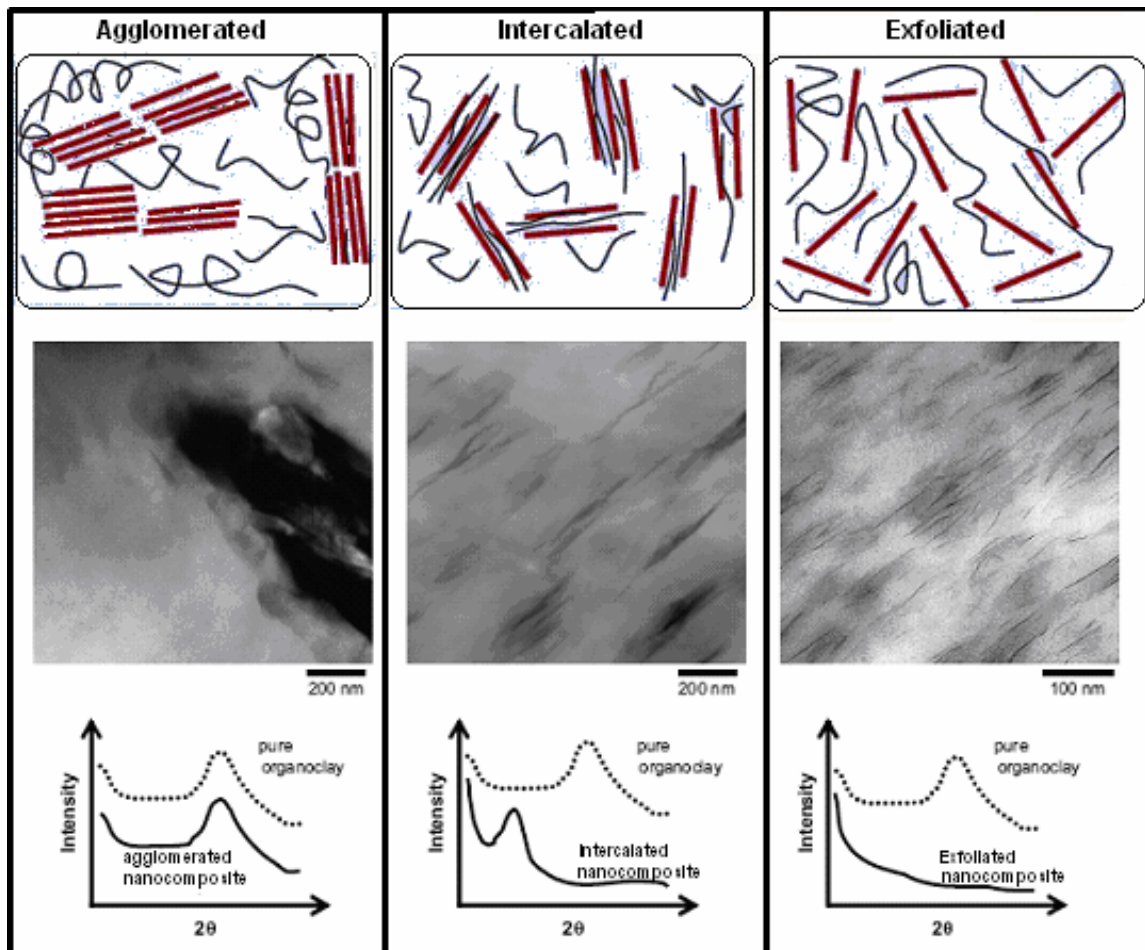


Fig.1.5. Structure of clay in nanocomposites with corresponding wide angle X-ray scattering (WAXS) and transmission electron microscopy (TEM) results [28]

Although the intercalation chemistry of polymers when mixed with appropriately modified layered silicates has long been known,[17,20] the field of polymer/clay nanocomposites has gained momentum only recently. Two major findings have stimulated the revival of interest in these materials: first the report from the Toyota research group of a nylon-6 (PA-6)/montmorillonite nanocomposite,[21] which showed pronounced improvements in thermal and mechanical properties; and second the observation by Vaia et.al that it is possible prepare nanocomposite by melt mixing the polymers with layered silicates.[44]

Applications and commercial developments of PNCs

Many applications of polymer nanocomposites based on clays have emerged owing to their markedly improved performance in mechanical, thermal, barrier, optical, electrical, and other physical and chemical properties. An increasing number of commercial products have

become available. Current and potential commercial applications of nanocomposites have been described in the literature.[45,46] Some of the commercial products available in the market, their characteristics and their applications are listed in the [Table 1](#). These polymer nanocomposites offer high performance with significant weight reduction and affordable materials for applications in automotive and aerospace industry.

Table1.1: List of the main applications of nanocomposite polymers [28]

Reference market	Nanofiller	Polymer matrix
Barrier films	Organic clays	Nylon 6
Packaging	Organic clays	PP
Electro conductive materials	Nanotubes	Nylon 12, PETG, PBT, PPS, PC, PP
Colored parts in the automotive sector	Nanotubes	PPO/nylon
Bottles and films	Organic clays	Nylon 6
Cables and wires	Organic clays	EVA
Various uses	Organic clays	Nylon 6
Injection	Organic clays	PP
Beer bottles	Organic clays	Nylon MDX6
Transport, the sea sector	Organic clays	Unsaturated polyester
Various uses, electroconductive materials	Organic clays	Nylon 6, PP
Flame-retardant materials	Clay, mica	Nylon 6
Various uses	Clay, mica	POM
Various uses	Organic clays	Nylon 6, 12
Fuel systems for cars	Organic clays	Nylon 6, 66
Various uses	Organic clays	Nylon 6

1.3. Electrospun Nanofibers

Exploitation of electrostatic forces for spinning fibers is not a new approach, since it has been known for more than one hundred years. The recent interest in nanotechnology has brought to a rediscovery of the electrospinning technique, due to its capability of yielding fibers in the submicron range to nano range.[47,48] Mainly because of this reason, electrospun nanofibers attracted a huge interest in research community, as testified by the ever increasing scientific

literature on the subject. Most of these reports are focused on the use of nanofibers in fields such as nanocatalysis, tissue scaffolds, protective clothing, filtration, and optical electronics. It is very surprising, though, that very few works exist on the use of such fibers as fillers in polymer-based composites.

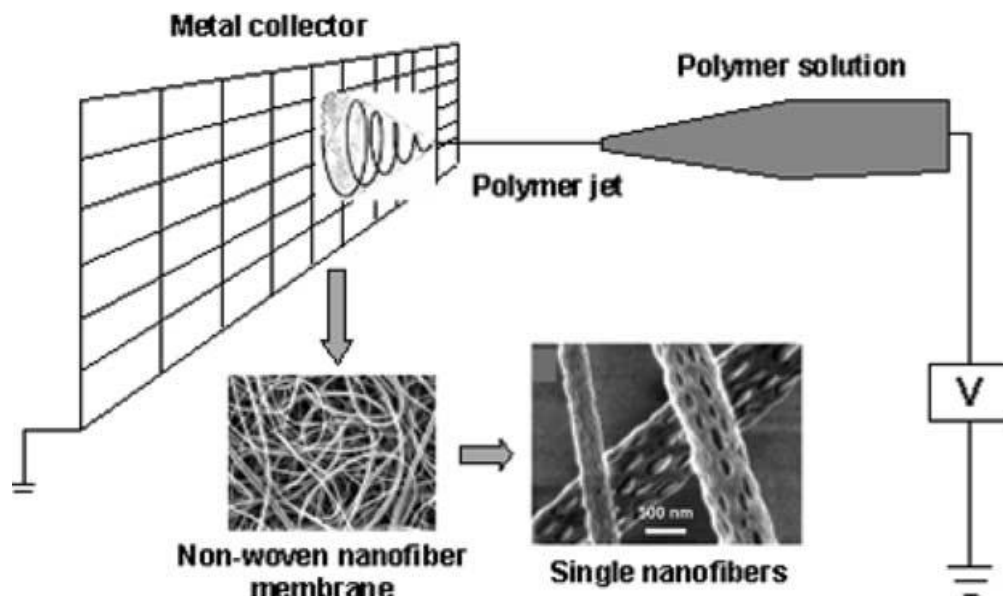


Fig.1.6. Schematic diagram to show polymer nanofibers by electrospinning [48]

Electrospinning is currently the only technique that allows the fabrication of continuous fibers with diameters down to a few nanometers. The method can be applied to synthetic and natural polymers, polymer alloys, and polymers loaded with chromophores, nanoparticles, or active agents, as well as to metals and ceramics. Fibers with complex architectures, such as core-shell fibers or hollow fibers, can be produced by special electrospinning methods. It is also possible to produce structures ranging from single fibers to ordered arrangements of fibers. Electrospinning is not only employed in university laboratories, but is also increasingly being applied in industry. In 1745, Bose described aerosols generated by the application of high electric potentials to drops of fluids.[49] Electrospinning, also known as electrostatic spinning, has its basis in early studies. Electrospinning, first introduced by Formhals[50] and later revived by Reneker[51,52] uses high voltage (about 10-20 kV) to electrically charge the polymer solution for producing ultra-fine fibers (diameters ranging from a few nanometer to larger than 5 μm).[51] [Figure 1.6](#) shows a schematic illustration of the basic electrospinning setup, which essentially consists of a pipette or a syringe filled with polymer solution, a high voltage source and a grounded conductive collector screen. In

addition, a metering syringe pump can be used to control the flow rate of the polymer solution. The needle of the syringe typically serves as an electrode to electrically charge the polymer solution and the counter electrode is connected to the conductive collector screen. [Figure 1.7](#) shows examples of Scanning Electron Microscopy (SEM) and Transmission Electron Microscopy (TEM) images of Polyamide (PA) and Polylactide (PLA) respectively.

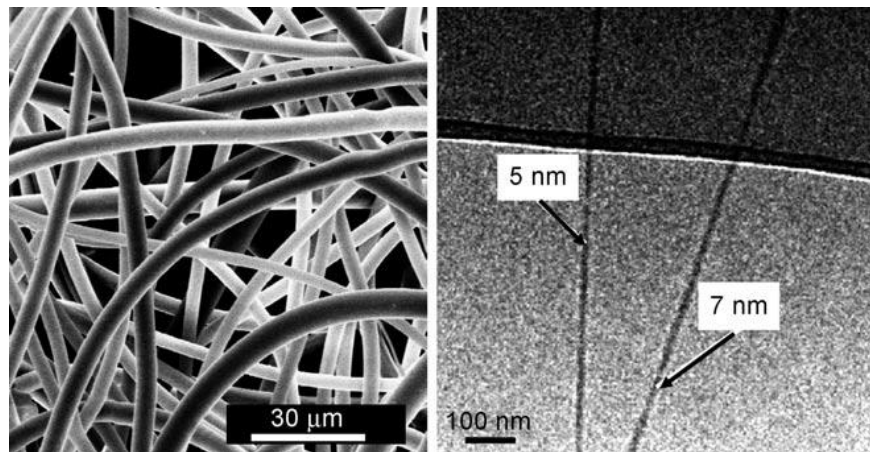


Fig.1.7. Left: SEM image of fibers of PA produced by melt electrospinning. Right: TEM image of fibers of PLA produced by solution electrospinning [53]

The scope of possibilities presented by electrospinning encompasses a multitude of new and interesting concepts. This rapid development is reflected by the increasing numbers of scientific publications and patents. [Figure 1.8](#) shows year by year increase in number of publications based on electrospinning.

Ultra-fine fibers of biodegradable polymers produced by electrospinning have found potential applications in tissue engineering due to their high surface area to volume ratios and high porosity of the fibers.[54-57] Moreover, the flexibility of seeding stem cells and human cells on the fibers makes electrospun materials most suited for tissue engineering applications.[58,59]

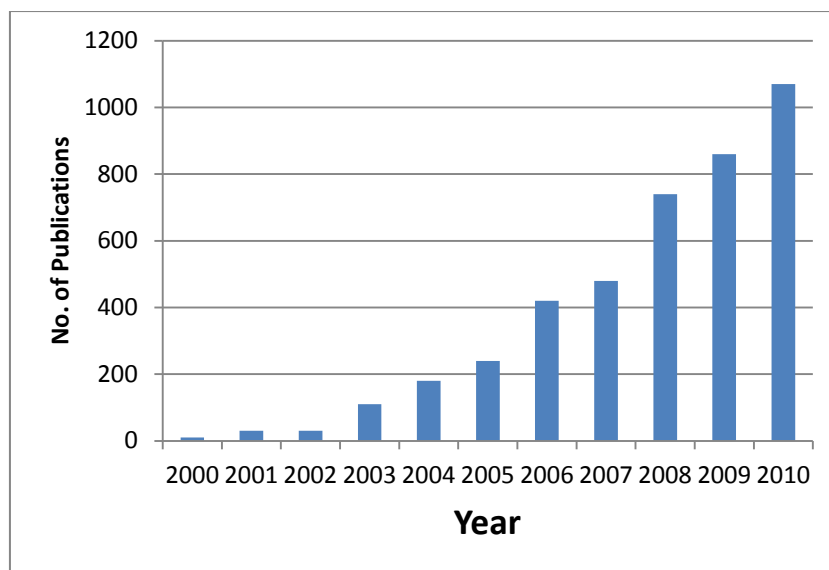


Fig.1.8. Number of scientific publications per year (2000–2010) with the keyword “electrospinning” (source: Web of Science)

The fibers produced can be used systematically to design the structures such that they do not only mimic the properties of the extracellular matrix (ECM), but also possess high strength and high toughness. Although electrospun fiber reinforced polymer composites have significant potential for development of high strength/high toughness materials and materials with good thermal and electrical conductivity, very few studies have investigated the use of electrospun fibers in composites.[60-63] Traditional reinforcements in polymer matrices can create stress concentration sites due to their irregular shapes and cracks propagate by cutting through the fillers or travelling up, down and around the particles. However, electrospun fibers have several advantages over traditional fillers allowing extending the nanocomposite concept to fiber-reinforced materials.[61]

1.4. Polymer matrices

The large varieties of polymers were used for the preparation of polymer nanocomposites using different fillers, such as, nylon, polypropylene, polyethylene, polybutene, polyurethanes, etc. After the pioneer work by Toyota group, enormous amount of work has been carried out on preparation of polymer based nanocomposites. Now the focus is moving towards polymer nanocomposites which are light, possessing good mechanical properties, and eco friendly i.e. bio compatible/degradable, for mainly two reasons: environmental concerns and the realization that our petroleum resources are finite. In this regard, several

research groups developed different nanocomposites based on bio compatible/degradable polymers which are obtained from fossil sources, as well as from renewable resources. Particularly, more attention has been paid on polymers from renewable resources because they allow adding value to agricultural products, which is economically important for many countries. So far, different biocompatible/degradable polymers were used such as poly caprolactone (PCL), poly lactic acid (PLA), poly hydroxybutyrate (PHB), poly butylene succinate (PBS), natural rubber, starch, cellulose etc. Several researchers also reported nanocomposites based on blends of biocompatible/degradable polymers or obtained blending these polymers with non-degradable polymers.

CHAPTER 2

SCOPE AND OBJECTIVES

2. Scope and Objectives

The reinforcement of polymers using fillers, whether inorganic or organic, is common in modern plastics. Polymer nanocomposites or, with a more inclusive term, polymer nanostructured materials, represent a radical alternative to these traditional filled polymer compositions. In contrast to ordinary polymer systems where reinforcement is on the order of microns, polymer nanocomposites are exemplified by discrete constituents on the order of a few nanometers. The nanoparticles may be spherical, plate like nanolayers or nanowires. Uniform dispersion of these nano sized fillers produces a very large increase of the interfacial area between the nanoparticles and the host polymer. The immense internal interfacial area and the nanoscopic dimensions between nanoparticles fundamentally differentiate polymer nanostructured composites from normally filled plastics and composites.[64] This allowed obtaining multifunctional, high-performance properties much improved with respect to those attainable with traditionally filled polymeric materials. In the past decade polymer/clay nanocomposites have emerged as a new class of materials and attracted considerable interest in research and development worldwide after initial reports from the Toyota group on Nylon 6 / clay nanocomposites.[21] Enormous amount of work has been done on preparation and characterization of polymer/organoclay nanocomposites because by this approach it is possible to impart much improved mechanical, thermal, electrical properties with respect to their macro and micro counterparts.[27,28,44,46,65-67] There is a large potential associated to the preparation and analysis of nanocomposites filled with a wide spectrum of nanoparticles, which are available commercially, and many others, which can be prepared easily in the laboratory. However there are limitations in the use of these organoclay-based nanocomposites, especially because of the difficulties in homogeneously dispersing the filler in the matrix, and therefore in efficiently increasing the interfacial area.

The analysis of structure and morphology of the dispersed nanoparticles, polymer phase and the interface of the nanocomposites plays a major role in understanding the properties of these materials. These can be studied by using various techniques such as wide angle X-ray diffraction (WAXD), small angle X-ray scattering (SAXS), optical microscopy, scanning electron microscopy (SEM), transmission electron microscopy (TEM), differential scanning calorimetry (DSC), polarized light optical microscopy (PLOM), thermogravimetric analysis (TGA), etc. A thorough characterization of the structure and morphology of these materials is

key for optimizing their formulation and for exploiting the properties of the nanofillers to their fullest extent. The structure and morphology of the nanocomposites obtained can be assessed by WAXD by which one can understand the intercalation of the polymer in the interlayer gallery if any and the semicrystalline structure of the polymer phase. SAXS allows exploring smaller angles than WAXD, so larger periodicities, typical of intercalated systems, Marigo et.al for example proposed a SAXS approach for a quantitative and very detailed description of the dispersion of the filler in polymer matrices.[68] SEM study can give the morphology of the tactoids formed and the topology of the surface of the polymer. TEM studies can help in understanding the dispersion of the nanoparticles in the polymer matrix; DSC analysis helps in understanding the crystallization kinetics of the nanocomposites, melting behavior etc. TGA allows studying the thermal degradation of prepared compositions.

This project is focused on preparing high-performance nanocomposites using bio degradable polymers such as PCL, PLA and PBSA reinforced with different kinds of nano fillers like organo clays and electrospun nano fibers. A fundamental part of this work deals with the characterization of all prepared composites in order to study the effect of the used nano fillers on their polymer matrix. We studied the effect of nanofillers on structure, morphology, thermal behavior, physical-mechanical properties and degradation behavior of polymer matrices. These polymers are now not economically viable because their low physical mechanical properties do not balance their higher cost. Therefore, objective of this study is to develop biodegradable polymer nanocomposites reinforced with economically cheap nano fillers to enhance their properties.

CHAPTER 3

EXPERIMENTAL SECTION

3. Characterization Techniques

3.1. Wide angle X-ray diffraction (WAXD)

WAXD transmission patterns were recorded by a diffractometer GD 2000 (Ital Structures), working in Seeman-Bohlin geometry and with a quartz crystal monochromator on the primary beam ($\text{CuK}_{\alpha 1}$ radiation). When the basal spacings of clay were of interest, WAXD patterns were recorded by a Philips X'Pert PRO diffractometer, working in the reflection geometry and equipped with a graphite monochromator on the diffracted beam (CuK_{α} radiation). The application of the least-squares fit procedure elaborated by Hindeleh and Johnson [69] gave the degree of crystallinity by weight which was then transformed in degree of crystallinity by volume (Φ_{WAXD}).[70]

3.2. Small angle X-ray scattering (SAXS)

The SAXS patterns of the samples were recorded by a MBraun system, using a CuK_{α} radiation from a Philips PW 1830 X-ray generator. The data were collected by a position sensitive detector and were successively corrected for blank scattering, desmeared and Lorentz-corrected.

Finally, the Lorentz correction was applied: $I_l(s) = 4\pi s^2 I(s)$, where $I_l(s)$ is the one-dimensional scattering function and $I(s)$ the desmeared intensity function, being $s = (2/\lambda)\sin\theta$. [68,71-73]

SAXS Data Analysis

A fitting method of SAXS patterns was developed on the basis of a theoretical model referring to the Hosemann model [74] that assumes the presence of lamellar stacks having an infinite side dimension. This assumption takes into account a monodimensional electron density change along the normal direction to the lamellae.

The intensity profile was evaluated as:

Where:

$$I(s) = I^I(s) + I^{II}(s) \quad (1)$$

$$I^I(s) = \frac{(\rho_C - \rho_A)^2}{4\pi^2 s^2 D} \times \frac{|1 - F_C|^2 (1 - |F_A|^2) + |1 - F_A|^2 (1 - |F_C|^2)}{(1 - F_C F_A)^2} \quad (2)$$

$$I^{II}(s) = \frac{(\rho_C - \rho_A)^2}{2\pi^2 s^2 DN} \times \text{Re} \left\{ \frac{F_A (1 - F_C)^2 (1 - (F_C F_A)^N)}{(1 - F_C F_A)^2} \right\} \quad (3)$$

In these equations, F_C and F_A represent the Fourier transforms of the distribution functions of the crystalline and of the amorphous regions, respectively, ρ_C and ρ_A are the electron densities of the crystalline and amorphous regions, respectively, N is the average number of polymeric lamellae in the stacks and D the average long period. A fitting procedure of the calculated one dimensional scattering functions with the experimental ones allows to optimize the values of the crystalline (C) and amorphous (A) region thicknesses. Crystallinity (Φ_{SAXS}) was evaluated as the ratio between the thickness of the crystalline regions over the long period $D=A+C$. Employment of a two-phase model was justified by the fact that all the samples shared the same transition layer thickness of 20 Å, as evaluated according to Ruland.[75]

3.3. Scanning electron microscopy (SEM)

SEM pictures were obtained by an XL30 Scanning Electron Microscope (Philips). All considered specimens were gold coated. Samples were fractured in liquid nitrogen before they were gold coated.

3.4. Field emission scanning electron microscopy (FESEM)

The morphology of the electrospun Nylon 6 and poly vinyl pyrrolidone (PVP) mat was investigated by Field Emission Scanning Electron Microscopy (FE-SEM, S-4700, Hitachi Co., Japan) at an accelerating voltage of 10 kV after sputter coating the specimens with OsO₄.

3.5. Infrared spectroscopy

Infrared (IR) absorption spectra were acquired on a FTIR Nicolet 5700 spectrometer equipped with a Germanium Attenuate Total Reflectance accessory Thermo Smart Performer. The spectral region spanned from 4000 to 600 cm⁻¹, with a resolution of 4 cm⁻¹. Two hundred and fifty-six acquisitions were gathered. A cross section of the materials was sampled, in order to detect the signals of both electrospun fibers and matrix.

3.6. Transmission Electron Microscopy (TEM)

For TEM, 80 nm ultra-thin sections were prepared by an ultramicrotome (Ultracut E, Reichert-Jung) with a 35° Diamond knife (Diatome, Switzerland) at room temperature. TEM pictures were obtained by a TEM LEO 912 (Zeiss, Germany) at an accelerating voltage of 120 kV.

3.7. Differential scanning calorimetry (DSC)

All the measurements were carried out with a TA Instruments mod.2920 calorimeter operating under N₂ atmosphere. Polymer samples weighing about 5 mg closed in aluminum pans were used throughout the experiments. Indium of high purity was used for calibrating the DSC temperature and enthalpy scales.

3.8. Polarized light optical microscopy (PLOM)

The crystallization behavior of the samples was studied with a Leica DM400M polarized light microscope. The samples were placed between a glass slide and a cover slip and were kept at 180°C for 10 min, to ensure uniform melting and to delete their thermal history. The slide was then transferred to a Mettler FP82HT hot stage set at 100°C. The photomicrographs were taken between cross-polarizers with a Leica DFC280 digital camera. In order to suitably compare the behavior of different samples, photomicrographs were taken for all samples after 20 minutes of isothermal crystallization.

3.9. Thermogravimetric Analysis (TGA)

Thermogravimetric analysis (TGA) was performed with a TA Instruments SDT 2960 simultaneous TG/DSC system. The scans were recorded at a heating rate of 10°C/min in a temperature range from 25 to 900° C. Experiments were done under nitrogen atmosphere. The onset of the degradation (T_{onset}) was calculated as the intersection between the starting mass line and the line of maximum gradient tangent to the TG curve.

3.10. Universal testing machine (UTM)

The tensile properties of the samples were measured using an Instron Model 3345 mechanical tester at room temperature. The strain rate was 5 mm min⁻¹. Five measurements were performed for each sample. The stress at break (in MPa), strain at break (in %), the stress at yield (in MPa), the strain at yield (in %), and Young's modulus (in MPa) have been measured.

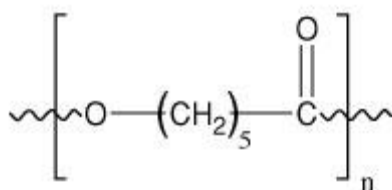
CHAPTER 4

PCL BASED COMPOSITES

4. Poly (caprolactone) (PCL) based Nanocomposites

4.1 Introduction

PCL is linear semi crystalline polyester, characterized by a relative low glass transition temperature (T_g -60°C) and produced by the ring opening polymerization of ϵ -caprolactone, the repeating unit of PCL is showed below.



Even though it is a synthetic polymer, it is biocompatible and biodegradable, either through hydrolytic or enzymatic cleavage along the macromolecular chain. Its potential uses are currently being examined in biodegradable packaging materials,[76] in pharmaceutical controlled release systems and other medical applications, such as suture filaments. The attractiveness of PCL can be further improved through the enhancement of its properties by preparation of nanocomposites. Some of such composites have been reported in the literature[76-95] and they exhibit excellent flexibility, low density and easy processability of polymers in conjunction with the high strength, rigidity and heat resistance of inorganic materials. The observed enhancements are on mechanical properties, thermal stability, gas barrier properties, electric properties, even on biodegradation rates.

Additionally, although a lot of work has been done with PCL nanocomposites with different nanofillers, still there is a possibility to improve the performance of such material. This chapter is discussed in three parts, first the preparation of PCL nanocomposites reinforced with organo clay nanoparticles and the effect of organo clay on PCL matrix. In second part, we prepared PCL composites filled with electrospun nylon fibers. Finally, in third part we discussed the preparation of PCL composites with two different types of electrospun fibers i.e. nylon6 and polyvinyl pyrrolidone (PVP) and mixture of these two fibers as reinforcement. In all cases, we tried to explore the effect of the filler on structure, morphology, thermal behavior, physical-mechanical properties and the degradation of matrix polymer i.e. PCL.

4.2 Structure, Morphology, and Biodegradability of Poly (ϵ -caprolactone)-Based Nanocomposites

Although a lot of work has been done on the synthesis, properties, and characterization of PCL nanocomposites, little attention has been paid toward the relationship between molecular weight, structure, morphology, and biodegradation of PCL nanocomposites. In this work, biodegradable PCL/organically modified clay nanocomposites were prepared by a solvent casting method using different amounts of organoclay and polymer matrices with different average molecular weights. The structure of the nanocomposites was characterized using WAXD and SAXS. Biodegradation studies were carried out and the influence of structure on the degradation of nanocomposites was studied by WAXD. DSC was used to understand the crystallization behavior of the prepared nanocomposites. Tensile properties were also measured. Finally the degradation behavior of prepared composites was studied in compost environment.

Experimental

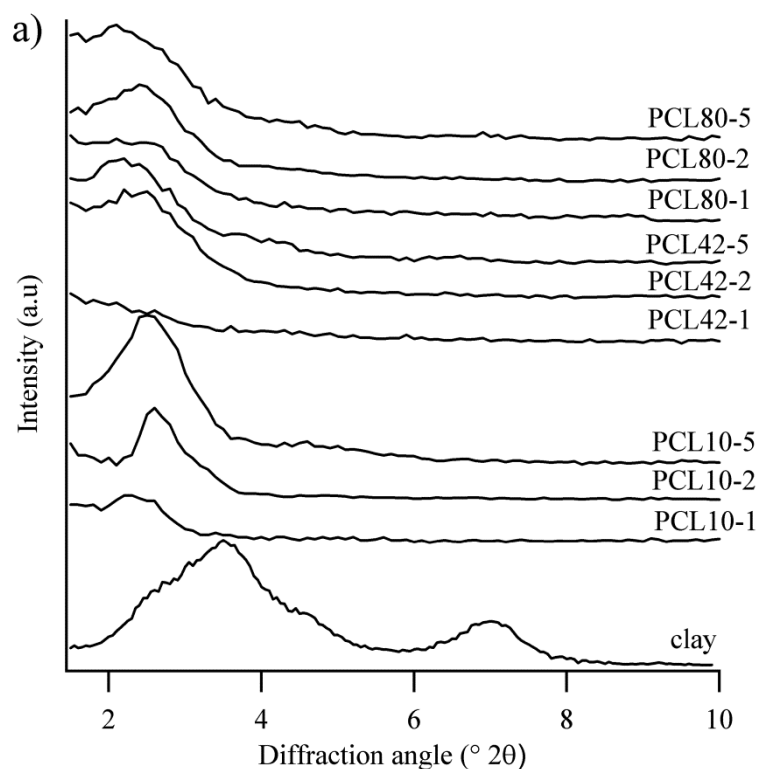
Sample Preparation For the preparation of composites, three PCL matrices differing in number average molecular weight (\overline{M}_n), that is, 80,000, 42,500, and 10,000 g/mol, were purchased from Sigma-Aldrich and used as received. The organoclay was Cloisite 15-A (Southern Clay Products). Cloisite 15A is a commercial montmorillonite organomodified by ion-exchange with dimethyl dehydrogenated tallow quaternary ammonium salt. All the nanocomposites were prepared by a solvent casting method using different amounts of organoclay (1, 3, and 5% by weight) and polymer matrices with different average molecular weights. Samples were coded as PCLx-y, where x indicates the average molecular weight of the matrix (80 for $\overline{M}_n = 80,000$ g/mol; 42 for $\overline{M}_n = 42,500$ g/mol; 10 for $\overline{M}_n = 10,000$ g/mol), and y indicates the filler content. 10 grams of PCL were completely dissolved in 200 mL of tetrahydrofuran. Subsequently, the appropriate mass of clay was added, under vigorous stirring. Mixing time was not less than 6 hr. After such time, the solvent was allowed to evaporate by bland heating at 40°C, and a solid composite was obtained. To carry out the subsequent analyses, the materials were compression molded into films by application of heat and pressure in a press (Alfredo Carrea, Genova, Italy) at 90°C for 5 min, followed by

quenching in ice and water. The samples obtained were evenly white-yellow in color, except for those containing 5% clay, which were more brownish and much less homogeneous.

The structure of the nanocomposites was characterized using WAXD and SAXS. Biodegradation studies were carried out and the influence of structure on the degradation of nanocomposites was studied by WAXD. DSC was used to understand the crystallization behavior of the prepared nanocomposites. Tensile properties were also measured.

Results and discussion

The structure and morphology of the nanocomposites were studied by WAXD and SAXS. [Figure 4.2.1\(a\)](#) shows WAXD patterns, in the low angle region where clay basal peaks appear, of the nanocomposites based on PCL with different molecular weight.



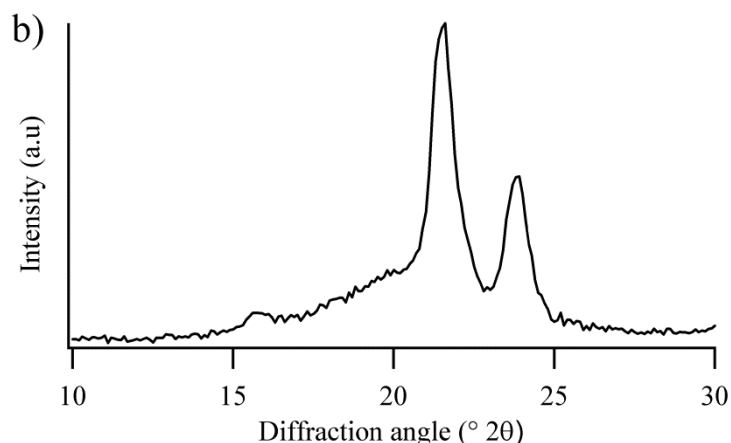


Fig. 4.2.1. a) WAXD traces of the composites and of the neat filler in the angular region of the basal peaks of clay. b) WAXD trace of sample PCL80-1, in the angular range of the diffraction signals of the polymeric crystalline cell

In all the composites, the 001 basal peak shifted toward lower angles from its original position, that is, $3.5^\circ 2\theta$, with a correspondent increase in interlayer space of about 8 Å. Kiersnowski [87] reported that the height of two caprolactone molecules is 7.4 Å. Chen and Evans [76] assessed the height of a monolayer of PCL as 4 Å. Our results are therefore consistent with a flat arrangement of polymer chains creating bilayers of PCL absorbed onto the silicate platelets inside the gallery [87]. For the two series of samples based on PCL with the lowest molecular weights, the shift is more significant for low clay contents. The basal peak is severely weakened in sample PCL42-1, meaning that most of the regularity in the stacking of the aluminosilicatic layers is lost, and an exfoliated structure is approached. Differently from the composites prepared with matrices of lower average molecular weight, the composite based on PCL80 with the largest increase in clay interlayer spacing was the one containing 5% clay.

The region of the WAXD spectra at angles wider than those of [Figure 4.2.1\(a\)](#) showed the reflections due to the polymeric matrix. [Figure 4.2.2\(b\)](#) shows an example of the obtained WAXD patterns in this angular range, the other samples displayed WAXD spectra superimposable to this. The patterns of all the samples were those typical of PCL with two major peaks at $21.3^\circ 2\theta$ and at $23.7^\circ 2\theta$. Such WAXD traces were fitted, deconvoluting the contribution of the crystalline and amorphous domains of the specimens and thus obtaining the degree of crystallinity. The degree of crystallinity evaluated by WAXD (Φ_{WAXD}), was about 44% for

both the matrices and the composites, irrespectively of their average molecular weight. Clay did not have a measurable effect on this feature of the structure, because the degree of crystallinity remained constant as a function of filler content.[80,81]

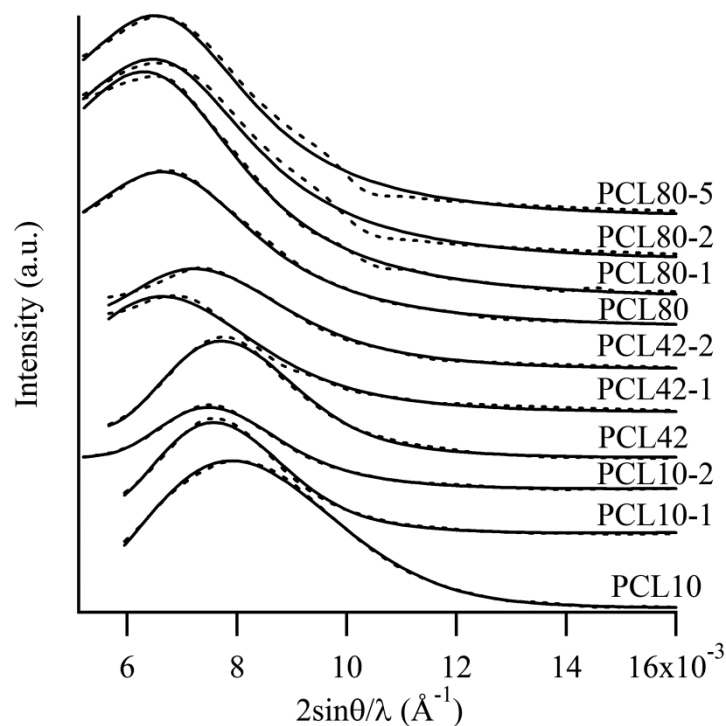


Fig. 4.2.2. SAXS patterns (dotted lines) of the considered samples. Traces calculated during the fitting procedure (solid lines) are also shown

SAXS was used to investigate the semicrystalline framework of the material on a larger scale, typical of lamellar stacks. The SAXS experimental traces are shown in [Figure 4.2.2](#) and were fitted according to a method, which was shown [73,96] to reliably determine the thicknesses and distributions of the crystalline and amorphous layers, the long period and the crystallinity, along with their distribution, associated to lamellar stacks.

[Table 4.2.1](#) shows the data describing the morphology of the stacks in all the considered samples. It can be noted that SAXS crystallinity (Φ_{SAXS}), that is, the crystallinity associated to lamellar stacks, tends to increase as a function of clay content with all molecular weights of PCL.

In other instances, it was highlighted that the nanofillers may exert a minor role in shaping the structure at a crystalline cell level, but it has its most significant effects on polymer lamellae.[97-103] This is exactly what was observed in our case. The crystallinity detected by WAXD was unaltered by addition of clay, whereas SAXS, which probes the lamellar morphology of the matrix, evidenced a significant modification as a consequence of the presence of the filler.

Table 4.2.1: Morphological parameters of the lamellar stacks obtained by SAXS analysis of the samples. The thickness of the crystalline (C) and amorphous layer (A), the long period (D), and the crystallinity (Φ_{SAXS}), along with their relative distributions ($\sigma_C/C = \sigma_A/A$, σ_D/D) are shown. Samples PCL10-5 and PCL42-5 are not shown, since their SAXS patterns were barely detectable and were not fittable.

Sample	C (Å)	A (Å)	D(Å)	Φ_{saxs} (%)	σ_C/C	σ_A/A	σ_D/D
PCL10	67	47	114	58	0.24	0.24	0.17
PCL10-1	76	51	127	59	0.25	0.25	0.18
PCL10-2	85	50	135	63	0.33	0.33	0.24
PCL42	73	53	126	58	0.27	0.27	0.19
PCL42-1	85	57	142	60	0.39	0.39	0.27
PCL42-2	85	54	139	61	0.39	0.39	0.28
PCL80	81	81	163	50	0.47	0.47	0.34
PCL80-1	84	83	167	50	0.46	0.46	0.33
PCL80-2	84	81	164	51	0.47	0.47	0.33
PCL80-5	86	77	164	53	0.46	0.46	0.32

Moreover, Φ_{SAXS} is always larger than Φ_{WAXD} , which in our samples is never higher than 45%. This divergence can be explained considering the difference between the two techniques. SAXS is only sensitive to the crystalline regions organized in lamellar stacks, whereas WAXD allows the detection of all the regions contributing to the semicrystalline framework, including the amorphous phase located between the lamellar stacks. Therefore, WAXD crystallinity (Φ_{WAXD}) is lower because the contribution of crystalline domains is “diluted” by the interstack amorphous. The difference between Φ_{WAXD} and Φ_{SAXS} is much lowered using PCL80 rather than PCL42 or PCL10 as a matrix. This means that in the samples with larger PCL chains, the quantity of interstack amorphous material is much

lowered, and that most of the noncrystalline material is confined within the lamellar stacks. It appears that the lamellar morphology of low molecular weight matrices is affected by the presence of clay more than high-molecular weight matrices. This is also reflected by the considerable increase in the thickness of the crystalline layer of the composites with respect to the matrix, which is much larger in the case of PCL10 than for PCL80. Moreover, the distributions of the thickness of the crystalline layer, of the thickness of the amorphous layer, and of the long period were increased by increasing the clay content when the low molecular weight matrices were used. However, this effect was not observed in PCL80 samples. Finally, the fact that the lamellar stacks of lower molecular weight matrices are more sensitive to the presence of clay is evidenced by the fact that the SAXS diffractograms of the samples with 5% of clay are so severely weakened to be not fittable for PCL10-5 and PCL42-5, because of the disruption of the ordered lamellar stacks. The presence of a fittable SAXS signal for PCL80-5 is a sign that PCL80 as a matrix is more resistant to the interference of clay. Kiersnowski et.al [87] reported contrasting results with respect to ours. They found that the composites had thinner lamellae and a lower Φ_{SAXS} with respect to the matrix polymer. However, they studied in situ polymerized PCL composites, in which the attainment of the structure and morphology were dictated also by the polymerization process and also by the excellent exfoliation of the filler, which can be achieved by this technique. In our case, only intercalation could be attained, so the mobility of the chains was different and thus the crystallization conditions.

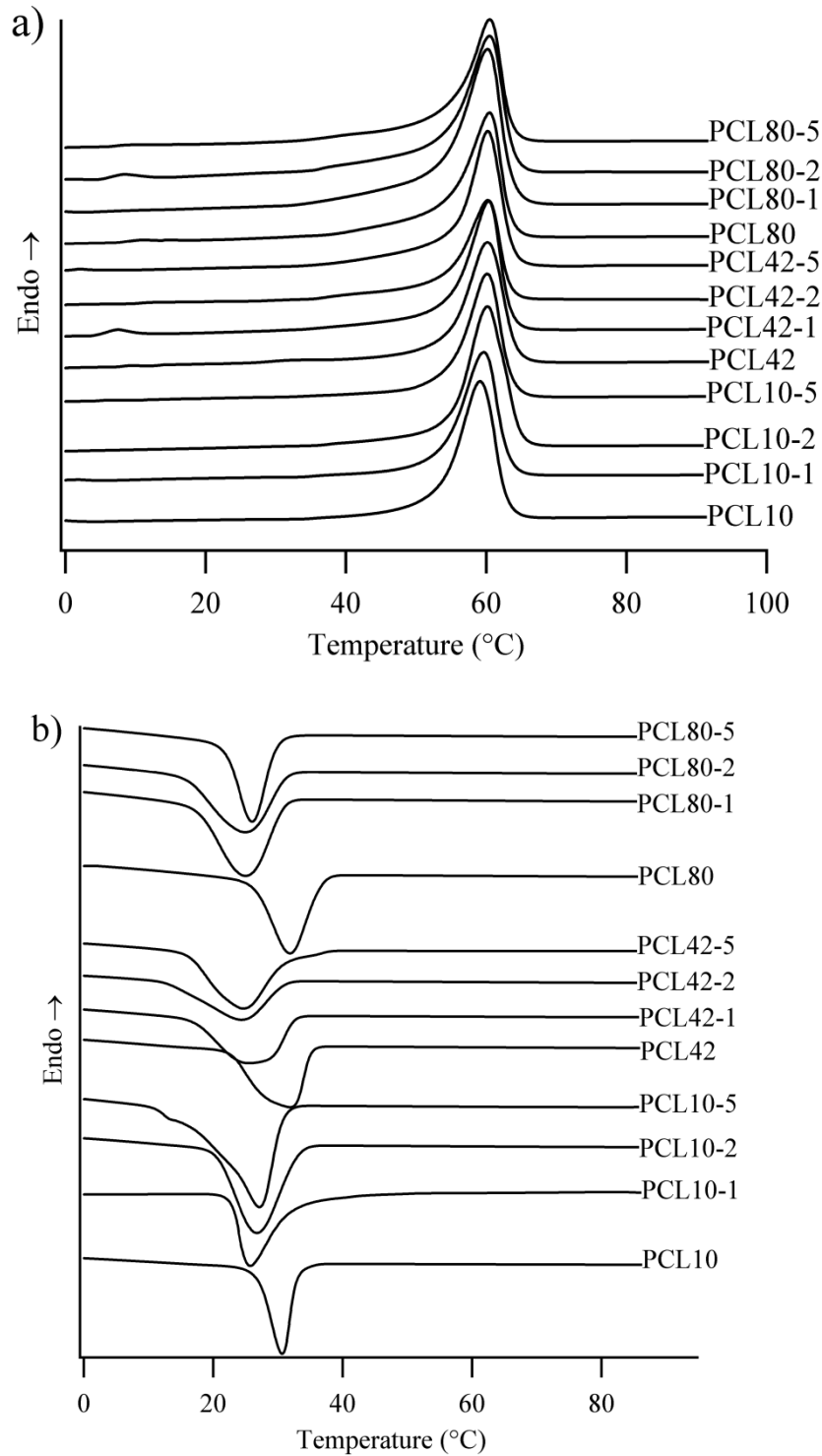


Fig.4.2.3. DSC patterns for a) the first heating ramp and b) cooling ramp of the considered samples

The crystallization behavior of the samples was studied by DSC (Fig. 4.2.3). No difference in melting temperature was noted between the matrix and the composites (Fig. 4.2.3(a)), whereas the crystallization temperature decreased by adding clay to the polymer matrix (Fig. 4.2.3(b)). Saturation of this effect was observed, that is, further addition of clay did not

further modify the crystallization temperature. For example, in the composites based on PCL42, the crystallization temperature decreased from 31°C in the matrix to 26°C in the composites. This reflects an inhibiting effect on crystallization due to clay. Analogous results were obtained with the other molecular weights. This effect could appear to be reverse than which has been frequently reported, that is, clay normally acts as a nucleating agent.[76,79,93,94,104,105] Actually, it has been argued that clay has not a univocal influence on the rate of crystallization, but the quantity and dispersion of this filler is a key in tuning its nucleating effect, because the presence of dispersed clay can actually slow down the crystal growth rate. Kiersnowski and Pigłowski [88] noted that too large a quantity of filler, that is, in their case more than 10%, reduces the crystallization rate, whereas smaller quantities increase it. Chen and Evans [76] and Pucciariello et.al [93] observed nucleation only with exfoliated clay, whereas this effect was severely weakened or was reversed for intercalated nanocomposites. The inhibition effect brought about in our samples has a double, conflicting consequence. On one hand, it slows down and hinders the crystallization process, and on the other hand, at the same time, it allows a longer time for the polymer to attain a more regular ordering. The constancy in the degrees of crystallinity measured by WAXD is consistent with a balance between these two effects. Such a behavior has been observed before, for example, in polyethylene [106-108] or polypropylene [103,109].

Table4.2. 2: Tensile properties of the samples based on the PCL80 andPCL42 matrices

Sample	Modulus (MPa)	Stress at yield (MPa)	Strain at yield (%)	Stress at break (MPa)	Strain at break (%)
PCL42	352 ± 25	15.7 ± 0.9	7.0 ± 0.4	15.9 ± 0.2	467 ± 31
PCL42-1	338 ± 29	14.0 ± 0.8	12.1 ± 0.7	15.7 ± 0.1	884 ± 37
PCL42-2	312 ± 30	12.4 ± 0.6	10.0 ± 0.8	17.2 ± 0.3	1120 ± 56
PCL42-5	283 ± 11	14.8 ± 0.7	14.4 ± 0.9	12.6 ± 0.3	52 ± 15
PCL80	283 ± 21	14.9 ± 0.5	10.1 ± 0.8	17.3 ± 0.2	637 ± 32
PCL80-1	274 ± 26	12.1 ± 0.1	13.5 ± 0.9	14.4 ± 0.2	792 ± 45
PCL80-2	238 ± 23	11.5 ± 0.6	17.9 ± 0.7	16.7 ± 0.1	1170 ± 54
PCL80-5	418 ± 36	11.2 ± 0.6	11.9 ± 0.6	14.5 ± 0.3	848 ± 43

The tensile properties of the samples based on the PCL42 and PCL80 matrices were measured with a universal testing machine and are summarized in [Table 4.2.2](#). The stress

versus strain curves are shown in Fig. 4.2.4. No measurement was performed on the samples based on PCL10, because they had very poor mechanical properties, which did not even allow preparing suitable specimens for testing. The composites retained the modulus, stress at yield, and stress at break of their respective matrix. It is noteworthy that large increases in the strain at yield and strain at break were obtained. In other words, addition of clay does not influence their stiffness but greatly enhances its ductility. This behavior is highly unusual in nanocomposites. Previous reports on the preparation of PCL nanocomposites with a variety of fillers normally reported an increase in modulus, at the expense of elongation at break. [81,89,91,92,94,95,110] Physical–mechanical properties obtained for the PCL42-5 sample are worse than the other compositions, and this behavior may be due to the higher amount of clay, which in turn leads to nonhomogenous dispersion of clay in polymer matrix.

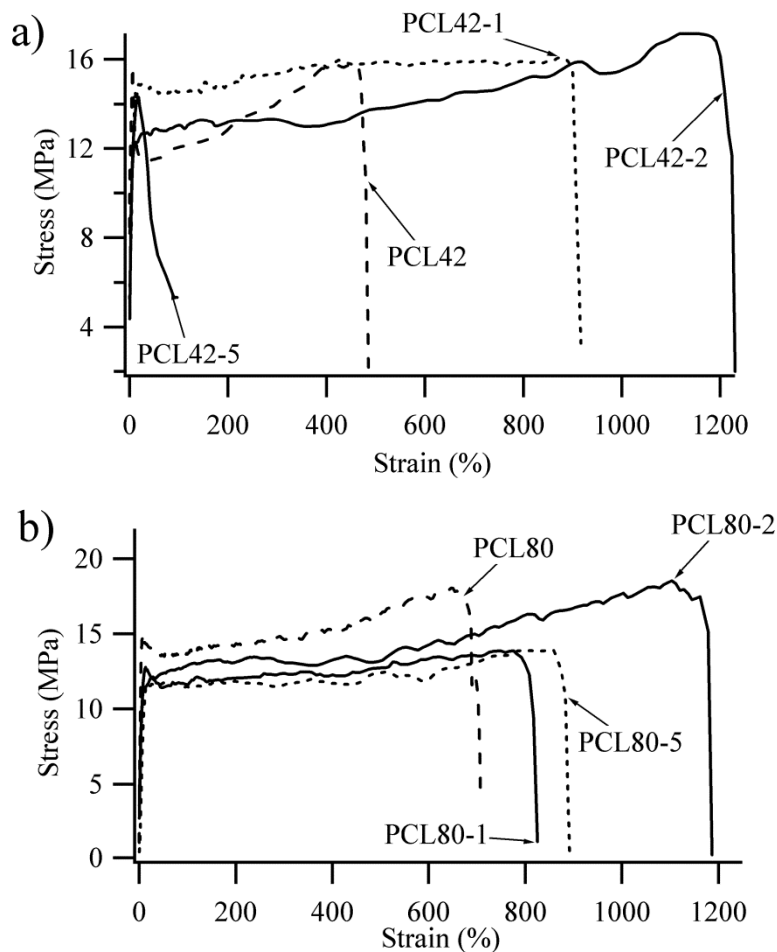


Fig.4.2.4. Tensile stress vs. strain curves of the samples of the a) PCL42 and b) PCL80 series

The biodegradability of the PCL/clay nanocomposites was evaluated by burying specimens in organic compost. The tests were carried out in a crystallizer at room temperature at 100% relative humidity. Samples were retrieved at given time intervals and weighted. The nanocomposites based on PCL10 were very brittle, so we were unable to take them out to weight, but samples were completely disappeared after 8 weeks in compost. Images of buried samples of the PCL42 and PCL80 series are shown in [Figs. 4.2.5 and 4.2.6](#), at time 0 and after 13 weeks.

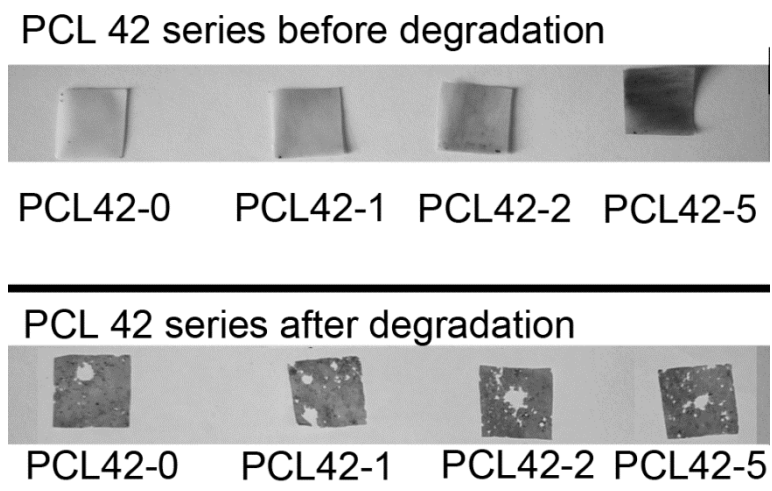


Fig.4.2.5. Samples of the PCL42 before the biodegradation experiment and after 13 weeks in compost

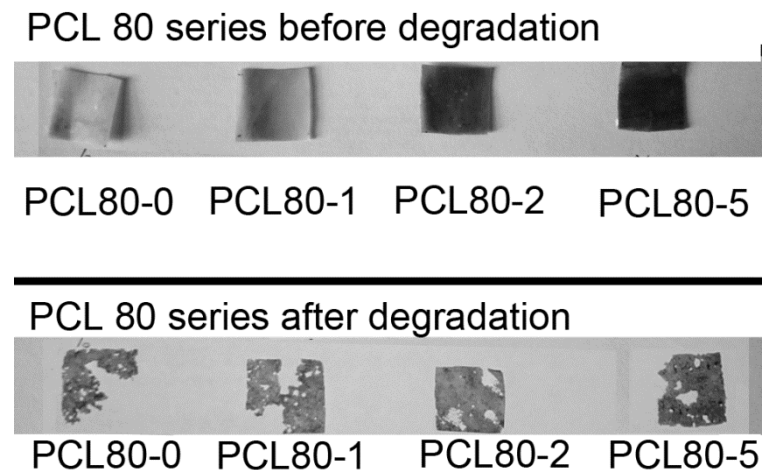


Fig.4.2.6. Samples of the PCL80 series before the biodegradation experiment and after 13 weeks in compost

For PCL10 samples, we did not collect the images due to their unavailability at week 13. [Figures 4.2.7 and 4.2.8](#) show the trend of the mass residue as a function of time for the samples of the PCL42 and PCL80 series, respectively.

In all cases, rapid loss in weight was observed after 8 weeks. The rate and extent of biodegradation decreased in the composites with respect to the matrix. It is surprising that among the many articles on PCL-based nanocomposites, very few works report studies on biodegradation. Wu and coworkers [95] reported that clay-containing nanocomposites underwent a more difficult degradation by bacteria, and they argued that it may possibly due to the recalcitrant nature of clay towards biodegradation. Lee et.al [90] attributed the hindering effect of clay toward biodegradation to the fact that the barrier effect due to the filler prevents water from exerting hydrolysis. Along with the role that clay exerts per se, it is likely that also the structure of the matrix may be important also.

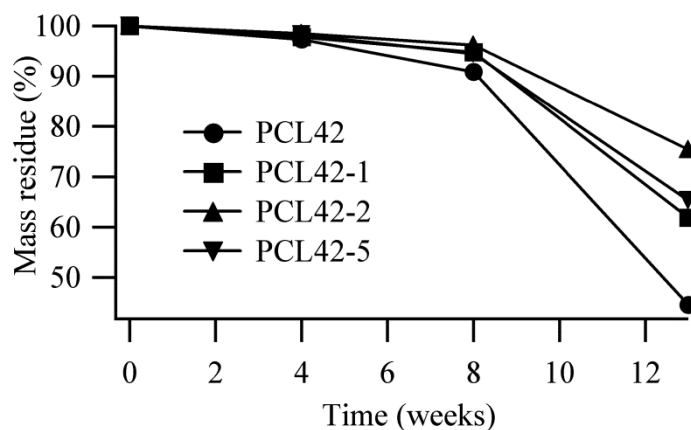


Fig.4.2.7. Mass residue of the samples of the PCL42 series as a function of time

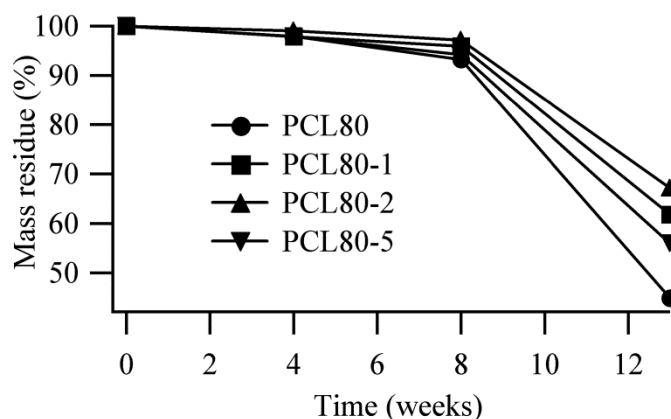


Fig.4.2.8. Mass residue of the samples of the PCL80 series as a function of time

To understand the effect of the structure on biodegradation, the degree of crystallinity of the samples of the PCL42 and PCL80 series was measured by WAXD at time zero and after 13 weeks, and the results are tabulated in [Table 4.2.3](#).

Table 4.2.3: Crystallinity degree of the samples of the PCL42 and PCL80 series before and after biodegradation

Sample	% of crystallinity at time 0	% of crystallinity after 13 weeks
PCL42500	44	46
PCL42500 1%	44	49
PCL42500 2%	44	51
PCL42500 5%	44	48
PCL80000	44	51
PCL80000 1%	44	47
PCL80000 2%	42	47
PCL80000 5%	42	45

Samples with PCL10 were not included in the comparison, due to their unavailability after 13 weeks. After exposing to the biodegradation, in all samples the degree of crystallinity increased, meaning that the less ordered portion of the sample was preferentially degraded. GPC measurements made on samples before and after degradation showed an increase in the average molecular weight as a result of biodegradation. Degradative processes therefore preferentially attack shorter chains, those which tend to be more involved in the amorphous phase, and therefore, they subtract short chains from the system, resulting in an increase in average molecular weight. Biodegradation thus affects the amorphous domains of the matrix, and it appears to be favored by a less crystalline framework. The composites exhibit thicker lamellae and more crystalline stacks, and therefore, they degrade slowly and to a lesser extent. In the case of our samples, there is not a clear and univocal trend of biodegradation rate or residue as a function of either crystallinity degree or clay dispersion. For example, samples PCL 80-1 and 80-2 share a very similar semicrystalline framework, because they have the same crystallinity by WAXD and a very similar lamellar morphology, nevertheless PCL80-1 degrades faster than PCL80-2. Obviously, a complex interplay of various factors influences the biodegradation behavior; nevertheless the role of the semicrystalline framework appears to be important.

Conclusions

Intercalated PCL/organoclay nanocomposites were successfully prepared by solution mixing using THF as a solvent. The thickness of crystalline lamellae increased in low-molecular weight polymer nanocomposites by increasing clay amount, and this effect was weakened in the case of nanocomposites with high-molecular weight polymer. Crystallization temperature was decreased by adding clay, and therefore, in these systems, the filler acted as an inhibitor of crystallization, rather than as a nucleant, as it has been frequently reported. The modulus of the prepared nanocomposites was unaltered, but their ductility increased, which is an unusual behavior in nanocomposites. In all cases, biodegradation started after 4 weeks and rapid change occurred after 8 weeks. Biodegradation rate was reduced with the addition of clay to polymer, coherently with the observed increase in the lamellar thickness brought about by this filler. Along with the effect on biodegradation of clay dispersion and quantity, in this report, it was shown that the semicrystalline framework has a role as well. Monitoring of the degree of crystallinity before and after biodegradation showed that in this process the amorphous regions are preferentially attacked. Although further investigation is still needed to single out the effect of all the relevant factors, this could offer a strategy for calibrating the biodegradability of PCL, by tuning the relative quantities of amorphous and crystalline domains.

4.3 Poly (ϵ -caprolactone) filled with electrospun nylon fibers: A model for a facile composite fabrication

In this work, a fabrication approach is presented that allows to prepare composites based on polycaprolactone filled with nylon 6 (NY) nanofibers by compression moulding. This work is intended as a proof of concept for the use of electrospun fibers as cheap and easily prepared fillers. PCL was chosen as a matrix because it is a very attractive biodegradable and biocompatible material, although not with outstanding physical mechanical properties. [111] The possibility to improve the performance of such material could open a wide array of possible applications, also allowing the substitution of some less environmentally friendly materials. Moreover, PCL has a quite low melting point, so it was a very suitable candidate for the proposed fabrication approach, which is based on the percolation of the molten matrix

within the pores of the electrospun nylon fibers mat. Care was taken to use a small amount of nylon fibers, since the availability of electrospun nanofibers on a large scale is still difficult, and also to avoid possible problems in the waste management of the materials.

Experimental

Samples and sample preparation

The matrix used for the samples was polycaprolactone, purchased from Sigma–Aldrich (Milano, Italy). This material is reported by the producer to have a melt index of 1.9 g/10 min (80°C/0.3 MPa), average molecular weight $\overline{M}_n \sim 42,500$ and $\overline{M}_w \sim 65,000$. Nylon 6 electrospun nanofibers were used as fillers. Nylon pellets (relative viscosity of 2.8) were obtained from Kolon Industries, Inc., Republic of Korea. The pellets were dried in vacuum oven at 100°C to remove adsorbed moisture. Electrospinning was carried out by taking 22 wt% (viscosity, 1320 cps) nylon solution in formic acid/acetic acid (80/20, wt/wt) with an applied voltage of 22 kV and tip to collector distance of 12 cm. Just after electrospinning, nylon 6 nanofibers were placed under vacuum to remove residual solvent. The porosity, total pore area, average pore diameter and bulk density of the fiber mat was 67.7%, 1.71 m²/g, 10.8 μm and 0.1463 g/mL, respectively, as measured by mercury porosimetry (Auto Pore IV 9500 V1.05, Serial: 243, Micrometrics Instrument Corporation, USA). Preparation of the composites was made by impregnation of the electrospun fibers mat with the molten PCL, by the compression moulding approach schematized in [Fig. 4.3.1](#) and [Table 4.3.1](#). The nanofibers mat was sandwiched between PCL films. By application of heat and pressure in a press (Alfredo Carrea, Genova, Italy) at 90°C, PCL was melted and percolated between the voids in the mat, constituting a continuous phase in which the fibers were dispersed. Three composites were prepared, differing by fiber content and by preparation procedure. Sample PCL/NY3 was prepared as a sandwich of one layer of nylon mat between two PCL films. PCL/NY5 was obtained from two layers of nylon mat alternated by PCL films. PCL/NY8 was prepared interposing all the nylon fibers between two PCL layers.

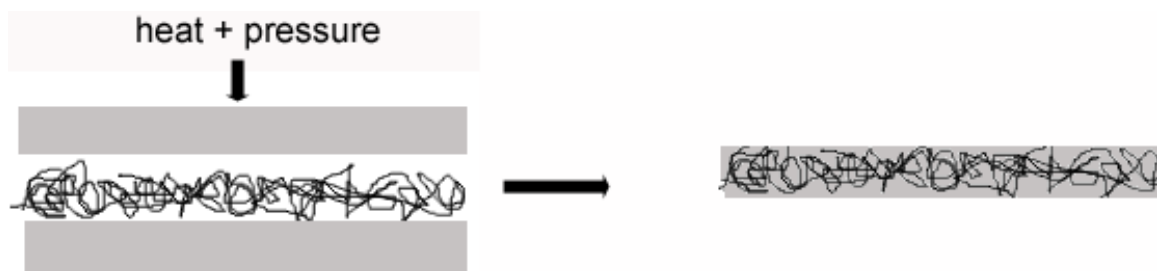

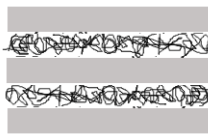
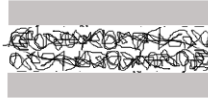


Fig.4.3.1. Preparation procedure of the PCL/NY composites

The structure of the nanocomposites was characterized using WAXD and SAXS. Interfacial adhesion was studied by SEM; DSC was used to understand the crystallization behavior of the prepared nanocomposites. The melting behavior was studied by melting the samples with a ramp from room temperature to 250°C at 10°C/min. The crystallization behavior was studied in two ways. In the first one, the thermal history was cancelled by a 5 min long isotherm at 100°C, subsequently the samples were cooled down to room temperature at 10°C/min. In the second one, cancellation of thermal history was made by a 5 min long isotherm at 250°C, followed by a cooling at 10°C/min to room temperature. Both cases were followed by a further heating ramp to 250°C, to observe the melting peaks of the constituents of the material. The tensile properties of the samples (dimensions 30 mm X 10 mm X 0.5 mm) were measured using an Instron Model 3345 mechanical tester at room temperature. The strain rate was 5 mm min⁻¹. Five measurements were performed for each sample. The stress at break (in MPa), strain at break (in %), the stress at yield (in MPa), the strain at yield (in %), and Young's modulus (in MPa) have been measured with relative errors of max. 9%.

Table 4.3.1: Composition and preparation procedure of the samples

Sample	Fibre content (% w/w)	Preparation setup
PCL	0	
PCL/NY3	3	
PCL/NY5	5	
PCL/NY8	8	

Results and discussion

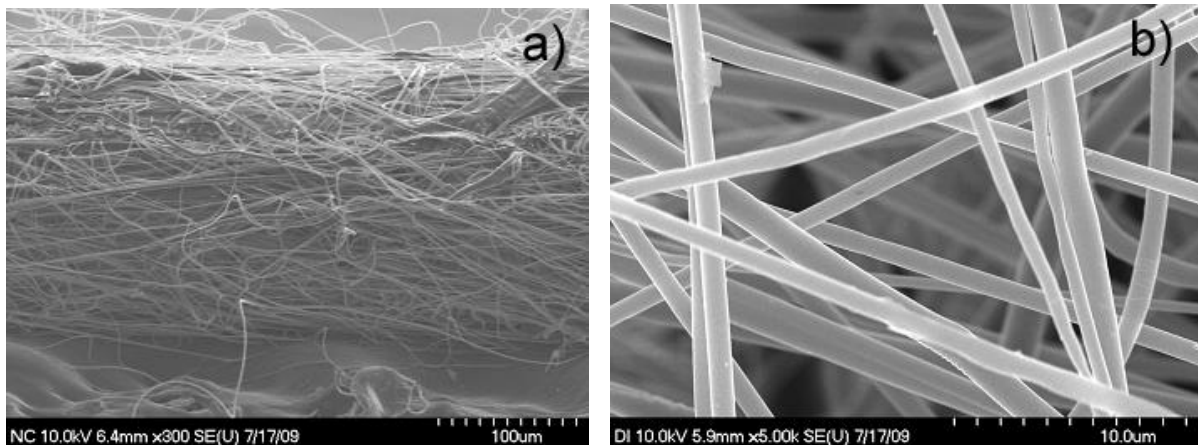


Fig.4.3.2. FE-SEM micrographs of (a) the cross section of the fiber mat and (b) of a detail of the fibers

Figs. 4.3.2 and 4.3.3 show FE-SEM and SEM micrographs of the electrospun nylon fibers employed in this work. Compared to the fiber diameter obtainable by conventional melt spinning, i.e. about 30 μm , [63] the average diameter of our electrospun fibers was 800 nm.

These can hardly be considered electrospun nanofibers, nevertheless their diameter is about one order of magnitude smaller (i.e. their specific surface areas are more than 10-times larger) [112] than ordinary nylon fibers. The quality of the fibers was good, with a smooth surface and no trace of beads.

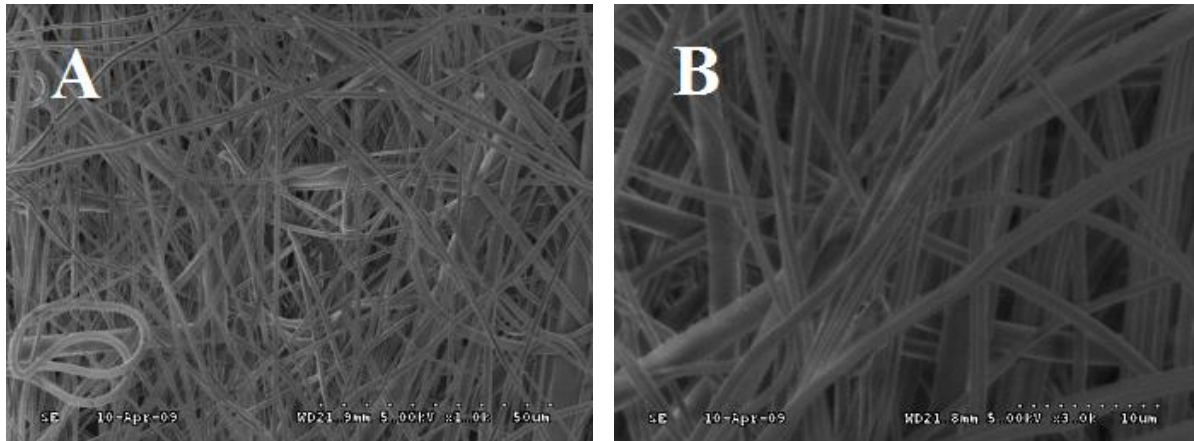


Fig.4.3.3. SEM micrographs of the nylon electrospun fibers at different magnifications (A) 1000x, (B) 3000x

As better detailed in experimental section, inclusion of the fibers in a continuous PCL matrix was done by percolating, in a compression moulding press, molten PCL within the interstices of the fibrous mat (Fig. 4.3.1). The electrospun fiber mat included in the matrix was isotropic. Operating at an intermediate temperature between the melting points of PCL ($T_{mPCL} = 60^{\circ}\text{C}$) and of nylon ($T_{mNY} > 210^{\circ}\text{C}$), i.e. working at 90°C , it was possible to preserve the network of the electrospun fibers, while at the same time creating a homogenous PCL polymeric matrix.

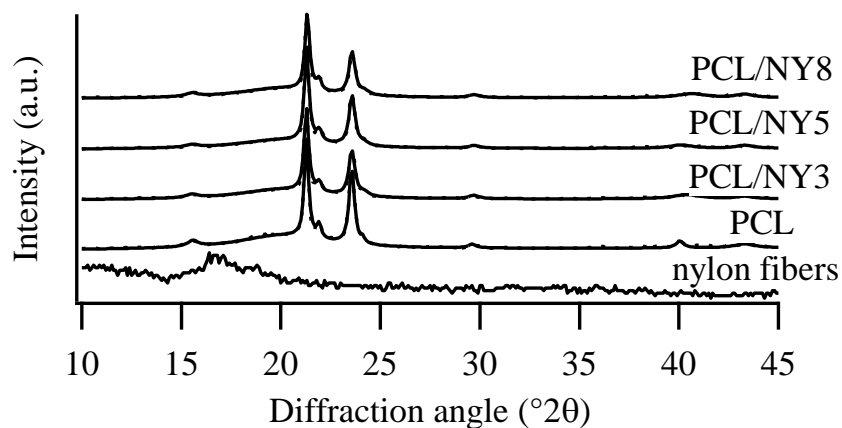


Fig.4.3.4. WAXD traces of blank PCL matrix, of pure electrospun fibers and of the composites

Table 4.3.1 summarizes the composition of the samples and also shows a schematic of the precursor assembly of materials before the compression moulding step. The effect of such a preparation procedure on the structure and morphology of the composites was studied by wide angle X-ray diffraction (WAXD). Fig. 4.3.4 shows the diffractograms of the blank PCL matrix, of pure electrospun fibers and of the composites. The entity of crystalline peaks is very weak in electrospun nylon fibers, with respect to the amorphous halo that dominates the diffractogram of this material. Obviously the polymer was not allowed enough time, during the electrospinning processing, to properly crystallize. The patterns of all the other samples were those typical of PCL with two major peaks at 21.3° and at 23.7° 2θ , [105] without the appearance of nylon peaks, due to the low quantity and crystallinity of this filler. The trend of the degrees of crystallinity as measured by WAXD (Table 4.3.2) showed an increase, albeit slight, of the crystallinity of the composites with respect to the pristine matrix.

Table 4.3.2: Degree of crystallinity obtained by WAXD and morphological parameters of the lamellar stacks obtained by SAXS analysis of the samples. The thickness of the crystalline (C) and amorphous layer (A), the long period (D), and the crystallinity (Φ_{SAXS}), along with their relative distributions ($\sigma_C/C = \sigma_A/A$, σ_D/D and $\sigma_\varphi/\varphi_{\text{SAXS}}$), and number of lamellae (N) are shown.

Sample	φ_{WAXD} %	C Å	A Å	D Å	σ_C/C	σ_D/D	Φ_{SAXS} %	$\sigma_\varphi/\varphi_{\text{SAXS}}$	N
PCL	49	101	42	144	0.06	0.04	70	0.01	48
PCL/NY3	52	79	64	143	0.02	0.02	55	0.02	47
PCL/NY5	51	83	64	147	0.04	0.02	57	0.02	50
PCL/NY8	55	88	64	152	0.01	0.01	58	0.02	50

DSC confirmed the presence of a nucleating effect due to the fibers. As said in experimental section, the crystallization behavior was studied in two ways. In the first one, the thermal history was cancelled by a 5 min long isotherm at 100°C , which was a temperature high enough to melt PCL, but not the nylon fibers. In this way, the nucleating effect of the fibers could be evaluated. In the second set of thermal experiments, cancellation of thermal history was made by a 5 min long isotherm at 250°C , therefore melting both the matrix and the electrospun fibers before starting the cooling ramp, so excluding the effect on nucleation of the fibrous morphology of nylon. Both cases were followed by a further heating ramp to

250°C, to observe the melting peaks of the constituents of the material. Results are summarized in [Table 4.3.3](#).

Table 4.3.3: Thermal data obtained in the DSC experiments. Data regarding melting of nylon are not shown, since they were constant in all the tests.

Sample	Before cancellation of thermal history		After cancellation of thermal history at 100°C (fibrous nylon network preserved)			After cancellation of thermal history at 250°C (fibrous nylon network destroyed)		
	T_m^{PCL} (°C)	ΔH_m^{PCL} (kJ/mol)	T_c (°C)	T_m^{PCL} (°C)	ΔH_m^{PCL} (kJ/mol)	T_c (°C) †	T_m^{PCL} (°C)	ΔH_m^{PCL} (kJ/mol)
PCL	59.3	76	28.0	56.9	58	31.3	55.6	64
PCL/NY3	60.1	74	34.3	57.2	58	33.6, 191.3	57.3	62
PCL/NY5	60.4	77	35.0	57.9	56	33.7, 191.5	57.5	63
PCL/NY8	59.0	71	35.0	57.3	55	33.6, 192.1	56.7	60

† The lower temperature corresponds to the crystallization peak of PCL, the higher temperature corresponds to the crystallization of nylon.

A significant and consistent increase of the crystallization temperature (T_c) was observed in the composites with respect to the matrix. It is interesting to note that this increase in T_c was observed both after selective melting of only the PCL matrix and also after melting of both PCL and nylon, but it was larger in entity in the first case, when the large interfacial area of electrospun nylon fibers could be exploited as a nucleating surface. This nucleating effect seems to be saturated, i.e. adding further filler did not bring about significant increases in the crystallization rate, probably because at that point the rate determining step became crystal growth rather than crystallite nucleation. No other marked effect was exerted by the presence of fibers on the thermal behavior.

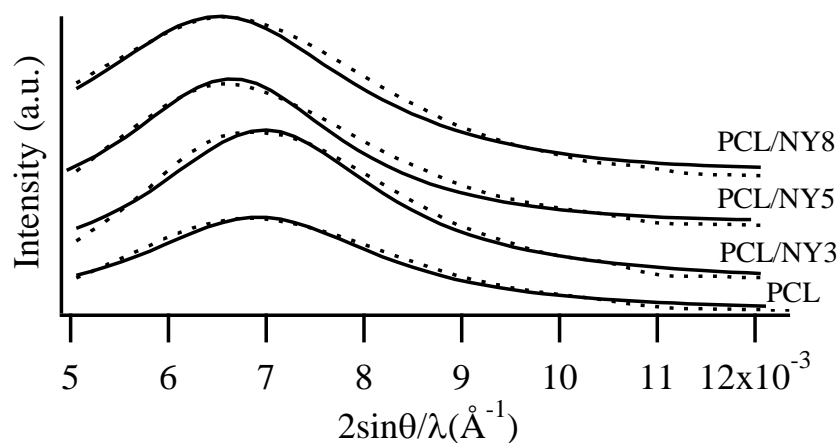


Fig.4.3.5. SAXS patterns (dotted lines) of the considered samples. Traces calculated during the fitting procedure (solid lines) are also shown

Fig. 4.3.5 shows the SAXS patterns of the considered samples. The experimental traces due to the matrix and to the samples with electrospun fibers were fitted according to a method, [113-115] which was shown [115] to reliably determine the thicknesses and distributions of the crystalline and amorphous layers, the long period and the crystallinity, along with their distribution, associated to lamellar stacks. The results are shown in Table 4.3.2. The model used for the best fitting was that of a variable finite stack with a symmetric distribution. Addition of fibers decreased the thickness of the crystalline layer and, consequently, the crystallinity associated to lamellar stacks. It can be seen that the crystallinities assessed by SAXS have larger values relative to those estimated by WAXD. This divergence can be explained considering the difference between the two techniques. SAXS is only sensitive to the crystalline regions organized in lamellar stacks, whereas WAXD allows the detection of all the regions contributing to the semicrystalline framework, including the amorphous phase located between the lamellar stacks. Therefore, WAXD crystallinity is lower because the contribution of crystalline domains is “diluted” by the interstack amorphous. It can be seen that the difference between Φ_{WAXD} and Φ_{SAXS} is much lowered passing from the matrix to the composites. This means that in the composites the quantity of interstack amorphous material is much lowered, and that most of the non-crystalline material is confined within the lamellar stacks. This is reflected by the considerable increase in the thickness of the amorphous layer recorded for the composites with respect to the matrix.

A qualitative difference can be seen in the shapes of the SAXS peaks (Fig. 4.3.5), which are much sharper in the composites rather than in the neat matrix. This is reflected by the

quantitative data (Table 4.3.2), that show a sharpening of the distribution of the thicknesses of the layers, which decreased from $\sigma_C/C = 0.06$ and $\sigma_D/D = 0.04$ in the case of the pristine matrix to about $\sigma_C/C = 0.02$ and $\sigma_D/D = 0.02$ for the composites. The effect of the nanofibers on the structure and morphology of the composites was therefore that of increasing the overall crystallinity (Φ_{WAXD}), whereas at the same time producing a rather homogeneous population of stacks of thin lamellae and rather thick amorphous layers. The lamellar stacks of the composites contained in fact within themselves the amorphous material that, in the pure matrix, was dispersed in the interstack space, so the inclusion of nylon fibers had the effect of including all the amorphous phase within the lamellar stacks. This radical alteration of the morphology of the matrix at a lamellar level most probably plays an important role on the improvement of the tensile properties of the composite (Table 4.3.4). A number of authors stressed the importance of lamellar morphology in understanding the reasons of reinforcement.[97,102,107,116] Modulus, in particular, was shown to depend on the lamellar thickness and crystallinity.[117] Figure 4.3.6a shows that this correlation was valid in our samples as well. The trend of Young's modulus as a function of filler content was the same as the crystallinity of the sample, evaluated by WAXD. Increases of up to 172% in modulus and up to 126% in strain at yield were obtained in our samples, compared to the pristine matrix. Whereas the increases in such tensile features are quite easy to obtain, it is very remarkable that addition of filler brought about a larger strain at break,[118-122] which in our case increased by as much as 28%. A simultaneous increase in modulus, strain at yield, and strain at break and stress at break is quite unusually obtainable by addition of single filler.

Table 4.3.4: Tensile properties of the samples

Sample	Young modulus (MPa)	Stress at yield (MPa)	Strain at yield (%)	Stress at break (MPa)	Strain at break (%)
PCL	352	15.7	7	15.9	467
PCL/NY3	530	16.2	10	18.1	601
PCL/NY5	466	15.9	16	16.1	483
PCL/NY8	957	Does not yield	Does not yield	13.2	23

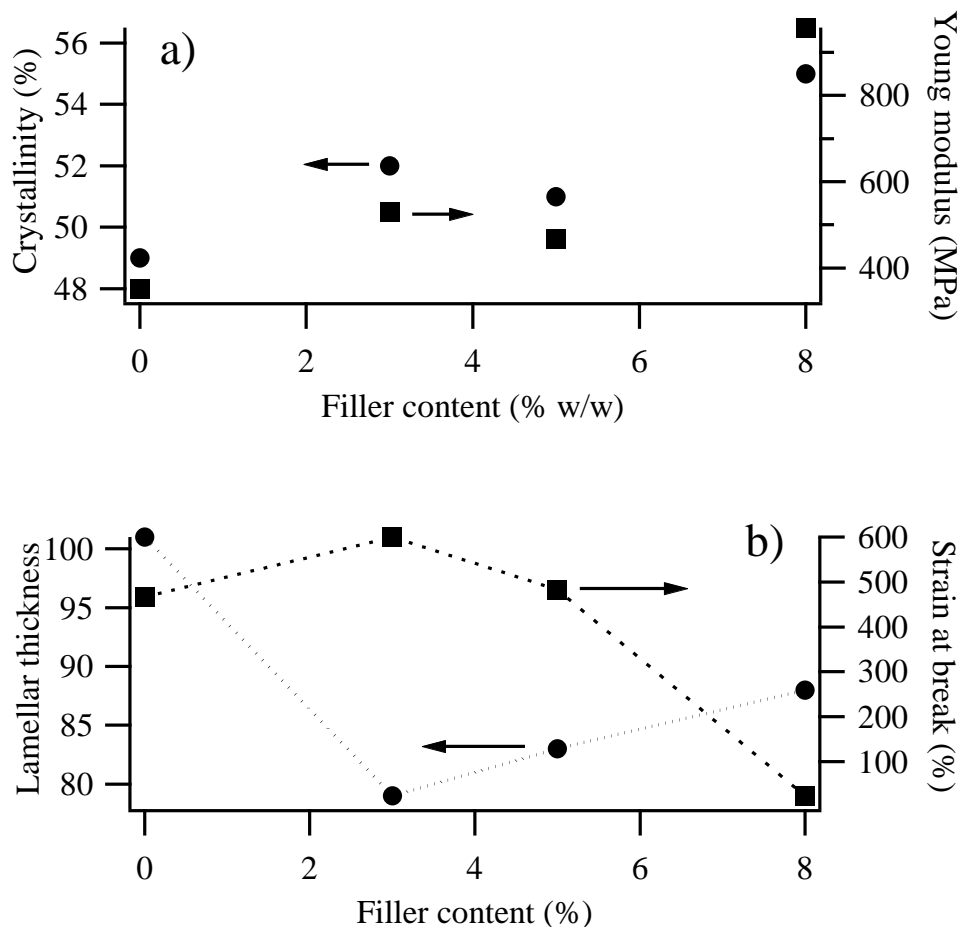


Fig.4.3.6. Trend of (a) the degree of crystallinity measured by WAXD and of Young's modulus, and of (b) ultimate strain and lamella thickness as a function of filler content

Obviously many factors are critical for the tensile behavior of polymer-based composites, among which dispersion, matrix–filler interactions, spherulitic texture, micromechanical deformation processes, skin–core structures and morphological features.[123] It is not possible, based on the data gathered in this work, to single out all of these factors. However, the role of the lamellar morphology in contributing to shaping the mechanical performance of the samples is suggested by [Figure 4.3.6b](#), that shows that the trend of the thickness of the crystalline lamella as a function of filler content is specular to that of ultimate strain, signifying that in this case thicker lamellae are detrimental for ductility. A correlation between tensile properties and lamellar features was previously noted for polyethylene and polypropylene composites filled with polyethylene-grafted multi-wall carbon nanotubes (MWNT) and polypropylene-grafted MWNT, respectively. [102,124] In that case, though,

the polymer chains grafted to MWNT probably participated in the formation of lamellae, thereby providing a physical link between matrix and filler. In this case, the interaction between the components of the composites is of a different nature.

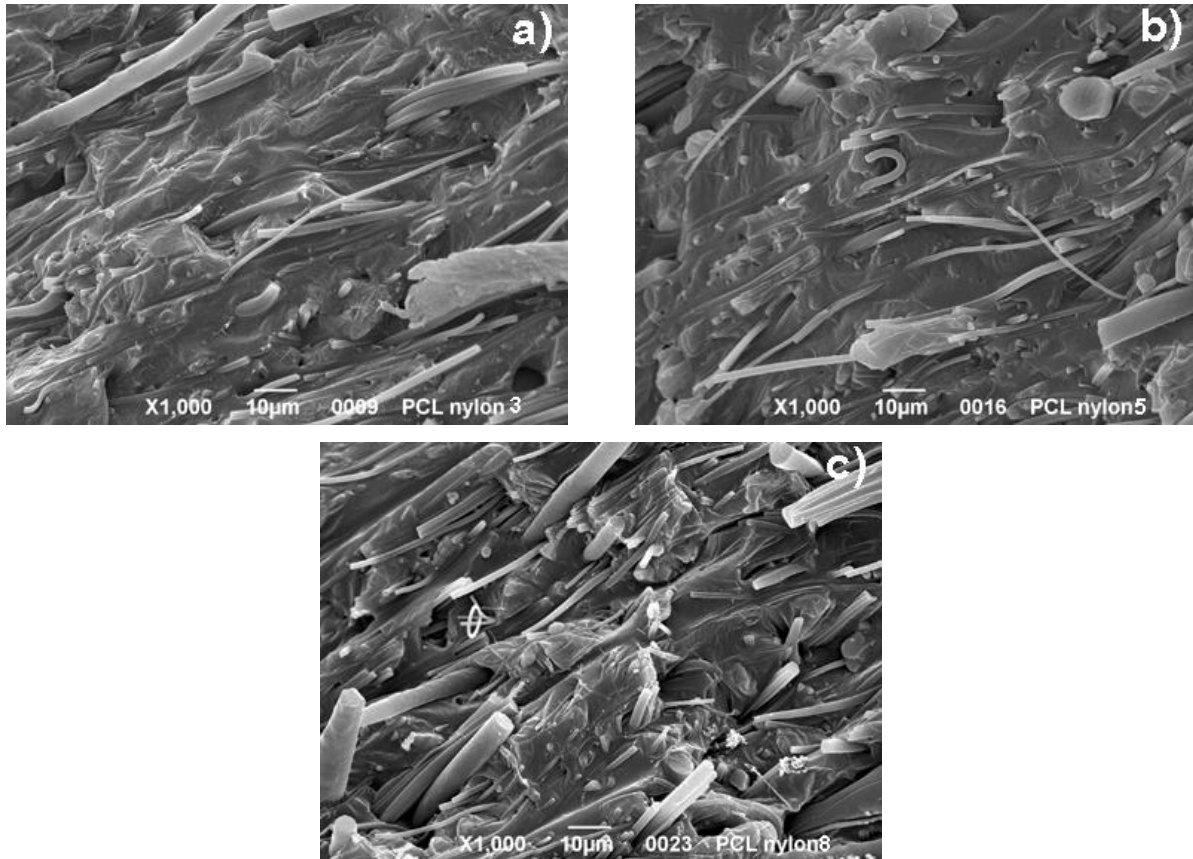


Fig.4.3.7. SEM micrographs of the cryogenic fracture surfaces of samples (a) PCL/NY3, (b) PCL/NY5, and (c) PCL/NY8

Addition of fillers brings a larger quantity of amorphous within the lamellae, with a possible concurrent increase in tie molecules and of entangled material that links lamellae together. Moreover, when tension is applied, the entangled fibers of the isotropic electrospun mat may tend to bridge the cracks. These factors can help rationalize the observed increase in ductility, only if the effect of interfacial adhesion is taken into account. SEM observations were performed to gather information on the morphology of the matrix/fiber interface. [Figure 4.3.7](#) shows low magnification pictures of the fracture surfaces of the three composites. Pulled-out fibers are visible in all three samples, but in PCL/NY8 a very large number of bundles and of loose fibers can be seen, whereas in the case of PCL/NY3 and PCL/NY5 bundles are less in number and the fibers are much more firmly embedded in the matrix.

Higher magnifications allow to better visualize the different interaction between matrix and filler that is observed at low and high filler loadings. [Figure 4.3.8](#) shows details of sample PCL/NY3. In [Figure 4.3.8a](#), it can be seen that the fibers with a larger diameter showed a much poorer interfacial adhesion. The fibers oriented perpendicularly to the fracture surface did not undergo pulling out, whereas those oriented tangentially to the fracture surface were pulled out and hanged loose, especially when bundles were formed. Along with these large fibers, a number of very fine filaments were present. These appear firmly embedded in the matrix ([Fig. 4.3.8b and c](#)): the exposed end of the fibers protrudes directly from within the matrix, without the presence of craters at their base due to debonding. On the contrary, an example of poor adhesion between matrix and filler can be seen in the bottom left corner of [Figure 4.3.7c](#), where a bundle of three fibers appears to loosely extend outwards from a hole in the matrix.

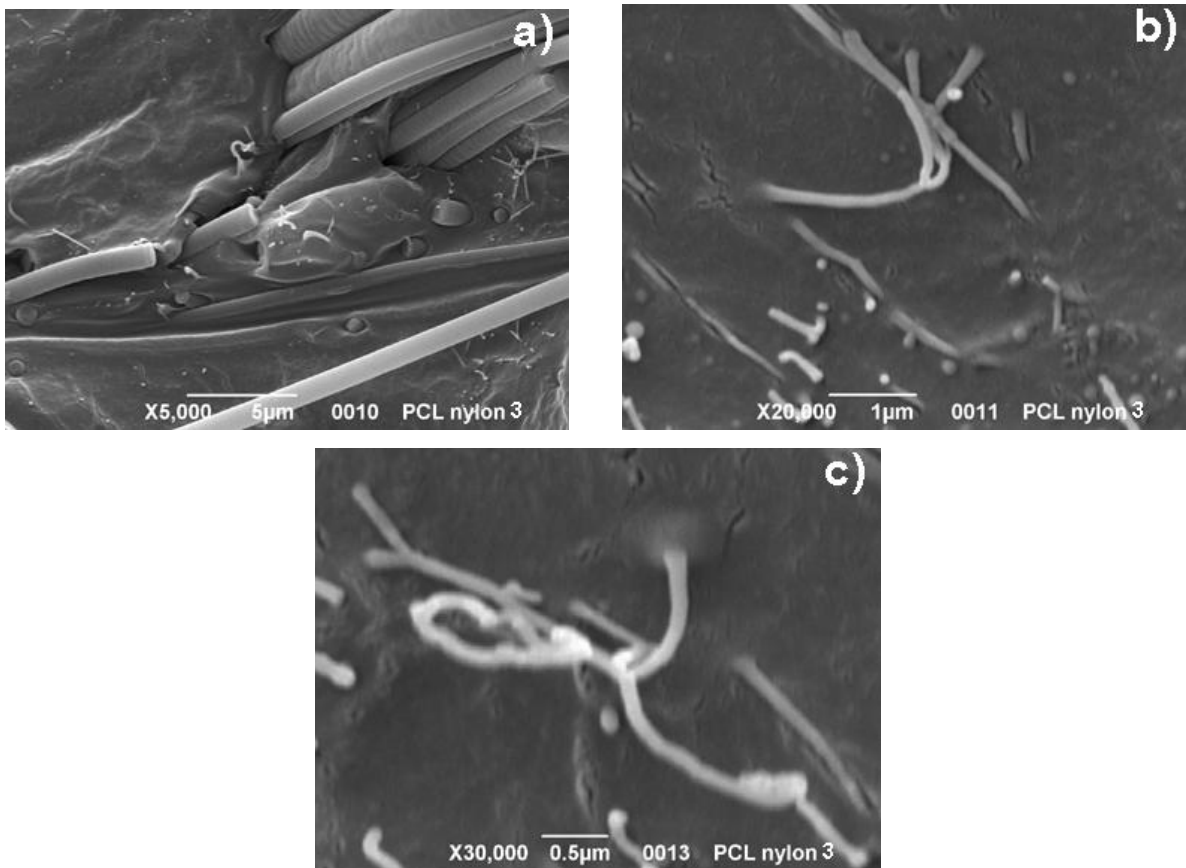


Fig.4.3.8. SEM micrographs at different magnification of the cryogenic fracture surface of sample PCL/NY3

The real advantage of using electrospinning for manufacturing the reinforcing fibers, is therefore the possibility to produce, within the fibrous mat, a subset of fibers with a very fine diameter, that are able to very efficiently interact with the matrix in which they are dispersed.

In order to be able to exploit this advantage, the average diameter must be kept as low as possible, but also the quantity of added filler must be accurately calibrated and kept low. This is evidenced by [Figure 4.3.9](#), in which high magnification details are shown of sample PCL/NY8. Compared with that of [Figure 4.3.8](#), the fracture surface appears in this case very rough, with several marks produced by detaching of the larger fibers. Smaller diameter fibers exist indeed, but their efficiency in improving the cohesion of the composite is reduced by the activity of larger bundles in initiating cracks and fractures. The poor interfacial adhesion of the fiber bundles with the PCL matrix is clear in [Figure 4.3.9](#).

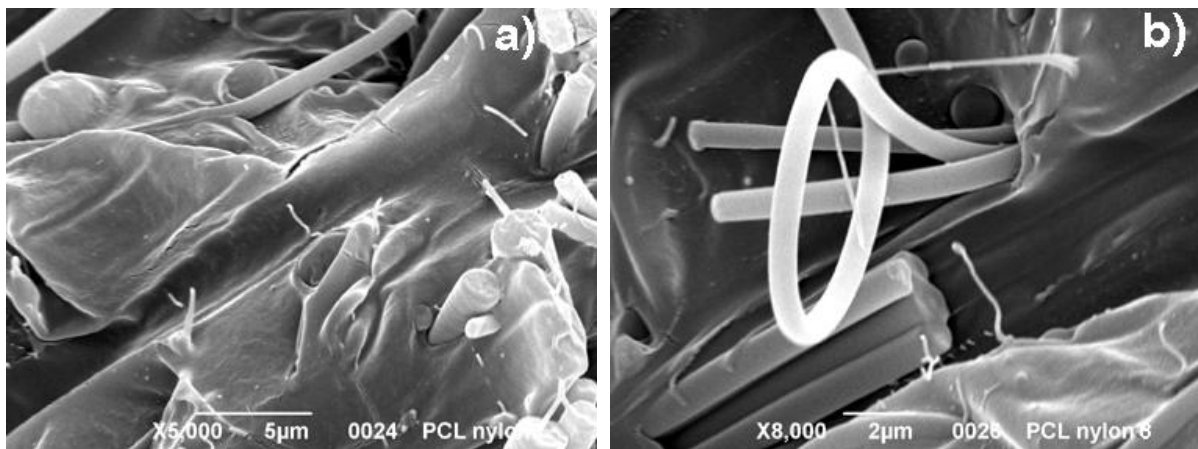


Fig.4.3.9. SEM micrographs at different magnification of the cryogenic fracture surface of sample PCL/NY8

Conclusions

In this paper, nylon electrospun fibers were used to reinforce PCL. At very low filler contents (3%), the obtained composites exhibited not only improved stiffness and strength, but also increased ductility. Previous reports on the preparation of PCL nanocomposites with a variety of fillers normally reported an increase in modulus, at the expense of elongation at break. [81,91,94,95,110,125] Chen and Evans [76] achieved a very sharp increase in elongation at break and an increase of modulus by 50%, with the addition of clay by melt processing. Addition of larger quantities of more expensive filler than our nylon fibers was necessary though for obtaining such improvements. Chrissafis et.al [78] investigated PCL-based nanocomposites with cloisite 20A, cloisite Na⁺, MWNT and SiO₂, and they found increases in modulus for all their samples, whereas elongation at break increased by 8% and 3%, just when cloisite 20A and cloisite Na⁺ were used, respectively.[78] In all cases the technique

used by these authors was in situ polymerization,[78] a very efficient approach, although less facile than the compression moulding method proposed in the present work. Moreover, the fillers employed are much more expensive than simple nylon 6 fibers used by us.

The presence of fibers with a very small diameter, typical of the products of electrospinning, favored a good interfacial adhesion between matrix and filler. Although the increases in tensile properties were not spectacular in magnitude, very encouraging indications emerged from this work:

- Decreasing the diameter of the fibers will most likely bring about a more effective reinforcement: the finest fibers were the ones that best adhered to the matrix;
- By this approach it is possible to simultaneously increase modulus and elongation at break, a quite difficult task with traditional nanofillers like montmorillonite clay or carbon nanotubes;
- Being of a similar order of magnitude than polymer lamellae, electrospun fibers can be used to shape the morphology of lamellar stacks, and therefore the final properties of the composites.

4.4 Improvement of tensile properties and tuning of the biodegradation behavior of polycaprolactone by addition of electrospun fibers

The aim of this work was to explore the effect of electrospun fibers of different chemical nature on the performance and on the biodegradation behavior of PCL-based composites. On one hand, nylon fibers were used, which had previously been shown to be able to improve the physical mechanical performance of the PCL matrix. On the other hand, polyvinylpyrrolidone (PVP) was used as fibrous filler, which was not expected to improve the tensile properties of the composite material, but that, being water soluble, could coadjuvate the biodegradation of the PCL matrix.

The structure of nanocomposites was characterized using wide angle X-ray diffraction (WAXD) and small angle X-ray scattering (SAXS) methods. Biodegradation studies were carried out with respect to time and the influence of structure on the degradation of nanocomposites was studied by WAXD. Differential Scanning Calorimetry (DSC) was used

to understand the crystallization behavior of nanocomposites prepared. Tensile properties were also measured. Biodegradation studies were analyzed in two different systems, one is in an all-purpose gardening soil kept moist at 100% relative humidity and the other one is in phosphate buffer solution (PBS) at 7.4pH at 45°C. The structure of the prepared samples was evaluated before, during and after degradation. In soil, samples were taken out for every one week until the first four weeks; later samples were taken out for weighing after every four weeks. In buffer solution, on the other hand, samples were taken out every 15 days until the experiments finished.

Experimental section

Samples and sample preparation

The matrix used for the samples was polycaprolactone, purchased from Sigma Aldrich (Milano, Italy). This material is reported by the producer to have a melt index of 1.9 g/10 min (80°C/0.3 MPa), average molecular weight $\overline{M}_n \sim 42,500$ and $\overline{M}_w \sim 65,000$. Nylon 6 fibers were prepared by electrospinning to be used as fillers. Nylon pellets (relative viscosity of 2.8) were obtained from Kolon Industries Inc., Republic of Korea. The pellets were dried in vacuum oven at 100°C to remove adsorbed moisture. Electrospinning was carried out by taking 22 wt% (viscosity, 1320 cps) nylon solution in formic acid/acetic acid (80/20, wt/wt) with an applied voltage of 22 kV and tip to collector distance of 12 cm. Just after electrospinning, nylon 6 nanofibers were placed under vacuum to remove residual solvent. Polyvinylpyrrolidone (PVP) fibers were spun by electrospinning to be used as fillers. A 7 wt% solution of polyvinylpyrrolidone (PVP, \overline{M}_w : 1,300,000 g/mol, Aldrich) in ethanol (AAPER alcohol) was prepared. The mixture was placed in an ice-water bath for 10 min, and drawn into a plastic syringe with a 21 gauge stainless steel needle. Electrospinning was carried out with an applied voltage of 20 kV and with a tip to collector distance of 15 cm. The collected polymer composite fibers were subsequently vacuum dried. Preparation of the composites was made by impregnation of the electrospun fibers mat with the molten PCL, by the compression molding approach like in previous work.

The nanofiber mat was sandwiched between PCL films. By application of heat and pressure in a press (Alfredo Carrea, Genova, Italy) at 90°C, PCL was melted and percolated between

the voids in the mat, constituting a continuous phase in which the fibers were dispersed. Three composites were prepared, differing by formulation (Table 4.4.1). The aim of such sample series was to evaluate the effect of fibers of different size and chemical nature on the morphology and performance of the composite materials.

The structure of the nanocomposites was characterized using WAXD and SAXS. Interfacial adhesion was studied by SEM; DSC was used to understand the crystallization behavior of the prepared nanocomposites. The melting behavior was studied by melting the samples with a ramp from room temperature to 250°C at 10°C/min. The crystallization behavior was studied in two ways. In the first one, the thermal history was cancelled by a 5 min long isotherm at 100°C, subsequently the samples were cooled down to room temperature at 10°C/min. In the second one, cancellation of thermal history was made by a 5 min long isotherm at 250°C, followed by a cooling at 10°C/min to room temperature. Both cases were followed by a further heating ramp to 250°C, to observe the melting peaks of the constituents of the material. The tensile properties of the samples (dimensions 30 mm X 10 mm X 0.5 mm) were measured using an Instron Model 3345 mechanical tester at room temperature. The strain rate was 5 mm min⁻¹. Five measurements were performed for each sample. The stress at break (in MPa), strain at break (in %), the stress at yield (in MPa), the strain at yield (in %), and Young's modulus (in MPa) have been measured with relative errors of max. 9%.

Biodegradation studies were analyzed in two different systems, one is in an all-purpose gardening soil kept moist at 100% relative humidity and the other one is in phosphate buffer solution (PBS) (7.4 pH) at 45°C. The structure of the prepared samples was evaluated before, during and after degradation. In soil, samples were taken out for every one week until the first four weeks; later samples were taken out for weighing after every four weeks. In buffer solution, on the other hand, samples were taken out every 15 days until the experiments finished.

Table 4.4.1: Formulation of the samples

Sample	Type of fiber	Fiber content (%)
PCL	-	0
PCLPvp	PVP	1.5
PCLNy	Nylon	3
PCLNyPvp	PVP + Nylon	4.5

Results and discussions

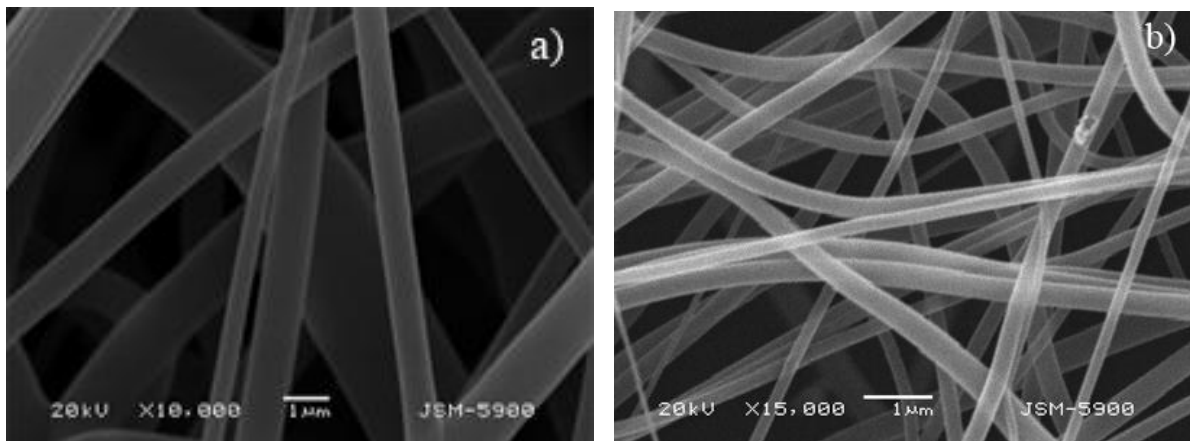


Fig.4.4.1. FESEM micrographs of a) the Ny fiber mat and of b) the PVP fiber mat

Fig. 4.4.1 shows FESEM micrographs of the electrospun Ny and PVP fibers employed in this work. Compared to the fiber diameter obtainable by conventional melt spinning, i.e. about 30 μm , the average diameter of our electrospun fibers were 800 nm in the case of nylon and 300 nm in the case of PVP. These diameters are about one order of magnitude smaller (i.e. their specific surface areas are more than 10-times larger) [112] than ordinarily spun fibers. A notable feature of the two mats is that PVP fibers are more homogeneous in diameter; on the contrary nylon fibers have a broader distribution of fiber size, with thin fibers which coexist with very large fibers, up to 3 mm in diameter. The quality of the fibers was good, with a smooth surface and no trace of beads.

As better detailed in the [Experimental section](#), inclusion of the fibers in a continuous PCL matrix was done by percolating, in a compression molding press, molten PCL within the interstices of the fibrous mat ([Fig. 4.3.1](#)). The electrospun fiber mat included in the matrix was isotropic. Operating at an intermediate temperature between the melting points of PCL ($T_{mPCL} = 60^{\circ}\text{C}$) and of nylon ($T_{mNY} > 210^{\circ}\text{C}$), i.e. working at 90°C , it was possible to preserve the network of the electrospun fibers, while at the same time creating a homogenous PCL polymeric matrix. PVP is an amorphous polymer, which therefore does not melt. Previously to the preparation of the composites, it was checked that the fibrous network was not significantly affected at the processing temperature of 90°C .

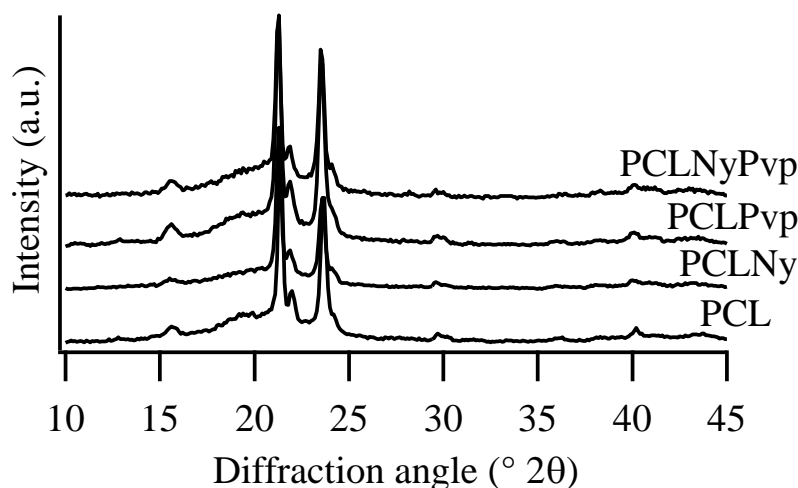


Fig.4.4.2. WAXD diffractograms of pristine PCL, and of the composites

The effect of fibers on the structure and morphology of the composites was studied by WAXD. [Fig. 4.4.2](#) shows the diffractograms of the blank PCL matrix, and of the composites. The WAXD patterns are those typical of PCL with two major peaks at 21.3θ and at 23.7θ , [105] no fiber peaks appear due to the low quantity and the virtual absence of crystallinity of the fillers. The trend of the degree of crystallinity (Φ_{WAXD}) was measured ([Table 4.4.2](#)) by fitting the diffractograms.

Table 4.4.2: Degree of crystallinity obtained by WAXD (Φ_{WAXD}) and morphological parameters of the lamellar stacks obtained by SAXS analysis of considered samples. The thickness of the crystalline (C) and amorphous layer (A), the long period (D), and the crystallinity (Φ_{SAXS}), along with their relative distributions ($\sigma_C/C = \sigma_A/A$ and σ_D/D) are shown.

Sample	Φ_{WAXD} (%)	Φ_{SAXS} (%)	C (Å)	A (Å)	D (Å)	σ_C/C	σ_D/D
PCL	49	70	101	43	144	0.06	0.05
PCLPvp	50	56	81	64	145	0.05	0.04
PCLNy	52	55	79	64	143	0.03	0.02
PCLNyPvp	52	59	88	61	149	0.01	0.01

Results showed that after addition of fibers an almost negligible increase in the degree of crystallinity occurred, as assessed by WAXD. This could probably be ascribed to the slight nucleating effect exerted by the fibers, which was reflected by the crystallization temperature, which increased by 3°C with respect to neat PCL, in a non-isothermal cooling ramp.

Fig. 4.4.3 shows the lamellar morphology patterns of the considered samples by SAXS. The experimental traces due to the matrix and to the samples with electrospun fibers were fitted according to a method which was shown [115] to reliably determine the thicknesses and distributions of the crystalline and amorphous layers, the long period and the crystallinity, along with their distribution, associated to lamellar stacks. The results are shown in Table 4.4.2. Very relevant differences were noted between the SAXS features of the composites and their respective matrices. This is not surprising because in other instances it was highlighted that the nanofillers may exert a minor role in shaping the structure at a crystalline cell level, but it has its most significant effects on polymer lamellae. [98-103]

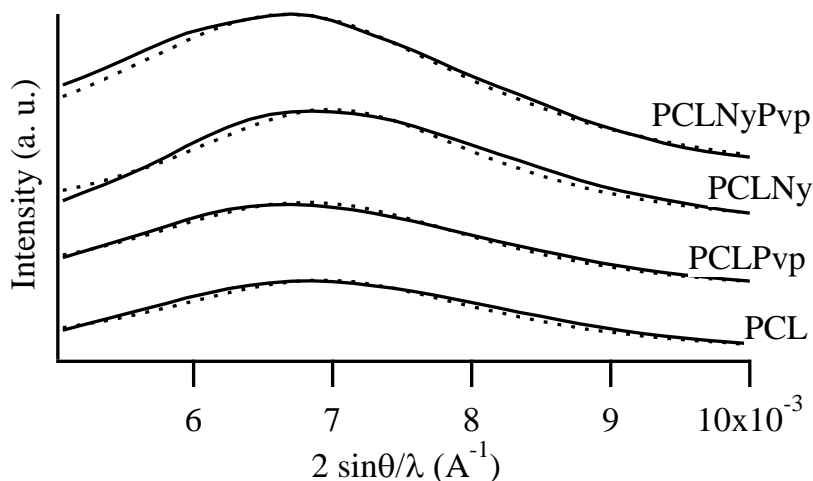


Fig.4.4.3. SAXS patterns (solid line) of the considered samples. Traces calculated during the fitting procedure (dotted line) are also shown

Addition of fibers decreased the thickness of the crystalline layer, C . Such a decrease in the value of C was coupled with a concurrent increase in the thickness of the amorphous layer. Consequently, the crystallinity associated to the lamellar stacks of the PCL matrix decreased after addition of fibers, irrespectively of the chemical nature of the fibers. It may be noted that crystallinities assessed by SAXS have larger values relative to those estimated by WAXD. This divergence can be explained considering the difference between the two techniques. SAXS is only sensitive to the crystalline regions organized in lamellar stacks, whereas WAXD allows the detection of all the regions contributing to the semicrystalline framework, including the amorphous phase located outside the lamellar stacks. Therefore, WAXD crystallinity is lower because the contribution of crystalline domains is “diluted” by the interstack amorphous. It can be seen that the difference between Φ_{WAXD} and Φ_{SAXS} is much lowered passing from the matrix to the composites. This means that in the composites the quantity of interstack amorphous material is much lowered, and that most of the non-crystalline material is confined within the lamellar stacks. This is reflected by the considerable increase in the thickness of the amorphous layer recorded for the composites with respect to the matrix. Such a behavior of fibrous fillers, i.e. in the case of carbon nanotubes and nylon electrospun fibers, has been reported earlier. [103,126]

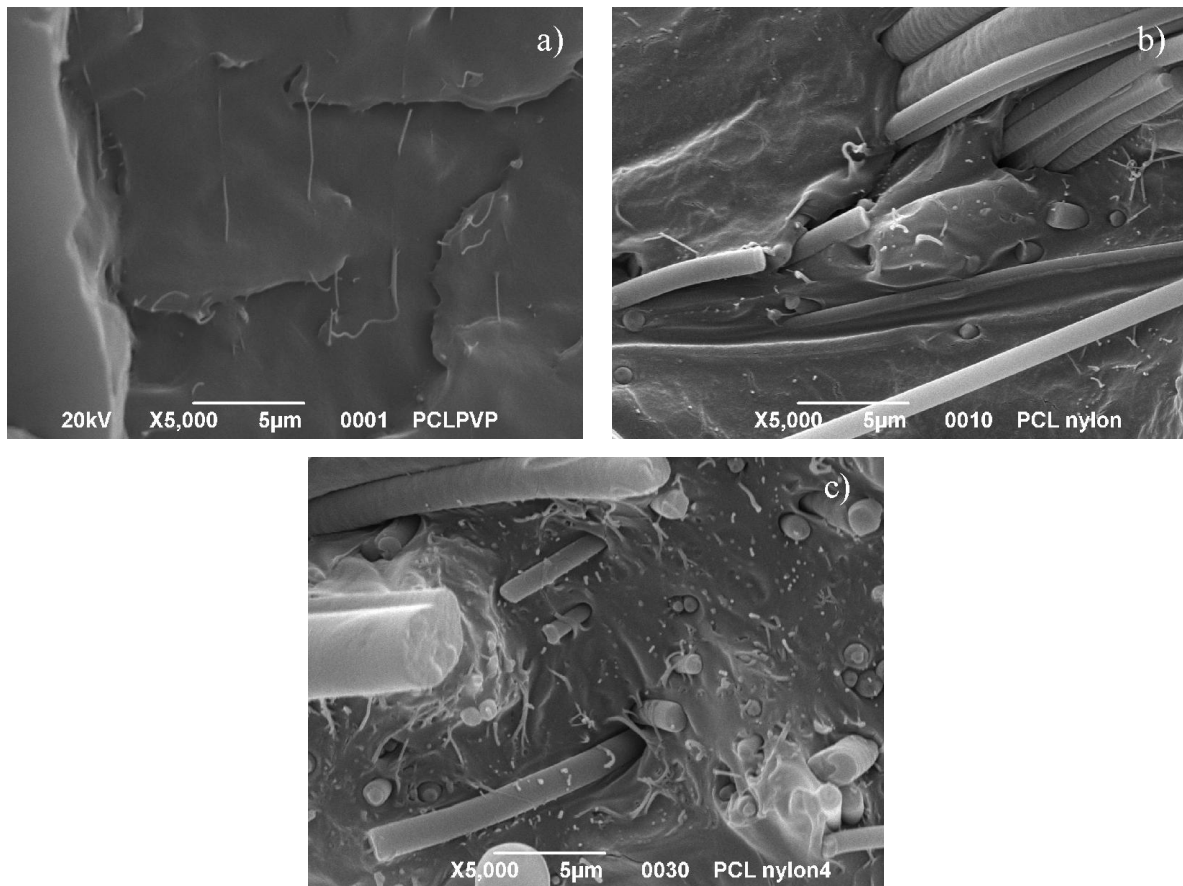


Fig.4.4.4. SEM micrographs of the cryogenic fracture surfaces of samples a) PCLPvp, b) PCLNy and c) PCLNyPvp

SEM observations were performed on composites in order to obtain information on the morphology of the matrix/fiber interface. Fig. 4.4.4 shows pictures of fracture surfaces of PCLPvp, PCLNy, and PCLNyPvp composites. Fig. 4.4.5 shows some higher magnification details, which show that the fibers with a smaller diameter are more firmly embedded in, and show a better interfacial adhesion to, the PCL matrix. Fig. 4.4.5a confirms what was observed in our previous work, [126] i.e. that very fine fibers were very firmly embedded into the matrix and displayed a very good interfacial adhesion toward the matrix. Figs. 4.4.4 and 4.4.5 show that, as the diameter of the fiber increases, the interfacial adhesion is decreased, and the exposed end of the fibers protrudes from a crater in the matrix, showing a significant degree of debonding.

Interestingly, when both nylon and PVP fibers coexist in the composites, interplay exists between the thicker nylon fibers and the thinner PVP fibers. The large diameter fibers are surrounded by the thinner ones (Fig. 4.4.5b). As will be noted later in this paper, this

morphological feature has no effect on the tensile properties of the composites, but it is very relevant in shaping the biodegradation behavior of the materials.

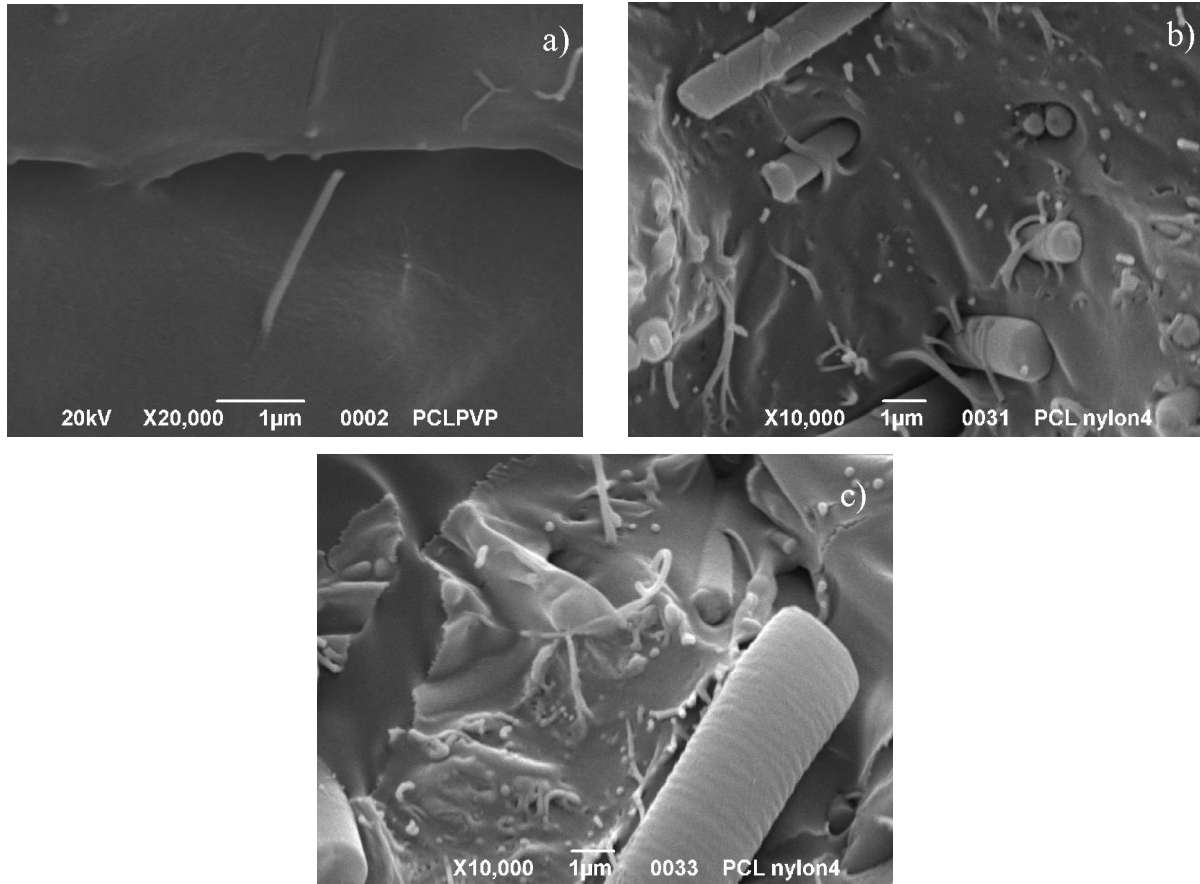


Fig.4.4.5. High magnification SEM micrographs of the cryogenic fracture surfaces of samples a) PCLPvp, b) and c) PCLNyPvp

Table 4.4.3: Tensile properties of the samples

Sample	Young modulus (MPa)	Stress at yield (MPa)	Strain at yield (%)	Stress at break (MPa)	Strain at break (%)
PCL	352	15.7	7	15.9	467
PCLNy	530	16.2	10	18.1	601
PCLPvp	345	16.0	6	16.2	440
PCLNyPvp	489	15.8	15	14.3	610

Table 4.4.3 shows the tensile properties of the considered samples. The addition of PVP did not bring about any improvement in the mechanical performance of the PCL matrix. It is worth noting, though, that even though PVP is a weaker polymer than PCL, the presence of PVP fibers in the PCL matrix is not detrimental as far as tensile properties are concerned. On the other hand, as previously noted,[126] nylon was efficient in upgrading the performance of PCL, simultaneously increasing the rigidity and ductility of the whole material. When both PVP and nylon fibers were added, the performance of the composite was comparable to that of the PCLNy composites. The PCLNyPvp, by comparison with the neat PCL matrix, increased its modulus by +39%, its strain at yield by +114%, and its strain at break by +31%. Stress at yield was unaltered, whereas stress at break decreased by -10% compared to the pure matrix. Rigidity and ductility were thus simultaneously increased: an unusual achievement in nanocomposites. These results confirm the viability of electrospun fibers for the upgrade of the physical-mechanical properties of a biodegradable matrix.

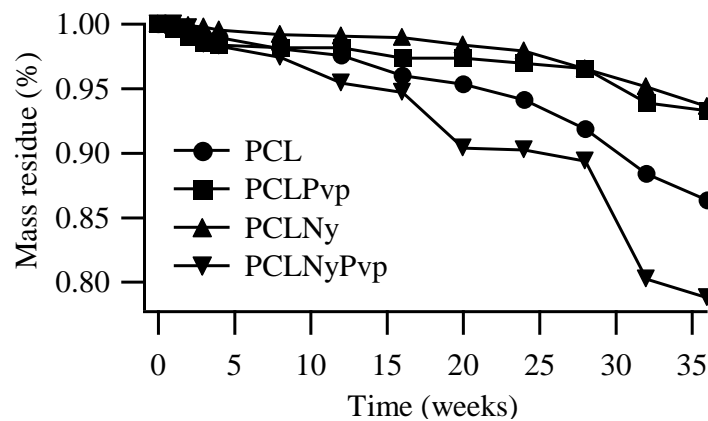


Fig.4.4.6. Mass residue of the samples as a function of time, obtained during biodegradation in soil

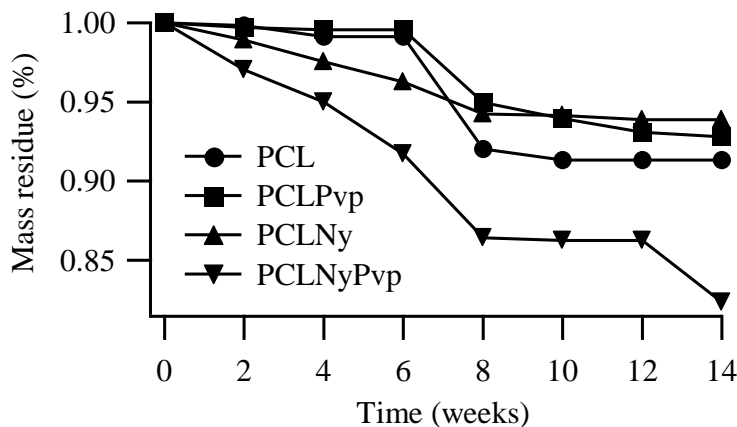


Fig.4.4.7. Mass residue of the samples as a function of time, obtained during biodegradation in buffer

It is interesting to note that in sample PCLNyPvp the coexistence of nylon and PVP fibers in the composites on one hand brings about improved tensile properties due to the reinforcing ability of nylon, but on the other hand it confers functional properties modifying the biodegradation behavior due to the action of PVP. Biodegradation studies were performed for all considered samples in two different systems; one consisted in burying the samples in soil and the second system was putting the samples in phosphate buffer solution with pH 7.4 at 45°C. Samples were taken at regular time intervals, and the trend of the mass of the specimens was noted as a function of time. Figs. 4.4.6 and 4.4.7 show the trend of weight loss of the samples in both soil and buffer, respectively.

In soil buried samples, degradation started at 8 weeks, whereas in buffer solution, degradation started after 30 days. Comparatively, in both cases, in soil and in buffer sample PCLNyPvp had the largest percentage of weight loss: 20% and 16% respectively. The modification of the structure due to biodegradation was studied for all the considered samples by WAXD. The degree of crystallinity of all prepared samples before and after biodegradation are tabulated in Table 4.4.4.

Table 4.4.4: Degree of crystallinity before and after degradation of the samples

Sample	Φ_{WAXD} before degradation	Φ_{WAXD} after 36 weeks in soil	Φ_{WAXD} (%) after 14 weeks in phosphate buffer
PCL	49	68	75
PCLPvp	50	72	78
PCLNy	52	62	75
PCLNyPvp	52	63	70

In all samples and in both systems, i.e. soil buried and buffer solution degraded samples, the degree of crystallinity increased after degradation, compatibly with the hypothesis that degradation happened preferentially in the less ordered portions of the sample. This is consistent with what was previously reported.[127-129]

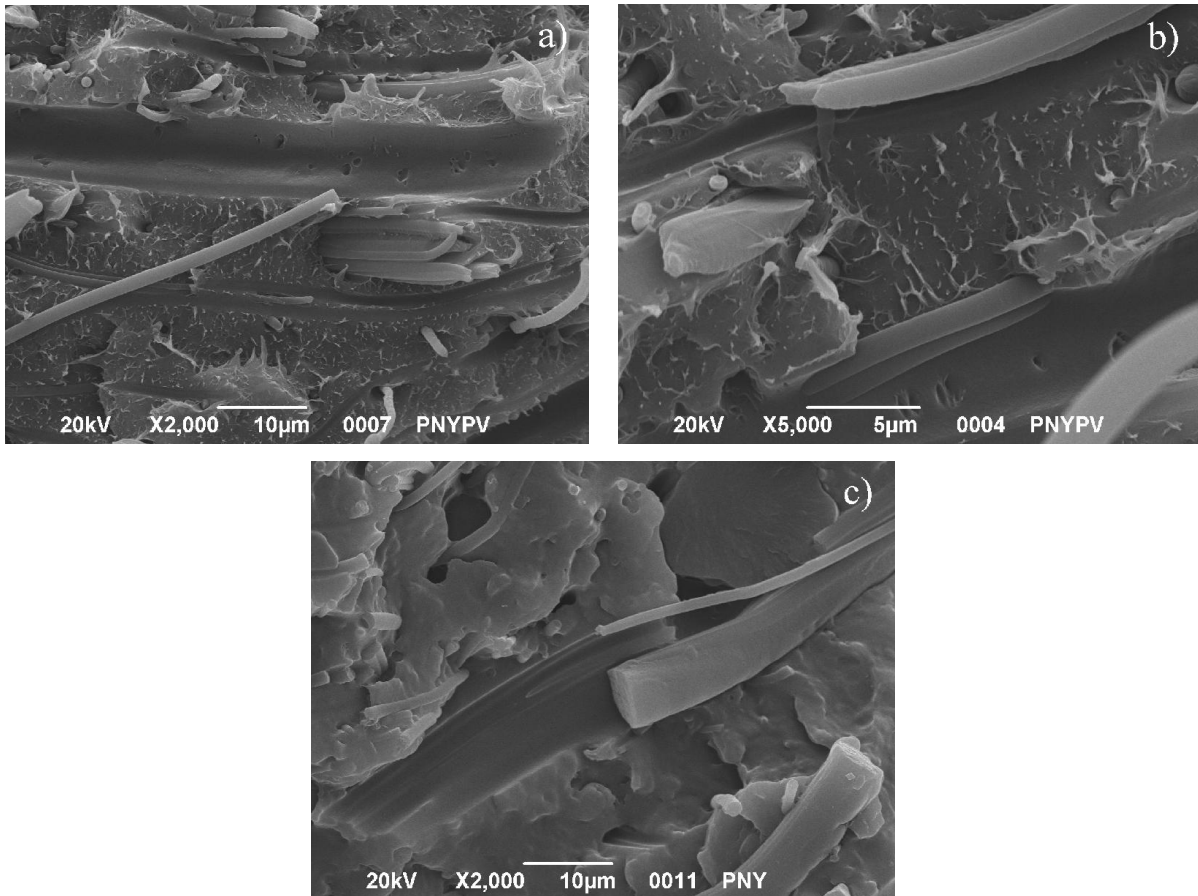


Fig. 4.4.8. SEM micrographs of the cryogenic fracture surfaces of samples PCLNyPvp (a) and (b), and PCLNy (c)

It is interesting to compare the two apparently conflicting behaviors of the composite sample containing PVP fibers and of the one containing both PVP and nylon fibers. Where only PVP fibers were added, biodegradation was virtually unchanged, and also slightly retarded, with respect to the neat matrix, whereas when both nylon and PVP fibers were used, degradation was quicker and more extensive. The semicrystalline morphology of the samples, i.e. the quantity of amorphous material at disposal for degradation is not so different to explain such divergence. The morphology of the fiber/matrix assembly could help in shedding light on this issue. As previously noted, PVP fibers adhere very firmly to the matrix, whereas nylon fibers, both because of their size and chemical nature, are more loosely embedded in the PCL matrix. PVP is a water soluble polymer, which is very easily degradable. It is therefore surprising that sample PCLPvp did not degrade more rapidly than PCL. When a more effective degradation medium was used, i.e. organic compost, the same PCL and PCLPvp samples showed an opposite result: The sample containing PVP degraded more and with a higher rate. This means that, as soon as the PVP fibers come into contact with water, they are

rapidly dissolved and thus leave the composite, decreasing its weight. Compost very suitably exploits the action of microorganisms, which attack the surface of the PCL surface, digging holes [127] that expose the fibers to the action of water. This effect was confirmed by examination of the samples degraded by mechanisms primarily based on hydrolysis, as in gardening soil and phosphate buffer. The mechanism of aliphatic polyester biodegradation is the bio-erosion of the material mainly determined by the surface hydrolysis of the polymer.[129] Fig. 4.4.8 shows a comparison between the fracture surfaces of the samples PCLNy and PCLNyPvp after degradation in buffer. These micrographs show particulars of the debonded surface where large nylon fibers detached from the matrix. As can be seen in Figs. 4.4.4(c), 5(b) and 5(c), thinner PVP fibers tended to wrap around larger nylon fibers. Fig. 4.4.8(a) and b show that, in PCLNyPvp, where large fibers debonded from the matrix, due to their poor interfacial adhesion, the thin fibers are not visible any more, and pores are present, which are ascribable to the dissolution of fine PVP fibers. In addition to a contribution to weight loss, the dissolution of PVP fibers formed channels which could vehicle water inside the composite, favoring a more thorough and rapid degradation of the PCL matrix. As a term of comparison, Fig. 4.4.8(c) shows that no such channels or pores were present in the composite containing just nylon fibers. In other words, PCLNyPvp was the more fastly degrading material because the imperfect adhesion between matrix and nylon fibers allowed the formation of preferential channels through which water could penetrate in the bulk of the material, and dissolve the PVP fibers. When only PVP fibers were present, the matrix/fiber assembly was much more compact (Fig. 4.4.4(a)), so water could reach the fibers only after the surrounding PCL matrix was degraded, significantly slowing the whole process. Armentano and coworkers [129] recently reviewed the effect of nanofillers on the degradation of biodegradable-polymer-based nanocomposites, and highlighted the role of nanofillers in favoring the exchange of water within the composites, thereby increasing the rate of degradation. Another interesting feature was observed during biodegradation studies.

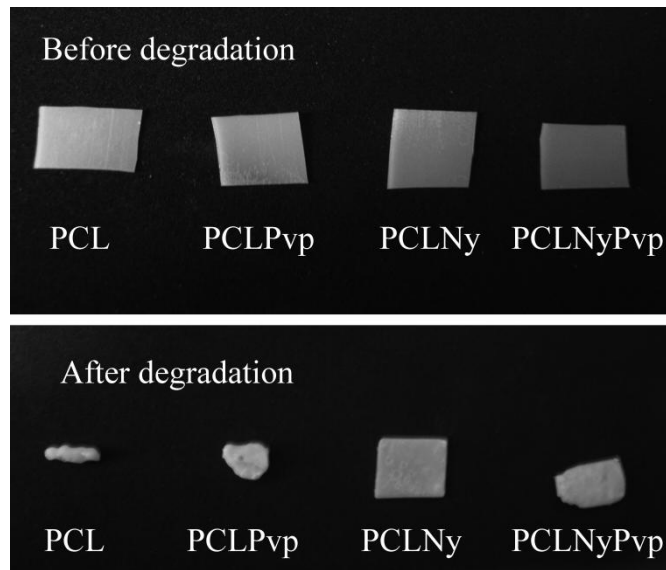


Fig.4.4.9. Pictures before and after degradation in buffer solution of PCL and composites

Fig. 4.4.9 shows the pictures of the samples before and after degradation in buffer. The PCL and PCLPvp samples severely changed their shape, whereas, when nylon fibers were used, the composites displayed an excellent dimensional stability. This is particularly notable in sample PCLNyPvp, in which even after a 20% weight loss due to degradation, the shape was perfectly retained. This is important under an applicative point of view, because it may allow the functionality of the biodegradable product also when the degradation process is quite advanced.

Conclusions

In this paper, electrospun fibers were used as fillers to improve the physical mechanical properties and to modify the biodegradation behavior of PCL-based nanocomposites. Nylon was chosen as the reinforcing material, whereas PVP was selected to tune the biodegradation rate. The characterization of the structure and morphology of such composites showed that fibers have an important role in shaping the semicrystalline framework of the material, especially at a lamellar level. A critical effect of fiber diameter on interfacial adhesion was observed, with thinner fibers adhering more firmly to the matrix, compared to thicker ones. The most interesting results regarded the physical mechanical properties and the biodegradation behavior. Despite being a weaker polymer than PCL, PVP was not detrimental to the tensile properties of the material. On the other hand, nylon fibers proved to be effective reinforcing fillers for the PCL matrix, also in co-presence with PVP fibers. PVP

fibers were, on the other hand, critical in shaping the biodegradation behavior. Water soluble PVP fibers located within the interstices between the matrix and the nylon fibers can be more easily reached by water, which penetrates through the erosion of the PCL surface. This produces hollow channels that allow to vehicle more water in the bulk of the composite, thereby increasing the rate and extent of biodegradation. In addition to producing such favorable morphology, nylon fibers greatly increase the dimensional stability. Even after 20% degradation, the nylon-containing samples retained their shape. These materials were therefore suited for applications in which it is desirable to maintain the functionality of the objects even after a significant advancement of the biodegradation process. In conclusion, in this paper we showed that electrospun fibers of different chemical nature and with different sizes could cooperate in improving the physical mechanical properties of a PCL matrix, at the same time tuning its biodegradation behavior.

Chapter 5

PLA BASED COMPOSITES

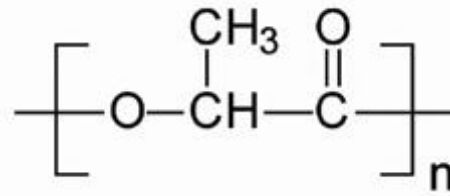
5. Poly (lactic acid) based Composites

Introduction

Modern society produces ever-increasing quantities of waste materials, which are causing environmental concerns. Most of the plastic wastes produced from polymers that are produced from fossil sources, once they are consumed and discarded into the environment, finally end up as un-degradable wastes and therefore contribute greatly to global pollution. Mainly plastic wastes are coming from single-use items like shopping bags and food packaging materials, etc. Increasing environmental awareness and inconsistency in petroleum pricing opened a way to develop eco friendly materials and to replace plastics which are mainly causing environmental problems. Research mainly focused on materials from renewable resources like agricultural products and thus polymeric materials from agro based products are not only gaining interest for environmental concerns and also for political reasons.[130-133]

The development of innovative biopolymer materials has been underway for a number of years, and continues to be an area of interest for many scientists. The most popular and important biodegradable polymers are aliphatic polyesters,[134-142] such as poly(lactic acid) (PLA), poly(glycolic acid) (PGA), poly(3-hydroxybutyrate) (PHB), and poly(ϵ -caprolactone) (PCL), among which PLA has attracted the most attention due to its renewable resources,[134] biodegradation, biocompatibility, superior thermal properties, and the transparency of the processed materials.[135] Therefore, PLA is widely used in medical application such as wound closure, surgical implants,[136] resorbable sutures,[137] tissue culture,[138] and controlled release. In this direction PLA is one of the most promising candidates amongst all bioplastics, because it is produced from renewable resources and readily biodegradable. PLA is linear thermoplastic polyester produced by the ring opening polymerization of lactide. Lactide is a cyclic dimer prepared by the controlled depolymerization of lactic acid, which is obtained from the fermentation of sugar feed stocks, corn, etc. Also, it is easy to process, and has good thermal plasticity and is thus a promising polymer for various end-use applications, also for good replacement for non degradable plastics. There is increasing interest in using PLA for disposable degradable plastic articles; however, there are properties such as flexural properties, gas permeability, impact strength,

etc. that are to be improved for so many end use applications of this polymer.[130,132,143]
The repeating unit of poly (lactic acid) is shown below.



5.1 The effect of different clays on the structure, morphology and degradation behavior of Poly(lactic acid)

Introduction

A wealth of investigations was carried out on PLA, to improve material performance. PLA was blended with some other bio polymers such as starch,[144] or cellulose.[145,146] PLA was copolymerized with some other co-monomers like caprolactone;[147], to improve material properties for many end use applications. PLA was also reinforced with natural fibers like kenaf.[148-150] wood [151] and flax fibers,[131] Clay based nanocomposites were also prepared, introducing clay nanoparticles into the PLA matrix. The most widely used clay is montmorillonite, because of its large cation exchange capacity. However, several kinds of clays, for example montmorillonite modified with several cations (mostly alkyl ammonium cations) were employed for the preparation of PLA nanocomposites in order to improve the material performances for end use applications.[132,152-154] Ogata et.al [152] first prepared blends of PLA and organically modified montmorillonite by solution casting method; several authors since then have prepared PLA/modified montmorillonite using different techniques.[155-157] They found only tactoids, which consisted of several stacked silicate layers, and as a result, the modulus of the composites was slightly higher than that of pure PLA. Bandyopadhyay et.al [153] reported the preparation of intercalated PLA/OMLS (organically modified layered silicates) nanocomposites with much improved mechanical and thermal properties. Hasook et.al [158] found that melt blending 5% organoclay (treated with dimethyl distearyl ammonium ions) with PLA increased the tensile modulus by 20%. Also,

several groups worked on PLA/clay nanocomposites, varying the process parameters.[159-161]

Compatibilisers can be added to improve properties of polymer composites, but have not been used in most studies of PLA nanocomposites to date. Ray et.al [154] reported a study of PLA nanocomposites where up to 3% PCL was added as a compatibiliser. They reported an enhancement of mechanical properties and a change in morphology, attributed to better stacking of silicate layers. Hasook and coworkers [158] reported a similar study of PLA nanocomposites where 5% PCL was added as a compatibiliser. They reported that addition of low molecular weight PCL decreased modulus, increased tensile strength, and did not change degree of dispersion, so they concluded that PCL was not acting as a compatibiliser.

On the other hand, PLA was also reinforced with layered double hydroxides.[162-164] Layered double hydroxides (LDHs), known as anionic clays, consist of a stacking of positive hydroxylated layers $[M_{1-x}^{2+} M_x^{3+} (OH)_2]^{x+}$ separated by interlayer anionic species and water molecules $[A_{x/q}^{q-} \cdot nH_2O]$, where M^{2+} is a divalent metal ion (such as Mg^{2+} , Zn^{2+}), M^{3+} is a trivalent metal ion (such as Al^{3+} , Cr^{3+}), and A is an anion with valency q (such as CO_3^{2-} , Cl^- , NO_3^-). [202 Leroux, F. 2005; } } Because of their highly tunable properties and unique anion exchange properties, LDHs are considered an emerging class of layered materials for the preparation of polymeric nanocomposites.[39,40] Most LDH layers disperse homogeneously in a PLA matrix in the nanometer scale yielding intercalated or exfoliated structures. Incorporation of organically modified LDH brings considerable increase in the crystallization rate of PLA, because of the heterogeneous nucleating effect. With the presence of LDH, the nucleation density increases and the spherulite size reduces. Besides, it was found that the incorporation of LDH has little or no discernable effect on the crystalline structure as well as the melting behavior of PLA. As a consequence, it is considered that LDHs could possibly be a kind of promising fillers for reinforcing the biodegradable polyesters to produce biocompatible nanocomposite materials.[164]

According to authors' knowledge, so far no work was reported in which the performance of cationic and anionic clays on PLA was compared. Moreover, no reports were found in literature discussing the correlation between the effect of these clays on the structure and morphology of PLA and the degradation behavior. This paper compares the effects of

cationic and anionic clays on structure, morphology, crystallization and degradation behavior of PLA with the aim of understanding the relationship between structure and degradation.

Materials

PLA, with D content of 1.1-1.7% was obtained from Unitika Co. Ltd. According to the supplier, it had a weight average molecular weight $\overline{M}_w = 200$ kg/mol, density = 1.25 g/cm³ (ASTM 1238). Two different cationic clays i.e. Dellite HPS (deriving from a naturally occurring especially purified montmorillonite) and Dellite 43B (montmorillonite modified with a quaternary ammonium salt, i.e. dimethylhydrogenated tallow ammonium) were purchased from Laviosa Chimica Mineraria s.p.a., Italy. Perkalite is an organically modified layered double hydroxide (purchased from Akzo Nobel Polymer Chemicals, Netherlands). All materials were dried at 50°C prior to use.

All composites were prepared with 3% of clay (W/W) in melt mixing in a camera mix (Brabender) at 190°C. The obtained lumps were sliced into small pellets and then melt pressed in a hot press at a temperature of 190°C in order to obtain films for further analysis. To obtain a crystalline material, all samples were annealed at 100°C for 4 hours. Only annealed samples were used for all further analysis. Filler level was kept constant in all cases, because it is reported that filler level above 5% is resulting in reduction of mechanical properties.[159,165] The samples were coded with type of clay used for the preparation of PLA nanocomposites. For example, the composite prepared with perkalite, has been given the code PLA-PERK.

The kinetics of crystallization was studied by subjecting each sample to the following thermal cycle: after erasure of previous thermal history by keeping the polymer at 200°C for 5 min, it was cooled at the maximum rate to the crystallization temperature (T_c). The heat evolved during the transition was monitored as a function of time during an isothermal at T_c of suitable length. The fraction X of material crystallized after the time t was estimated from the relation:

$$X = \int_0^t \left(\frac{dH}{dt} \right) dt / \int_0^\infty \left(\frac{dH}{dt} \right) dt$$

Where the numerator is the heat generated at time t and the denominator is the total heat of crystallization. The Avrami equation [166] was used to correlate X with time:

$$X = 1 - \exp[-K(t - t_0)^n]$$

K is the kinetic constant of crystallization, n is a coefficient linked to the time dependence and the dimensions of growth of crystallites.

For TEM, 80 nm ultra-thin sections were prepared by an ultramicrotome (Ultracut E, Reichert-Jung) with a 35° Diamond knife (Diatome, Switzerland) at room temperature. TEM pictures were obtained by a TEM LEO 912 (Zeiss, Germany) at an accelerating voltage of 120 kV. The PLA samples are very unstable in the TEM. That means they move themselves and cavitation occurs by the use of the electron beam. These cavities expand and the section is destroyed. Therefore a very low current was used, which was smaller than 1 μA .

Degradation studies were performed on all prepared samples in phosphate buffer solution (PBS) at pH 7.4. Samples were taken out from the media at different time intervals, washed thoroughly with distilled water and dried at room temperature for 24 hours, weighed and returned to the media.

Results and discussions

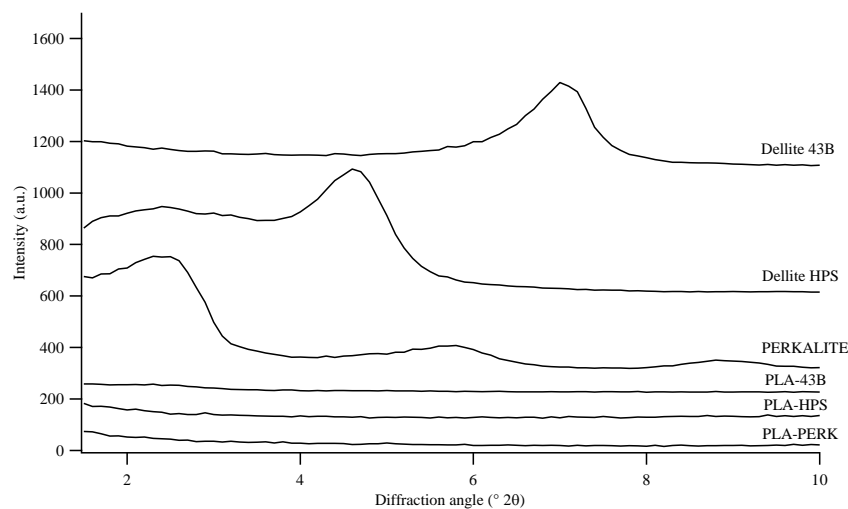


Fig.5.1.1. WAXD diffractograms for different clays and composites at lower angles

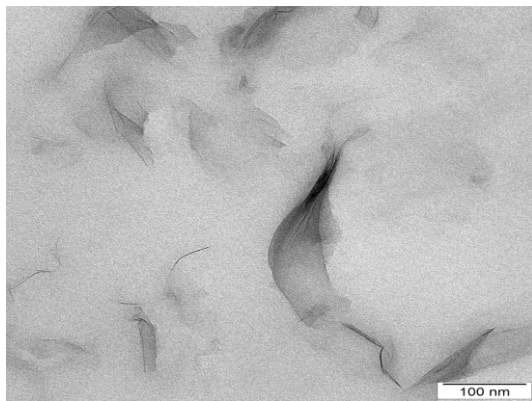
The dispersion of clay in the prepared composites was analyzed by WAXD. Peaks related to the pristine clays and of dispersed clay particles in the matrix polymer are shown in [Figure.5.1.1](#). Basal peaks were recognized at $2\theta \sim 2.3^\circ$, 4.6° and 7° for pristine perkalite, dellite HPS and dellite 43B respectively. These basal peaks disappeared when clays were mixed within the PLA matrix; this indicates that they have attained a very good dispersion in the composite. It is often reported in the literature that when the basal signal disappears, this is a sign that exfoliation occurred. Considerable attention should be exercised in taking this conclusion, though, because WAXD alone is not sufficient to prove exfoliation.[167-170]

In order to correctly assess the degree of interaction between polymer and clay, WAXD and SAXS must be used complementarily. Extensive intercalation could in fact separate clay layers to such an extent to be undetectable by WAXD but that can still be determined by SAXS.[171]

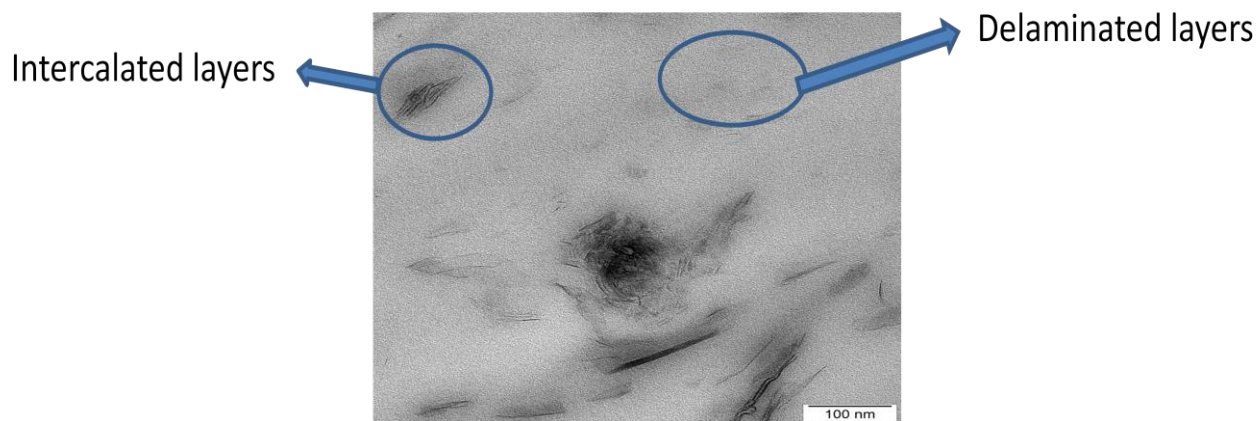
Only the disappearance of SAXS signals and Transmission Electron Microscopy (TEM) observations can confirm that exfoliation has occurred. Moreover a number of possible factors, such as the small sample size, when very low clay loadings are used, or orientation issues, could determine the disappearance or at least a dramatical weakening of the basal signal that could be misinterpreted as exfoliation.

Very interesting comparisons of WAXD and TEM data showed moreover that the WAXD signal can disappear even if some intercalation is present. The lack of Bragg scattering can suggest that a wide range of basal layer spacings is present within the tactoids. This variation in persistence lengths (which correspond to regions that have a constant value in the d -spacing) can result from a number of different reasons: incomplete exchange of the cations present in the pristine clay galleries with the organomodifier, uneven polymer intercalation, single clay layers organized in tactoids with large interlayer spacing and not regularly ordered, variable composition within a tactoid which affects clay surface charge, and small tactoid effects.[171] This latter situation, i.e. reduction of the size of tactoids to just two or three layers,[172] can be considered practically equivalent, as far as properties are concerned, to exfoliation.[173-176] SAXS traces in the periodicity region typical of clay were featureless, corroborating the WAXD observation that a significant disordering of clay tactoids was achieved in the composites.

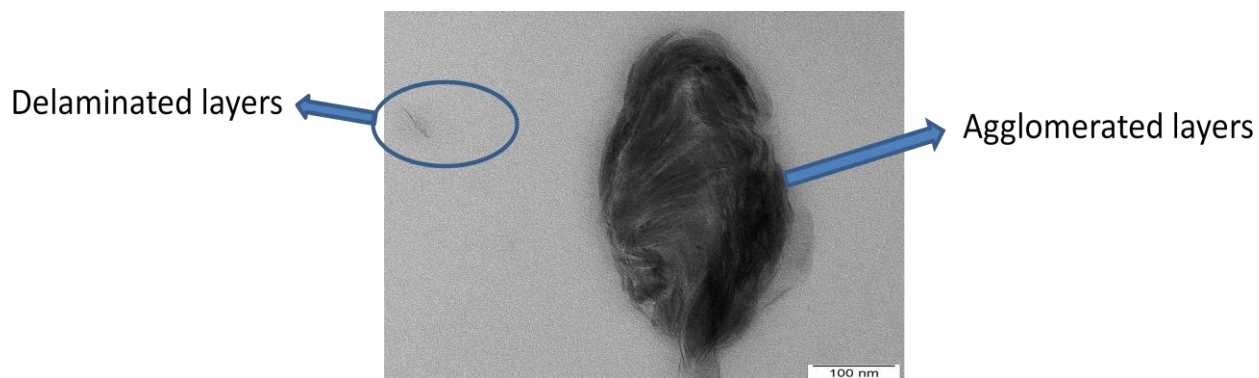
We performed TEM analysis in order to confirm the degree of dispersion of clay in our prepared composites. [Figure 5.1.2](#), shows TEM micrographs of the composites prepared using different clays.



(a)



(b)



(c)

Fig.5.1.2. TEM images of PLA43B (a); PLAPERK (b); and PLAHPS (c)

It is evident from TEM micrographs that all the nanocomposites prepared show the presence of delaminated clay layers, in accord with the very weak basal signals. We also observed, though, intercalated and agglomerated structures along with some delaminated structures, especially in PLAPERK (fig.5.1.2(b)) and PLA HPS (fig.5.1.2(c)). Hence, the absence of peaks in WAXD is not the confirmation of exfoliation or complete delamination of clay layers.

Delamination could be due to high shear stress, i.e. 100 rpm, in the preparation procedure. In a study, Bourbigot et.al [177] reported optimum conditions to achieve exfoliated structures as high shear stress, i.e. 100 rpm for 1 min at 185°C.

The WAXD patterns of the samples are those typically found for PLA (fig.5.1.3).[164,178] Macroscopically no effect of any clay was observed on the structure of matrix polymer. WAXD traces were fitted to calculate the degree of crystallinity (Φ_{WAXD}) by deconvoluting the contribution of the crystalline and amorphous domains to the diffraction pattern and corresponding results are reported in Table5.1.1. In all compositions, addition of clays brought about an increase in Φ_{WAXD} , especially in the case of the composite with perkalite.

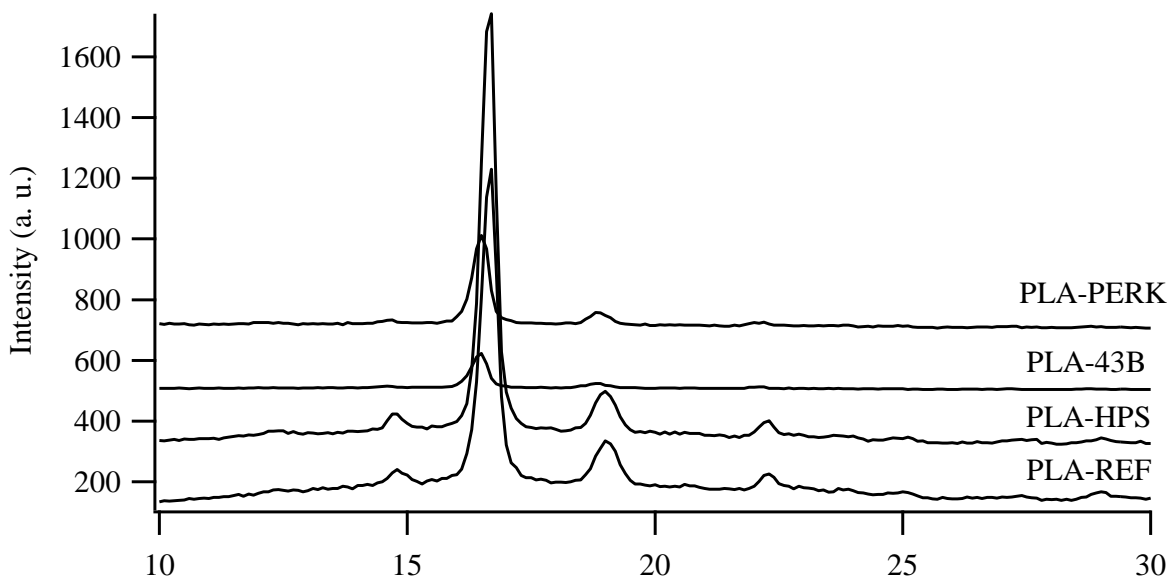


Fig.5.1.3. WAXD diffractograms of PLA and of its composites at higher angles

Table 5.1.1: Degree of crystallinity of all prepared samples measured by fitting WAXD traces

sample	Degree of crystallinity (Φ_{WAXD}) (%)
PLAREFB	54
PLAHPS	72
PLA43B	79
PLAPERK	84

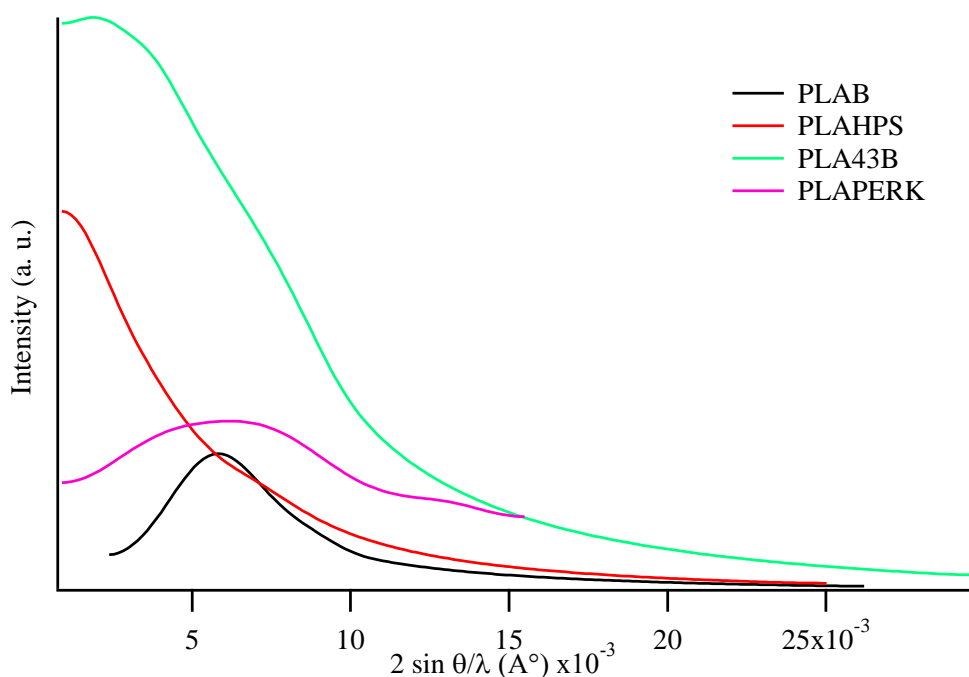


Fig.5.1.3. Lorentzian SAXS patterns of pure PLA matrix polymer and of its composites

The morphology of the polymer at lamellar level was studied by SAXS. Resulting SAXS patterns are reported in [Figure 5.1.4](#). In the pure matrix polymer, a sharp peak appeared, indicative of very well ordered crystalline lamellae. In the composites, on the other hand, the SAXS peaks were much less neat. The composite with perkalite retained the same long period of neat PLA, but with a significant broadening of the SAXS signal. This indicates that lamellar stacks are less homogeneous in size and morphology.[179] In the case of the materials with cationic clays, the SAXS signal disappears. SAXS data are coherent with a disruption of the order of the lamellar stacks due to a very intimate contact between matrix and filler. This is maybe because clay particles are dispersed thoroughly in the matrix polymer with delaminated structures due to high shear stress, and thus they function like obstacles for the free motion of polymer chains when crystalline lamellae were forming. This is not surprising because it is reported that nanofillers influence the shaping of the structure at

a crystalline cell level, but it has its most significant effects on polymer lamellae.[97-102,124]

Table 5.1.2: Isothermal crystallization kinetic studies at different temperatures

Sample	at 100°C		at 110°C		at 120°C	
	n	ln (k)	n	ln (k)	n	ln (k)
PLAREFB	1.9	-6.1	1.9	-6.0	1.7	-2.4
PLAHPS	1.9	-4.7	1.9	-4.2	1.7	-3.8
PLA43B	1.7	-4.2	1.6	-3.9	1.6	-3.2
PLAPERK	2.8	-3.4	2.0	-2.3	1.7	-4.4

As we mentioned before, no literature was found to compare the effect of clays on the degree of crystallinity of PLA. However, structural and morphological data are consistent with an effect of clay on the crystallization rate.

In order to better understand the influence of the different clays on the crystallization behavior of PLA, the crystallization kinetics was studied. Isothermal measurements at three different T_c (100, 110 and 120°C) were performed to establish the nucleating effect of clays on PLA matrix, and the obtained results were interpreted according to the Avrami equation.[166] Such data treatment allows to obtain two parameters describing the crystallization kinetics: $\ln K$, which is a kinetic constant, and n , which is a parameter related to the mechanism of nucleation and to the dimensionality of growth in the crystallization. It has been already reported that clay particles increase the crystallization rate and thus increase the number of spherulites formed in nanocomposites compared to pure PLA matrix.[132,180-183] Day et.al [181] reported that when the materials were crystallized in the temperature range 120–130°C the crystallization rate for the composite material was approximately 15 to 20 times faster than that for the neat PLA. In our study, we observed multiple effects of clays on the crystallization behavior of PLA. One is at low temperatures at 100 and 110°C, K is larger in composites compared to neat PLA, meaning that clays are showing nucleating effect on PLA matrix. On the other hand, when materials were studied at 120°C, neat PLA had larger K values than composites. This is not surprising because sometimes clays act as inhibiting agents rather acting as nucleating agents. In a work by our group,[127] Cloisite 15A had shown inhibiting effect on PCL rather than acting as nucleating agent as it has been reported. For what concerns the crystallization mechanism, n remained approximately

constant in all samples (~1.9) except in PLAPERK at 100°C, when it increased to 2.8. This indicates that no significant changes in the crystallization mechanism were brought about by clay except with perkalite. It is especially interesting to note the crystallization behavior of the samples at 100°C, which is the temperature at which they were annealed in the present work. K increases in the same order as Φ_{WAXD} , i.e. perkalite has the largest crystallinity and the fastest crystallization; on the contrary neat PLA is the least crystalline sample and crystallizes slowly. Moreover, a sharp difference in crystallization mechanism could be seen between composites, with cationic clays which have the same n of PLA, and that of PLA-PERK, in which the change in n is indicative of a change in crystallization mechanism. This difference in crystallization mechanism is reflected by SAXS data: PLA-PERK maintains a rather ordered lamellar morphology, whereas PLA-HPS and PLA-43B displayed a dramatic disordering of the lamellar stacks, which brought to featureless SAXS traces.

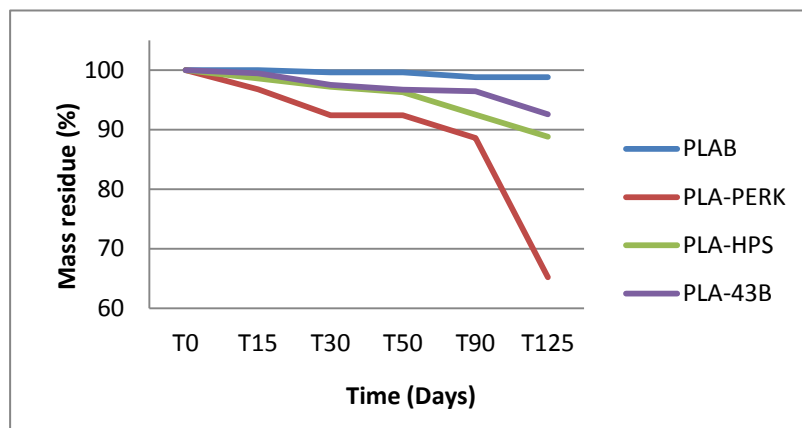


Fig.5.1.5. % of weight loss of pure PLA matrix and of its composites in PBS solution

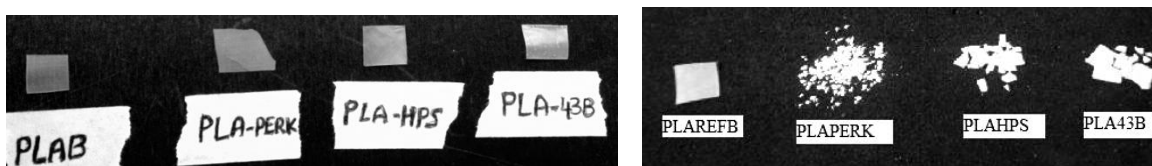


Fig.5.1.6. (a) before degradation studies (b) after degradation studies

Studies were performed to investigate the effect of clay on the rate of degradation (Figs. 5.1.5 and 5.1.6). Figure 5.1.6 shows the results after 125 days in PBS, PLA showed a negligible weight loss. On the other hand, the composites with cationic clays lost about 10% of their initial weight, whereas almost 40% of sample PLA-PERK degraded after 125 days in PBS. Differently from cationic clays, perkalite initiates degradation early in the first days of

exposure to PBS. The composites containing Dellites started losing mass after 15 days. This is somewhat an unexpected result. Hydrolytic degradation preferentially attacks the amorphous regions of the sample. PLA-PERK, the fastest-degrading sample, is also the most crystalline one, and the one showing the best dispersion of the filler. Such behavior is probably linked to the chemical nature of perkalite, which may allow a better interaction with the incoming water. Moreover, the better dispersion of the filler layers within the matrix increases the barrier effect,[132] so slowing down the penetration of water in the material. This allows a longer contact time between polymer and water, thus favoring the hydrolysis reaction. S. S. Ray et.al [160] reported the rate of degradation of neat PLA and of its composites with montmorillonite in compost environment. They reported that addition of clay to PLA promoted the rate of degradation in compost and it took only two months of time for complete degradation of the composite in compost. In our study, however, PLA and its composites are degrading more slowly, meaning that the degradation rate of PLA is slower in PBS media.

Conclusions

The structure, morphology and degradation behavior of PLA-based composites filled with different kinds of clay were compared. Even though a similar degree of dispersion could be achieved in cationic and anionic clays, these two kinds of fillers exerted different effects on the structure and morphology. The anionic perkalite clay induced higher crystallinity, a faster crystallization rate and also a modification of the crystallization mechanism. Moreover, when perkalite clay was used, the lamellar framework of PLA was preserved. These differences were reflected in the degradation behavior of the materials. This shows the potential of the addition of nanofillers for tuning the degradation rate of PLA, in order to widen the application range of this promising polymer.

5.2. Electrospun nylon fibers for the improvement of mechanical properties and for the control of biodegradation rate of poly (lactide)-based composites

Nylon fibers have been extensively employed as reinforcement of several polymer matrices, most notably poly (methyl methacrylate) (PMMA),[184] poly(ethylene terephthalate) (PET),[185] poly(carbonate) (PC)[186] and rubber.[187,188]

Recent literature reports showed the potential in property improvement of electrospun nylon fibers especially in poly(aniline) (PAN),[189] PMMA,[190] poly(caprolactone)[126,191] and dental resins.[60,61] In paragraph 4.3., PCL composites filled with electrospun nylon 6 (N6) fibers were prepared by a melt processing technique.[126,191] With very low filler content (3%) a simultaneous increase in strength, stiffness and ductility was observed, which is unusual in nanocomposites containing other types of fillers, where the increase in modulus normally happens at the expenses of elongation at break.[126] Such potential was corroborated also by other authors. Recently, Mallon and coworkers reported that electrospun fibers of polyacrylonitrile-graft-poly(dimethyl siloxane) were able to confer to a cross-linked poly(dimethyl siloxane) matrix not only strength and stiffness, but also a remarkable extensibility.[192] Moreover, electrospun fibers could modify the degradation rate of PCL.[191]

According to the authors' knowledge, PLA was never reinforced with any kind of electrospun fibers. In this work, we filled PLA with electrospun N6 fibers in order to study the effect of fibers on the structure, morphology, mechanical properties and biodegradation behavior.

Tensile mechanical properties of rectangular-shaped samples (30 mm × 10 mm × 0.5 mm) were measured using an Instron model 3345 mechanical tester at room temperature and 50% humidity. The strain rate was 5 mm. min⁻¹. At least five measurements were performed for each sample.

Degradation studies of the samples were performed in two different media. Firstly, the materials were exposed to phosphate buffer solution (PBS) at pH 7.4 for 4 months. Since in this medium no significant degradation was observed, the samples were moved into a NaOH (0.1 M) solution. Such degradation tests were carried out at 65°C. Samples were taken out from the media at regular time intervals, washed thoroughly with distilled water and dried at

room temperature for 24 h, weighed and returned to the media. Two specimens for each sample were tested in parallel to check the reproducibility of the procedure.

Experimental

PLA, with D content of 1.1-1.7% was obtained from Unitika Co. Ltd. According to the supplier, it had a weight average molecular weight $\overline{M}_w = 200$ kg/mol, density = 1.25 g/cm³ (ASTM 1238).

Ny electrospun fibers were used as fillers. Electrospinning was carried out on a 22 wt% (viscosity, 1320 cps) Ny solution in formic acid/acetic acid (80/20, wt/wt) with an applied voltage of 22 kV and tip to collector distance of 12 cm. All fibers were dried prior to use in vacuum oven at 100°C to remove adsorbed moisture and residual solvent. The characterization of the electrospun mat was done after this drying stage.

Two types of composites with different amounts of filler content were prepared as in our previous work.[126,191] The first composite, i.e. PLANY1.5, was prepared by keeping the N6 fiber mat between two PLA films, and applying pressure and heat in a press (Alfredo Carrea, Genova, Italy) at 180°C, PLA was melted and percolated between the voids in the mat, constituting a continuous phase in which the fibers were dispersed. The second composite, PLANY2.5, was prepared by keeping two Ny fiber mats alternated by PLA films. [Table 5.2.1](#) shows the sample codes and the wt% of filler content in the composites.

Table 5.2.1: Formulation and codes of the samples

Sample	Fiber content (%) W/W
PLAREF	0
PLANY1.5	1.5 ± 0.1
PLANY2.5	2.5 ± 0.1

All prepared samples were annealed in an oven at 100°C for four hours, because they were amorphous (confirmed by WAXD and DSC) right after treatment in the press.

The kinetics of crystallization was studied by subjecting each sample to the following thermal cycle: after erasure of previous thermal history by keeping the polymer at 200°C for 5 min, it was cooled at the maximum rate to the crystallization temperature (T_c). The heat evolved during the transition was monitored as a function of time during an isothermal at T_c of suitable length. The fraction X of material crystallized after the time t was estimated from the relation:

$$X = \int_0^t \left(\frac{dH}{dt} \right) dt / \int_0^\infty \left(\frac{dH}{dt} \right) dt$$

Where the numerator is the heat generated at time t and the denominator is the total heat of crystallization. The Avrami equation [166] was used to correlate X with time:

$$X = 1 - \exp[-K(t - t_0)^n]$$

K is the kinetic constant of crystallization, n is a coefficient linked to the time dependence and the dimensions of growth of crystallites.

This equation is linearized in the following way:

$$\ln[-\ln(1-X)] = \ln K + n \ln(t-t_0)$$

Plotting $\ln[-\ln(1-X)]$ vs. $\ln(t-t_0)$, and fitting with a straight line, n and K can be obtained by the slope and the intercept of the obtained line.

The crystallization behavior of the samples was studied with a Leica DM400M polarized light microscope. The samples were placed between a glass slide and a cover slip and were kept at 180°C for 10 min, to ensure uniform melting and to delete their thermal history. The slide was then transferred to a Mettler FP82HT hot stage set at 100°C. The photomicrographs were taken between cross-polarizers with a Leica DFC280 digital camera. In order to suitably compare the behavior of different samples, photomicrographs were taken for all samples after 20 minutes of isothermal crystallization.

Results and discussion

Figure 5.2.1 shows a SEM micrograph of the electrospun Ny fibers used in this work. The average diameter of these electrospun fibers was evaluated performing image analysis on

several micrographs, for a total of about 100 fibers, and was found to be 800 nm. [Figure 5.2.1](#) also shows in an inset the size distribution for the diameters of the fibers. These diameters are about one order of magnitude smaller (i.e., their specific surface areas are more than 10-times larger) than ordinarily spun fibers. A notable feature is the quite broad distribution of fiber size, with thin fibers coexisting with very large fibers, up to 3 μm in diameter. The quality of the fibers was good, with a smooth surface and no trace of beads.

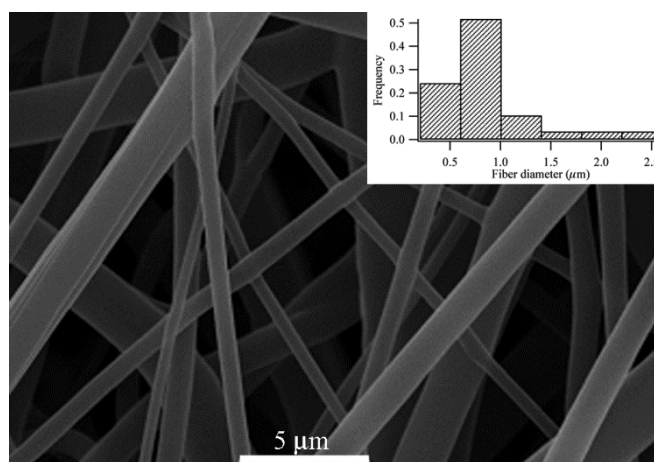


Fig.5.2.1. SEM micrograph of the nylon fiber mat. The inset shows the distribution of fiber diameters

As better detailed in the experimental section and in previous papers by our group,[126,191] inclusion of the fibers in a continuous PLA matrix was done by percolating, in a compression molding press, molten PLA within the interstices of the fibrous mat. The electrospun fiber mat included in the matrix was non woven. The preparation of the composites was done at 180°C which is a temperature high enough to melt PLA ($T_m = 150^\circ\text{C}$) but much lower than the melting point of the Ny fibers ($T_m > 210^\circ\text{C}$). It was therefore possible to preserve the network of the electrospun fibers, while at the same time creating a homogeneous PLA polymeric matrix. The effect of fibers on the structure and morphology of the composites was studied by WAXD. [Figure 5.2.2](#) shows the WAXD diffractograms of PLA and of its composites PLANY1.5 and PLANY2.5. In all compositions, a major crystalline peak at $2\theta \sim 16.6^\circ$, related to the α -phase (110) plane, was observed without the appearance of any crystalline peaks related to nylon. [Table 5.2.2](#) shows the degree of crystallinity evaluated by WAXD (Φ_{WAXD}) of concerned samples. A small increase in the Φ_{WAXD} was observed in the composites, but fibers are not showing much effect on Φ_{WAXD} .

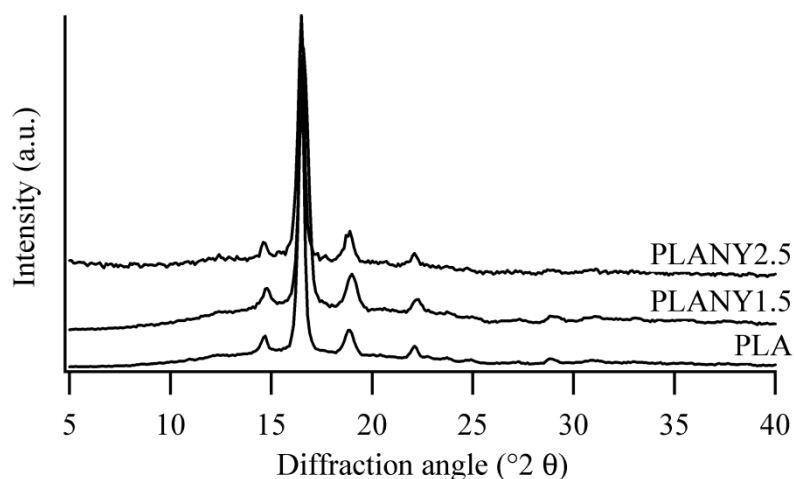


Fig.5.2.2. WAXD diffractograms of PLA, and of its composites with different amount of filler content

Table 5.2.2: Degree of crystallinity obtained by WAXD (Φ_{WAXD}) and morphological parameters of the lamellar stacks obtained by SAXS analysis of considered samples. The thickness of the crystalline (C) and amorphous layer (A), the long period (D), and the crystallinity (Φ_{SAXS}). $\sigma_{\text{C/C}}$, $\sigma_{\text{A/A}}$, $\sigma_{\text{D/D}}$ and $\sigma_{\Phi}/\Phi_{\text{SAXS}}$ are the distributions of the aforementioned parameters and can be interpreted as the relative deviation from the average of the values of such features

Sample	C (Å)	A (Å)	D (Å)	Φ_{WAXD} (%)	Φ_{SAXS} (%)	$\sigma_{\text{C/C}}$	$\sigma_{\text{A/A}}$	$\sigma_{\text{D/D}}$	$\sigma_{\Phi}/\Phi_{\text{SAXS}}$
PLAREF	109	53	162	63	67	0.3	0.3	0.2	0.1
PLANY1.5	164	54	218	67	75	0.1	0.1	0.1	0.2
PLANY2.5	127	42	169	66	75	0.1	0.1	0.1	0.1

The lamellar morphology of all prepared samples was studied using SAXS. [Figure 5.2.3](#) shows the experimental traces due to the matrix and to the samples with electrospun fibers. The experimental traces due to the matrix and to the samples with electrospun fibers were fitted according to a method [113,114,193] which was shown [115] to reliably determine the thicknesses and distributions of the crystalline and amorphous layers, the long period and the crystallinity, along with their distribution, associated to lamellar stacks. The fitted traces are

shown in Figure 5.2.3, and the morphological features obtained by this procedure are summarized in Table 5.2.2.

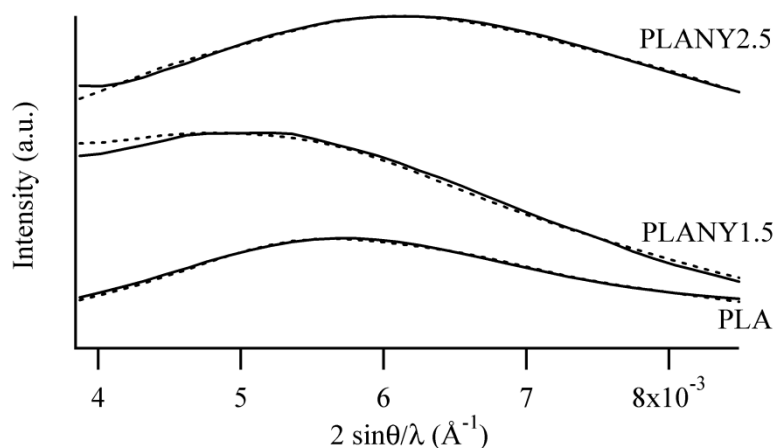


Fig.5.2.3. SAXS patterns (solid line) of the considered samples, traces calculated during the fitting procedure (dotted line) are also shown

The long period of the SAXS peak of the composite with the lowest filler content, i.e. PLANY1.5, was larger than that of the matrix, whereas when the amount of fibers increased, the SAXS peak shifted towards wider angles. In all composites, the thickness of the lamellae was increased with respect to the neat matrix, although the maximum thickness was achieved in sample PLANY1.5. The thickness of lamellae slightly decreased in PLANY2.5, with respect to sample PLANY1.5. Interestingly, also the thickness of the amorphous layer decreased going from PLANY1.5 to PLANY2.5, so the overall effect was that the crystallinity associated to the lamellar stacks of the composites was constant irrespectively of the fiber content. It is noteworthy that Φ_{SAXS} was significantly higher in the composites than in the neat matrix. The increase in crystallinity noted by WAXD is confirmed by SAXS, but the effect is magnified when the focus is posed on the characterization of the lamellar morphology. It has already been highlighted that the nanofiller often negligibly influences the structure at a crystalline cell level, but it has its most significant effects on polymer lamellae.[97,100-102,124]

This apparently conflicting behavior, i.e. that the presence of fibers increases the lamellar thickness, which on the other hand starts to decrease beyond a certain filler content can be

explained in analogy to other systems, such as composites filled by montmorillonite,[116,194-196] graphite[197] or CNTs.[198] Fibers have a double role in influencing the semicrystalline framework of the polymeric matrix. The presence of fibers has on one hand a nucleation effect, bringing about an increase of crystallization degree.[126,191,198] This was confirmed by DSC, as will be detailed later in this section. On the other hand, as previously observed for other nanofillers, for example CNTs or electrospun fibers, increasing the filler content, and therefore its surface area, some hindering effect on the free motion of macromolecular chains appear, leading to difficulties in attaining thick lamellae, as observed also in this work.[102,124,126,182,198-200]

In [Table 5.2.2](#), it can be seen that the crystallinities assessed by SAXS had larger values relative to those estimated by WAXD. This divergence can be explained considering the difference between the two techniques. SAXS is only sensitive to the crystalline regions organized in lamellar stacks, whereas WAXD allows the detection of all the regions contributing to the semicrystalline framework, including the amorphous phase located between the lamellar stacks. Therefore WAXD crystallinity was lower because the contribution of crystalline domains was “diluted” by the interstack amorphous. It can be seen that the difference between Φ_{WAXD} and Φ_{SAXS} increased passing from the matrix to the composites. This means that in the composites the quantity of interstack amorphous material is increased, and that much of the non-crystalline material is segregated outside the lamellar stacks.

Fillers such as talc, montmorillonite, carbon black or hydroxyapatite were shown to accelerate the crystallization rate of PLA.[182,201,202] Fibers have the same effect on the crystallization behavior of PLA, as noted for kenaf fibers and rice straw,[203] and for CNTs.[204] DSC was used to assess the nucleating ability of electrospun fibers. Isothermal crystallization was performed in the DSC instrument at $T_c = 110^\circ\text{C}$, observing a crystallization exothermal curve. Such pattern was linearized as better detailed in the experimental section,[166] and by fitting of the lines yielded by the experimental data (data shown in the Supporting Information) two parameters were obtained, which describe the crystallization kinetics: $\ln K$, which is a kinetic constant, and n , which is a parameter related to the mechanism of nucleation and to the dimensionality of growth in the crystallization.[166] The kinetic constant K was larger for the composites ($\ln K = -3.4$ and -3.3 for PLANY1.5 and PLANY2.5, respectively) than for the matrix ($\ln K = -3.8$). This implies that fibers have a nucleating effect, which was also confirmed by polarized light optical microscopy (PLOM).

Figure 5.2.4 compares pictures taken after 20 minutes of isothermal crystallization at 100°C for the neat matrix and for sample PLANY1.5. As can be seen, a larger number of spherulites appeared in the fiber-containing material, and the crystallization process is much closer to completion in the composite, rather than in the matrix.

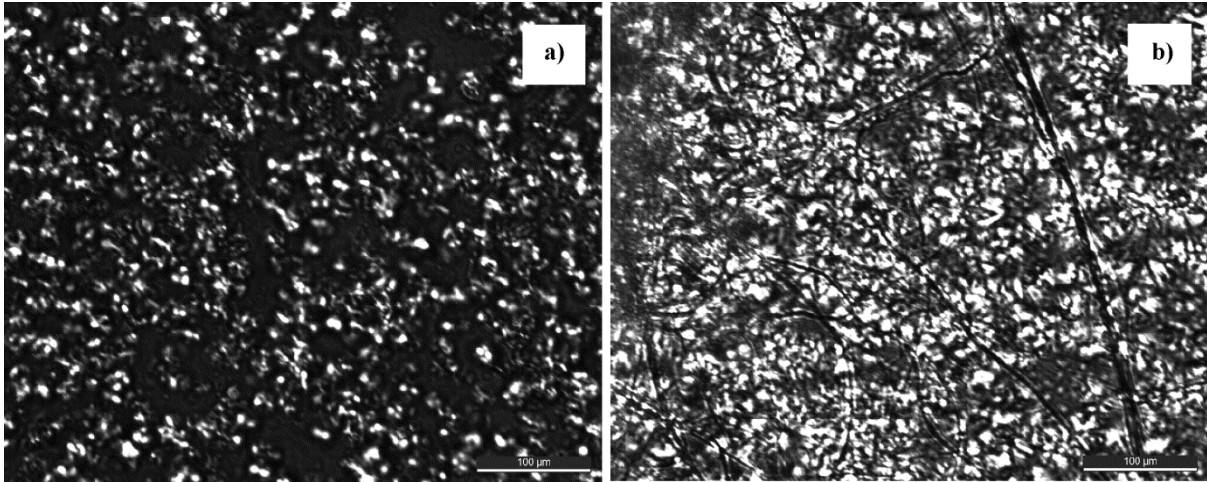


Fig.5.2.4. Polarized light optical micrographs of the spherulitic texture obtained after 20 minutes of isothermal crystallization at 100°C for a) the neat matrix and for b) sample PLANY1.5

In Figure 5.2.4(b) it can be seen that the spherulites are preferentially concentrated around the fibers. This corroborates DSC data in evidencing a nucleating ability by electrospun fibers, which was previously observed also in the case of poly(caprolactone) matrices.[126] The Avrami parameter n remained constant at 1.6 in all samples, indicating that no significant changes in the mechanism of crystallization are observed by the addition of filler. This is somewhat different from what previously observed for other nanofillers, which often induced a modification of the crystallization mechanism.[182,205]

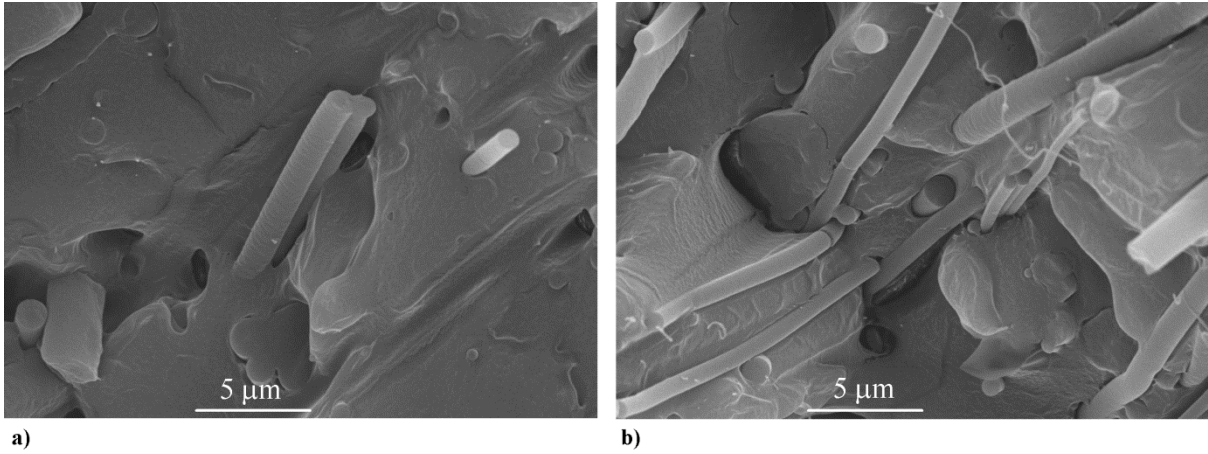


Fig.5.2.5. SEM micrographs of PLANY1.5 in a region where fibers are preferentially positioned a) perpendicular and b) parallel to the fracture surface

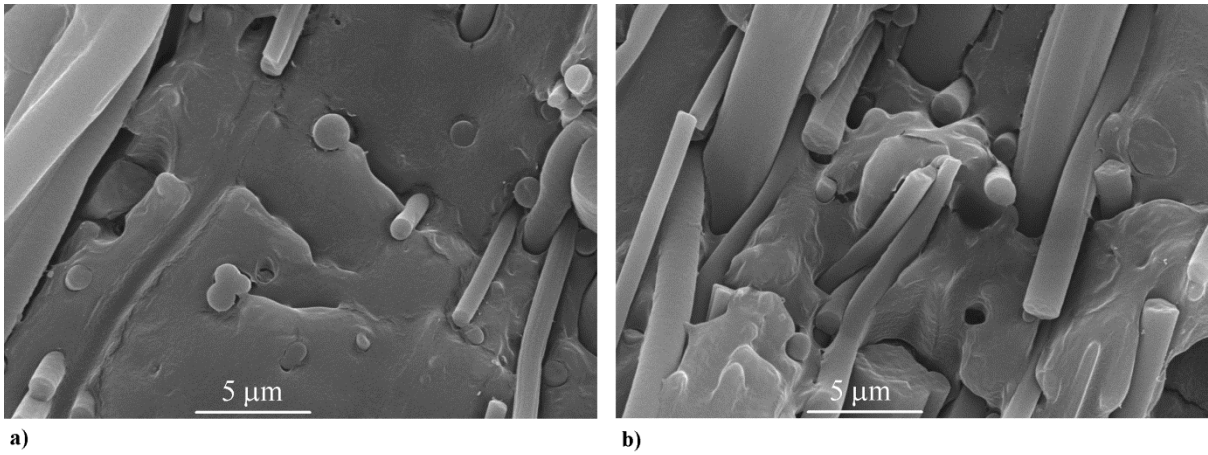


Fig.5.2.5. SEM micrographs of PLANY2.5 in a region where fibers are preferentially positioned a) perpendicular and b) parallel to the fracture surface

The adhesion between the matrix and the electrospun fibers was studied by observing the fractured surface of the samples using SEM. [Figures 5.2.5 and 5.2.6](#) show that PLA and nylon fibers had a good compatibility with each other, resulting in well embedded composite systems. Compared to composites of natural fibers and PLA,[206-208] in this case a much better adhesion was attained. Especially when fibers were disposed perpendicularly to the fracture surface, the sections of fractured fibers were perfectly embedded within the PLA matrix. The entity of adhesion decreased in the regions of the composites where many fibers are oriented tangentially to the fracture surface ([Figs 5.2.5\(b\) and 5.2.6\(b\)](#)). Also in such

zones of the sample, though, the fibers remained firmly rooted within the matrix, without the appearance of large craters or of debonded sites. The morphology of the composites studied in this work, especially of PLANY1.5, was somewhat different to the one previously observed in the case of PCL/nylon composites, where larger diameter fibers showed a poor interfacial adhesion, and bundles protruded from craters in the matrix.[126] Interestingly, in the composites studied in this work, all the fibers displayed the same optimal adhesion, irrespective of their diameter. On the contrary, in the case of PCL/nylon composites the finest filaments were firmly embedded in the matrix, their exposed end protruding directly from within the matrix, without the presence of craters at their base due to debonding, which was the case in the largest-diameter fibers. Increasing the filler content, such as in the case of PLANY2.5, the morphology became more similar to the one previously observed in PCL/nylon composites, although also in PLANY2.5 adhesion is globally considered very good. The quality of adhesion was also investigated by infrared spectroscopy. [Figure5.2.7](#) shows a comparison of the IR spectra of samples PLAREF, PLANY1.5, PLANY2.5, and of the electrospun nylon mat. Particular attention was posed to the signals at 3300 cm^{-1} (N-H stretching of nylon), at 1640 cm^{-1} (C=O stretching of nylon) and at 1540 cm^{-1} (N-H bending of nylon). The position and shape of such peaks are a function of the type and extent of hydrogen bonding which nylon molecules form. As may be seen, in the composites the signals due to the N-H bond of nylon, i.e. the stretching band at 3300 cm^{-1} and the bending peak at 1540 cm^{-1} are broadened and weakened so much that they disappear. On the other hand, the C=O stretching band moves from 1640 cm^{-1} in the neat fibers to 1647 cm^{-1} in the composites, indicating that the chemical environment of the amide groups of nylon are significantly modified by the interaction with the PLA matrix.

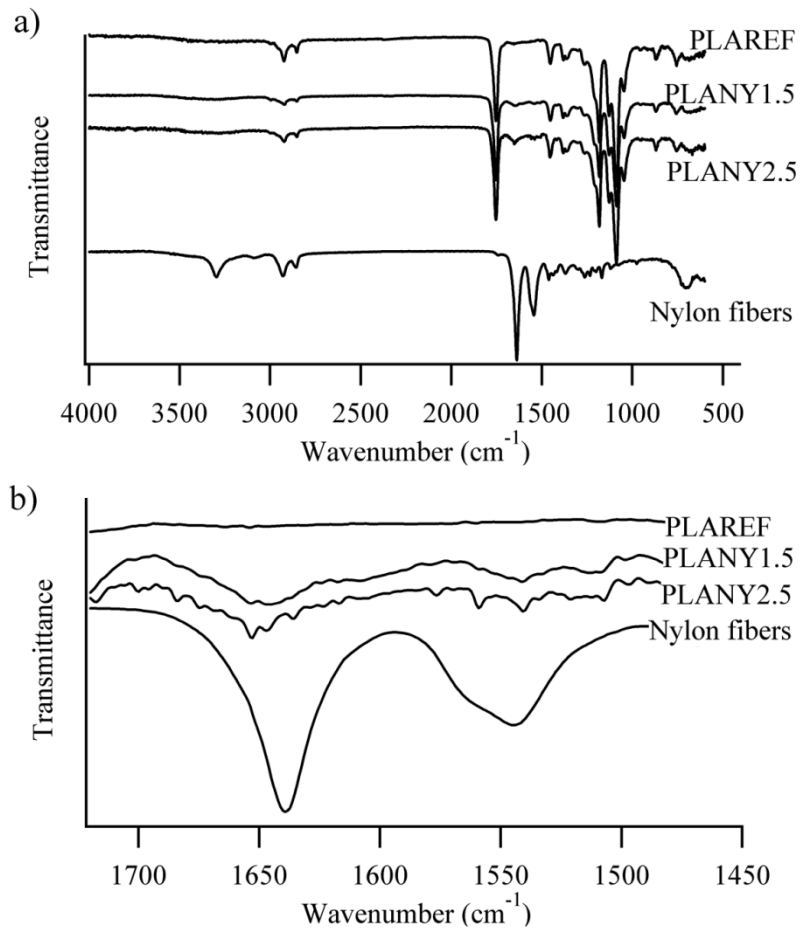


Fig.5.2.7. IR spectra of the reference matrix, of the composites and of the neat nylon fibers. Part a) shows the entire spectrum, part b) shows an enlargement of the spectral region where the C=O stretching ($\sim 1640\text{ cm}^{-1}$) and the N-H bending ($\sim 1540\text{ cm}^{-1}$) bands of nylon appear

Differences in the semicrystalline framework and in interfacial adhesion between matrix and filler were reflected by the mechanical properties displayed by the samples. [Table 5.2.3](#) summarizes the mechanical properties of the matrix and of the composites.

Table 5.2.3: Tensile mechanical properties of PLA and of its composites

Sample	Modulus (GPa)	Stress at break (MPa)	Elongation at break (%)
PLAM	2.4 ± 0.7	48 ± 6	3.6 ± 0.4
PLANY1.5	6.6 ± 0.4	46 ± 5	1.7 ± 0.3
PLANY2.5	3.6 ± 0.4	23 ± 4	3.2 ± 0.5

The materials were quite brittle, breaking before yielding, as expected from crystalline PLA. PLANY1.5, which was characterized by an optimal adhesion between matrix and fibers, with no bundles and with the thickest lamellae, increased its modulus almost three-fold with respect to the matrix. This sample retained the stress at break of the matrix, whereas its elongation at break decreased. As often observed in nanocomposites, the increase in stiffness of the sample was obtained at the expense of its ductility.

When the quantity of fiber bundles increased and the thickness of lamellae decreased, as in PLANY2.5, the effect of the fibers was much weakened, and the mechanical properties of the composite were the same, and in the case of stress at break even lower, as those of the matrix.

Similar results were obtained for natural fibers, although with a much larger filler content.[209] Oksman and coworkers, for example, reported very similar mechanical properties as ours, but a content of 30% of flax fibers [206] was necessary to achieve the same performance obtained with just 1.5% electrospun fibers. In another report by Misra and coworkers, 40% wood fibers were required to obtain a tensile performance similar to that of our composites.[151] Improvements in modulus slightly larger than those of our composites were obtained with ternary micro-nanocomposites containing, in addition to 40% wood fibers, also 5% nanoclay.[208]

The approach chosen by Yano and coworkers, who used submicrometric fibrillated cellulose [146] brought about increases in tensile modulus and strength, although to a lesser extent than in the composites of the present work. When 3% microfibrillated cellulose was added, no significant increases in tensile modulus and strength were observed, and just elongation at break decreased. However, tensile modulus was increased by 60% and tensile strength by 10% with the addition of 10% micro fibrillated cellulose.[146]

Simultaneous increases in tensile modulus and in elongation at break could be attained with small quantities of CNTs, which are, however, much more expensive than the electrospun fiber employed in the composites described in the present paper.[210]

The existence of an optimum level of filler, beyond which the properties decrease instead of increasing, is common in composites [206] and nanocomposites [159,161,211] and is often associated to the effect of the presence of the filler on the crystallinity of the matrix.[211]

A number of authors stressed the importance of lamellar morphology in understanding the reasons of reinforcement.[97,107,116] In particular, a correlation between tensile properties

and lamellar features was previously noted for polyethylene and polypropylene composites filled with polyethylene-grafted multi-wall CNTs and polypropylene-grafted CNT, respectively.[102,212] A clear relationship between lamellar features and mechanical properties was observed also in this case, as can be seen in [Figures 5.2.8 and 5.2.9](#).

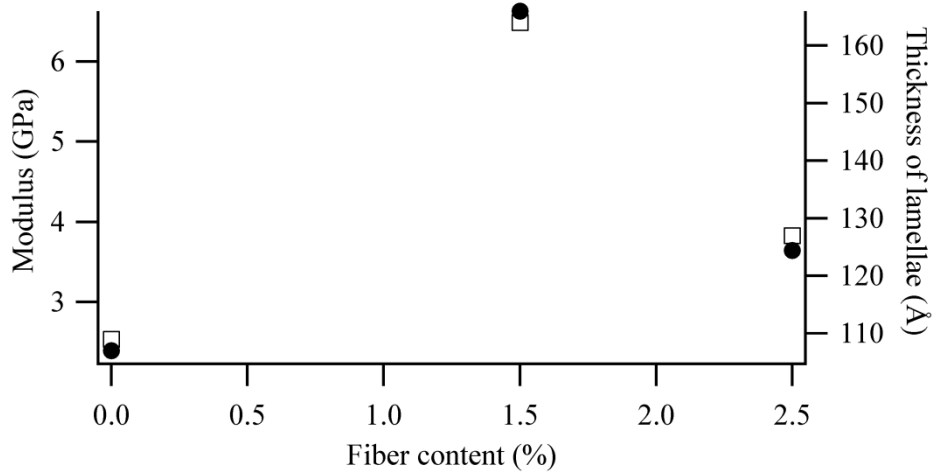


Fig.5.2.8. Comparison of the trend of tensile modulus (closed circles) and of the thickness of lamellae (open squares) as a function of fiber content

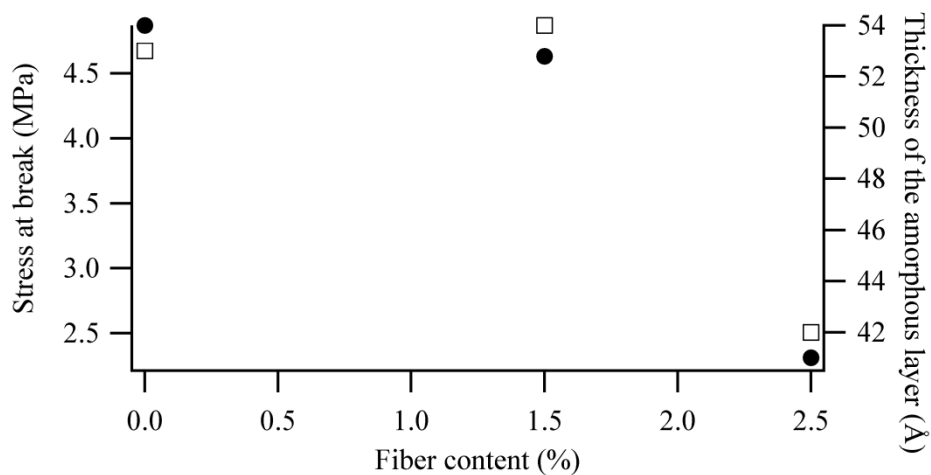


Fig.5.2.9. Comparison of the trend of stress at break (closed circles) and of the thickness of the amorphous layer between the lamellae (open squares) as a function of fiber content

The trend of Young's modulus as a function of filler content was the same as the trend of the lamellar thickness evaluated by SAXS ([Fig. 5.2.8](#)). Modulus is known to depend on the lamellar thickness and crystallinity.[117] In this case; lamellar thickness was the

preponderant factor influencing modulus, because although samples PLANY1.5 and PLANY2.5 have the same Φ_{SAXS} they displayed very different moduli.

Another example of correlation between lamellar morphology and tensile properties is shown in Figure 5.2.9, which displays the stress at break and the thickness of the amorphous layer in lamellar stacks as a function of fiber content. Also in this case, the trends are very similar.

Multiple factors are critical for the tensile behavior of polymer-based composites, among which dispersion, matrix-filler interactions, spherulitic texture, micromechanical deformation processes, skin-core structures and morphological features. Though the data gathered in this work may not be sufficient to single out all of above factors, a role of the lamellar morphology is strongly evident.

A particularly interesting effect of fibers was that of influencing the biodegradation behavior of the composites. Samples were exposed to degradation studies firstly in PBS for 4 months. Even after 4 months, samples showed negligible weight loss, i.e. 0.4%, in PBS. Subsequently, samples were moved to NaOH solution; in this medium samples were degraded very rapidly compared to PBS. Figure 5.2.10 shows the trend of mass residue as a function of residence time in NaOH.

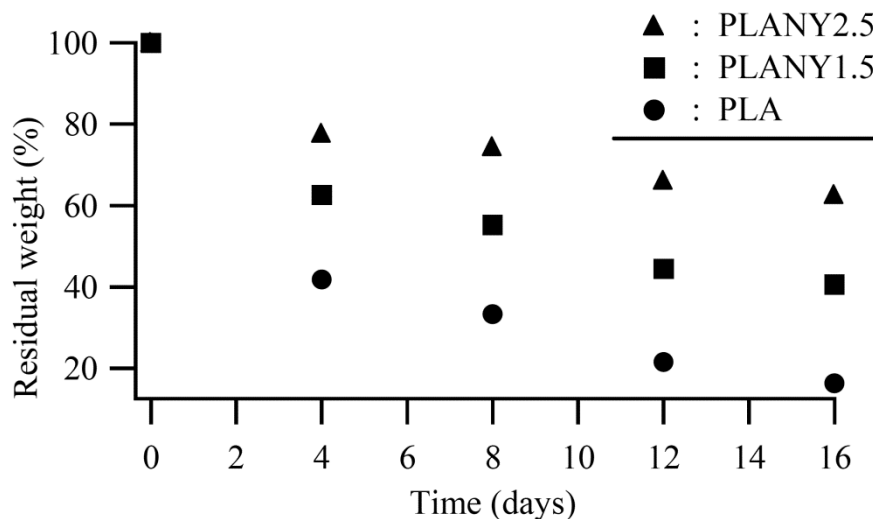


Fig.5.2.10. Residual weight of the samples as a function of residence time in NaOH solution

PLA was the sample which degraded more quickly, whereas addition of fibers made the composites more resilient to degradation. This effect is linear, as shown in [Figure 5.2.11](#), which displays the entity of the residue as a function of fiber content.

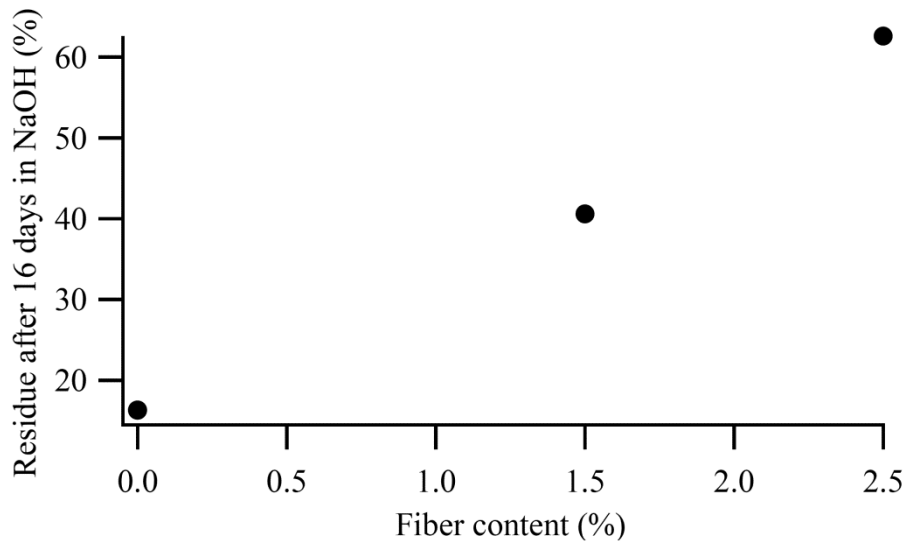


Fig.5.2.11. Residual weight of the samples at the end of the degradation experiments, as a function of fiber content

It has already been reported that degradation happens through a hydrolysis mechanism and preferentially in the less ordered portions of the sample, so the semicrystalline framework can be key for the control of the crystallization rate.[127,129,213] However, the semicrystalline morphology of the samples, i.e. the quantity of amorphous material at disposal for degradation was not so different to explain such divergence, because PLANY1.5 and PLANY2.5 had different degradation rates, but a similar degree of crystallinity. The morphology of the fiber/matrix assembly could help in shedding light on this issue. Armentano and coworkers [129] recently reviewed the effect of nanofillers on the degradation of biodegradable-polymer-based nanocomposites, and highlighted the role of nanofillers in favoring the exchange of water within the composites, thereby increasing the rate of hydrolysis-based degradation mechanisms. A number of reports observed that clay-containing nanocomposites had a higher degradation rate,[213-215] because such samples exhibited a high volume of polymer matrix in contact with the nanoclay edges and surface, resulting in easier water attack of the polymer chains as compared to the unfilled polymer.[213]

As previously noted, the composites displayed a very good interfacial adhesion between the matrix polymer and nylon fibers. Nylon fibers are not degraded by NaOH, so they acted as an obstacle to the diffusion of degrading solution inside the bulk of the sample. Obviously, the more the fibers, the more difficult it was for the NaOH solution to reach the inner regions of the composite. CNTs had the same effect: they acted as a physical barrier hindering the degradation process.[198,216] Moreover, the firm adherence between the fibers and the matrix inhibited the formation of channels at the interface which could vehicle water inside the composite, favoring a more thorough and rapid degradation of the PLA matrix. Previous investigations on PCL containing both N6 and polyvinylpyrrolidone (PVP) fibers indicated that such channels are very important for favoring degradation.[191] Despite being a water soluble and therefore readily biodegradable polymer, PVP fibers did not increase the degradation rate, because they were very firmly embedded in the PCL matrix, so water could reach the fibers only after the surrounding PCL matrix was degraded, significantly slowing the whole process.[191] The increase in degradation rate was achieved using simultaneously PVP and nylon fibers, in which thinner PVP fibers tended to wrap around larger nylon fibers. In this case, the dissolution of PVP fibers formed channels at the interface between matrix and nylon fibers which could vehicle water inside the composite, favoring a more thorough and rapid degradation of the PCL matrix.[191]

Another interesting feature was observed during biodegradation studies. [Figure 5.2.12](#) shows the pictures of the samples before and after degradation in NaOH. The PLA matrix totally lost its shape, whereas, when nylon fibers were used, the composites displayed an excellent dimensional stability, even after a weight loss of 40-60% the shape was perfectly retained. This is important under an applicative point of view, because it may allow the functionality of the biodegradable product also when the degradation process is quite advanced.

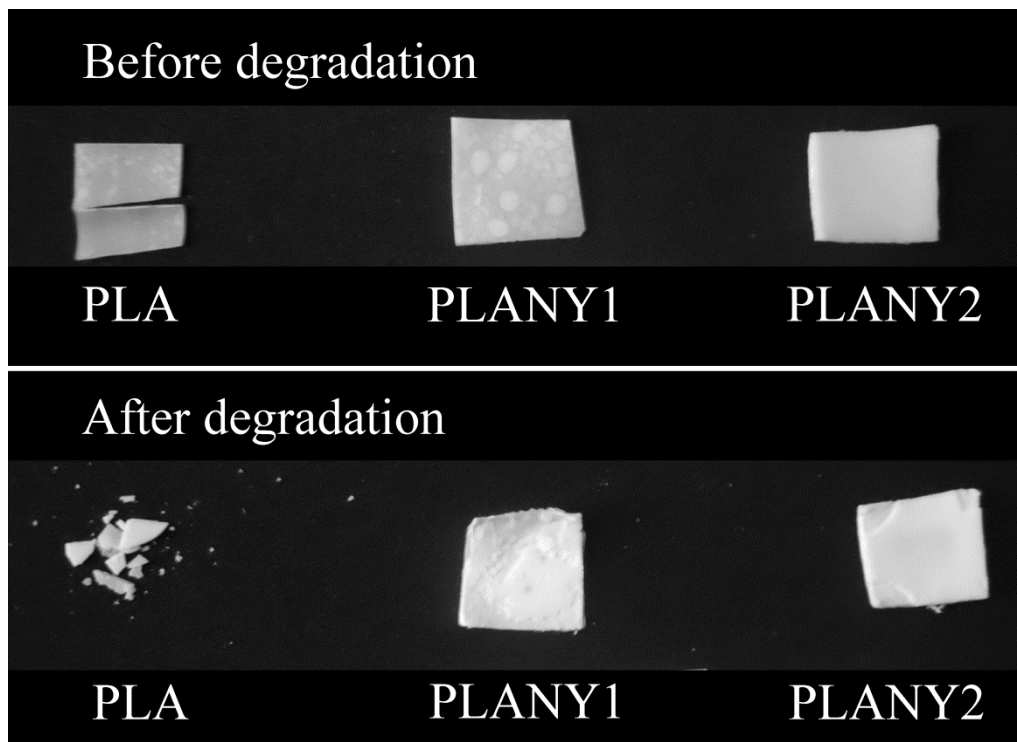


Fig.5.2.12. Images of the samples before and after degradation in NaOH solution

Conclusions

In this work, electrospun nylon fibers were used to prepare PLA-based composites, by a very simple compression molding method. The aim of this report was to show the viability of electrospun fibers as fillers for fiber-reinforced composites, a still rather underdeveloped field.

Electrospun fibers showed an interesting potential for the property improvement of biodegradable polymeric matrices because they are able on one hand to shape the semicrystalline framework at a lamellar level, therefore influencing the mechanical properties of the material, and on the other hand to tune the degradation rate. In other words, the interplay between good interfacial adhesion between matrix and filler and thickening of the lamellae induced by the presence of fibers allowed to increase the modulus of the composites 3-fold with respect to neat PLA, although at the expense of elongation at break. A larger quantity of fibers allowed increasing the modulus by 50%, while retaining the same elongation at break of the pristine matrix. The electrospun fiber mat used in this work was non woven and un-oriented, so the possibility to obtain oriented fibers promises to be even more effective for the control of the improvement of mechanical properties.

The morphology of matrix-filler interaction moreover slowed down the degradation rate of the material, at the same time improving the dimensional stability during the degradation process. This is a particularly interesting feature of the studied samples, because it shows that the addition of electrospun fibers can be a way to tune the durability of PLA-based products, widening the range of application of this promising material.

A remarkable advantage of this approach is its flexibility. In fact, the possibility to engineer by electrospinning the chemical nature and the morphological features of the filler allows an accurate design of the composites. This contrasts with most commonly used nanofillers, which derive from naturally occurring materials (clays) or are less tunable in chemical nature (carbon nanotubes), limiting the potential for a detailed design of the material.

5.3 Green Composites: PLA reinforced with Natural Fibers

The use of fiber reinforced polymer composites (FRPC) is increasing day by day in this modern society. Most of the FRPC have glass fiber or carbon fibers as reinforcement, which are known as conventional and traditional composites. On the other hand, recently researchers are using electrospun nano fibers for the preparation of FRPC.[184-188,190,191,191,217-225] The fibers which were used in their studies were obtained by electrospinning of synthetic polymers which are not degradable. Because composites are made using two dissimilar materials, they cannot be easily recycled or reused resulting in disposal problems after their intended life. So, disposal of the composites which has this kind of nondegradable synthetic fibers is very difficult. More importantly they are not from renewable resources. As awareness is increasing on using renewable materials for the preparation of different novel materials, researchers are reconsidering the idea of using natural fibers for the preparation of FRPC. So far, several FRPC were developed using natural fibers as reinforcement to prepare biodegradable composites. Different kinds of natural fibers were used such as sisal, banana, bamboo, coir, pineapple leaf fiber, and so on.[226-235] The natural fibers and fabrics have certain advantages over the conventional glass fibers such as environmental friendly nature, low cost, low density, non-toxicity, lower abrasion of equipment during processing and recycling. The properties of the reinforcement

and the matrix and the strength of their interfacial bonding determine the quality of a composite.

In this present work, we used *Hildegardia populifolia*. *Hildegardia* fibers have been used before as reinforcement for the preparation of FRPC, but very few articles exist in literature, [227,236-240] and no report was published on the use of *Hildegardia* with PLA. Rajulu et.al [236] examined the properties of this natural lignocelluloses fabric. This natural fabric is available with fibers in the uniaxial direction that are slightly interwoven and loosely bound with one another. *Hildegardia* fibers possess good mechanical properties with low density and can be used as reinforcement in polymer composites. *Hildegardia* was used as reinforcing filler in different polymer matrices such as polypropylene (PP), polypropylene carbonate (PPC), polypropylene carbonate-toughened epoxy, wheat protein etc. In a work Rajulu et.al [241], prepared polycarbonate toughened epoxy based composites using *Hildegardia* as reinforcing filler, and they reported increase in the mechanical properties with the addition of fibers. Li et.al [238] reported increases in the tensile properties of PP with the addition of *Hildegardia* along with compatibiliser. In a work by Li et.al [242] prepared PPC composites reinforced with short *Hildegardia* fibers by melt mixing method. They reported a dramatic increase in tensile strength and simultaneously a decrease in elongation at break and energy at break with increasing the fiber content in compositions. In another work by Rajulu et.al,[237] completely biodegradable composites were prepared using WPI as matrix and uniaxial *Hildegardia* as reinforcement. They used both natural *Hildegardia* and alkali treated *Hildegardia* fibers to prepare the composites with wheat protein isolate. They observed both tensile and flexural properties increased for fabric loading up to 10% (w/w) of reinforcement and decreased thereafter. The degradation was found to be extensive in soil burial method. The composites were found to degrade up to 95% in 35 days. The electron micrographs confirmed the degradation of the films and composites when exposed to microbes.

On the other hand, poly lactic acid (PLA) is gaining more interest day by day, because of the possibility to obtain this poly ester from agro based products. Moreover, it has got good thermal processibility like other commodity plastics. Also it is biodegradable polymer. So far PLA has been reinforced with different natural fibers. Most of them have until now been investigated as reinforcing materials for PLA. Composites based on PLA were prepared using flax, [206,243-245] jute, [246] kenaf, [247,248] abaca, [249,250] bamboo, [251,252] and wood flour [253-257] as cellulosic natural fibers have been reported for improvement of

mechanical properties. Recently, it has been reported that the impact strength of PLA composites is improved by using kenaf fibers from which fine particles have been eliminated. On the other hand, also wood pulp, microcrystalline cellulose, and cellulose whisker, which are derived from plant-based lignocellulose fibers [254,255,258,259] and rayon [260] and lyocell [261] which are known as cellulosic man-made fibers, have also been investigated as reinforcing materials for PLA.

In this present work, an attempt was made to produce biocomposites from PLA reinforcing with Hildegardia fabric by a melt press technique. The effect of fabric on crystalline structure, and thermal degradation behavior of PLA was studied. Adhesion between matrix polymer and Hildegardia fabric was analyzed using fracture surfaces of composites using scanning electron microscope. In addition we performed biodegradation studies by exposing the samples to soil environment. According to our knowledge, for the first time, we prepared biocomposites using this kind of natural fabric and thermoplastic resin by a simple melt press technique. So far several works are reported for the preparation of biocomposites by using natural fibers and thermoplastics, but they were prepared by melt mixing method. Thus, the natural fibers lost their original shape in composites. Whereas, in our study, even after the preparation of composites, it was possible to preserve the original shape of the fabric along with interwoven alignments between the individual fibers present in the fabric. Moreover, in this preparation method it is possible to keep all fibers oriented in the same direction in composites, whereas when composites were prepared in melt mixing method, the orientation of the fibers was not the same.

Experimental

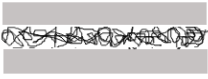
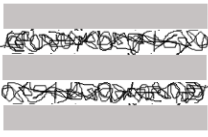
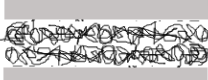
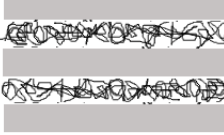
PLA, with D content of 1.1-1.7% was obtained from Unitika Co. Ltd. According to the supplier, it had a weight average molecular weight $\overline{M}_w = 200$ kg/mol, density = 1.25 g/cm³ (ASTM 1238). Hildegardia fabric was used as reinforcement. Sri Krishnadevaraya University of India supplied the Hildegardia fabric. The Hildegardia fabric was extracted by them from the branches of its tree and washed thoroughly with distilled water and then allowed to dry in the sun for about 1 week. The fabric was then dried in a vacuum oven maintained at 65°C for 3 days.

Alkali treatment for the fibers

The alkali-treated Hildegardia fabric was prepared by immersing the Hildegardia fabric in 5% aqueous NaOH solution for 4 h to remove the hemicelluloses and other greasy material. The alkali-treated fabric was neutralized with dilute acetic acid, washed thoroughly with distilled water, and then dried in a vacuum oven maintained at 65°C for 3 days.

Preparation of the composites

Table 1: Compositions and preparation procedure of the samples

Sample	setup
PLA	-
PLA1	 →
PLA2	 → →
PLA3	 →↑
PLA4	 ↑ →

* “→” indicates the direction of the fabric in composites

Composites were prepared by a simple compression molding technique by keeping fabric between PLA films like in our previous works.[126,191] Several compositions were prepared by altering the fabric content and procedure. [Table 5.3.1](#) shows the samples codes, fiber content and the procedure. The fabric content in all composites was about 7%.

Tensile mechanical properties of rectangular-shaped samples (30 mm × 10 mm × 0.5 mm) were measured using an Instron model 3345 mechanical tester at room temperature and 50% humidity. The strain rate was 5 mm. min⁻¹. At least five measurements were performed for each sample.

Degradation studies were performed on all prepared samples in compost environment. Samples were taken out from the media at regular time intervals, washed thoroughly with distilled water and dried at room temperature for 24 hours, weighed and returned to the media.

Degradation studies also were performed in alkali media i.e. NaOH solution (0.1M). Samples were taken out for every 3 days from the solution and thoroughly washed with distilled water and dried at room temperature, weighed and returned to the media.

Results and discussion

Figure 5.3.1 shows the SEM images of the fabric before and after NaOH treatment and images of composite PLA3. Figure 5.3.1c show the compatibility of Hildegardia fabric with PLA matrix.

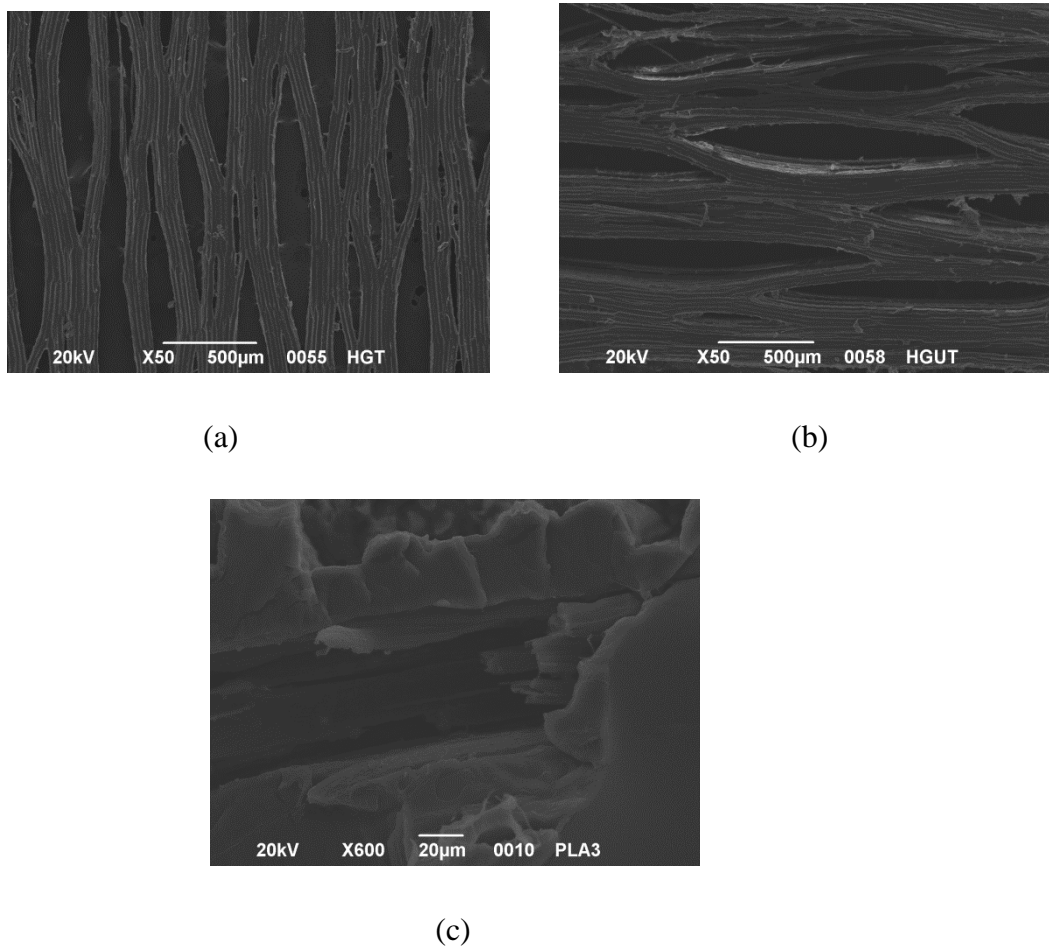


Fig.5.3.1. SEM micrographs of Hildegardia fabric and PLA/Hildegardia composites; a) treated Hildegardia, b) untreated Hildegardia c) PLA3

The treated fabric (Figure 5.3.1(a)) shows that hemicellulose is removed from the fabric after alkali treatment which is supporting the report by Rajulu et.al [236] Also they show that fabric is interwoven by fibers with several voids between fibers. Due to voids, PLA can enter into the fabric and can form very well embedded composite system. Figure 5.3.1(c) shows the interfacial adhesion between the fabric and PLA. It is observed that they have attained very good interfacial adhesion even in absence of any kind of compatibilizer. One can see in Figure 5.3.1(c) that fibers were broken while breaking the samples, showing that part of the load was transferred to the fibers from the matrix, effectively reinforcing the material.

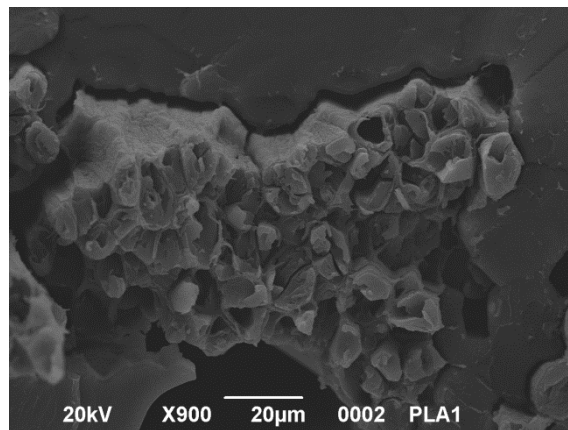


Fig.5.3.2. SEM micrograph of PLA1

In a work by Avella et.al [262] it was reported that kenaf fibers have poor interfacial adhesion with PLA matrix when there is no compatibilizer, whereas when a compatibilizer was used, kenaf fibers attained very good interfacial adhesion. However, in our study we observed that Hildegardia fibers attained good interfacial adhesion even in absence of compatibilizer. In Figure 5.3.2, it is clearly shown that the fabric has a good adhesion with the matrix without losing intermingling structures within the fabric. And it also showed that the void regions within the fabric are efficiently filled with matrix polymer.

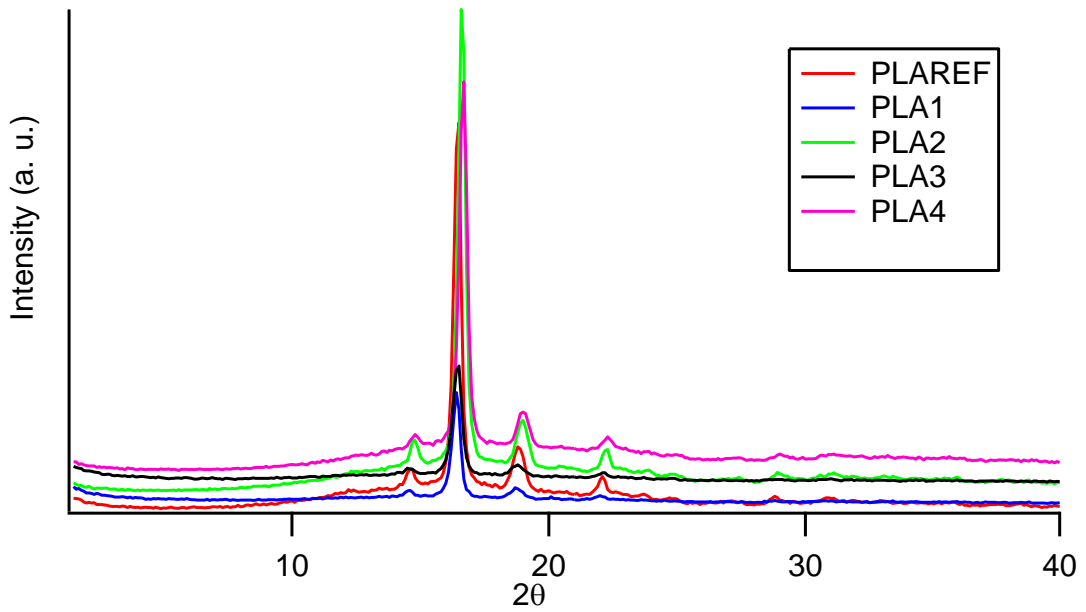


Fig.5.3.3. WAXD diffractograms of PLA and of its composites

The structure and morphology of PLA and of its composites was studied by WAXD, related diffractograms are shown in [Figure 5.3.3](#). Macroscopically no change was observed in semicrystalline structure with the addition of Hildegardia fabric to PLA. In all compositions, the typical diffraction pattern of PLA was observed without the appearance of any peaks related to Hildegardia.

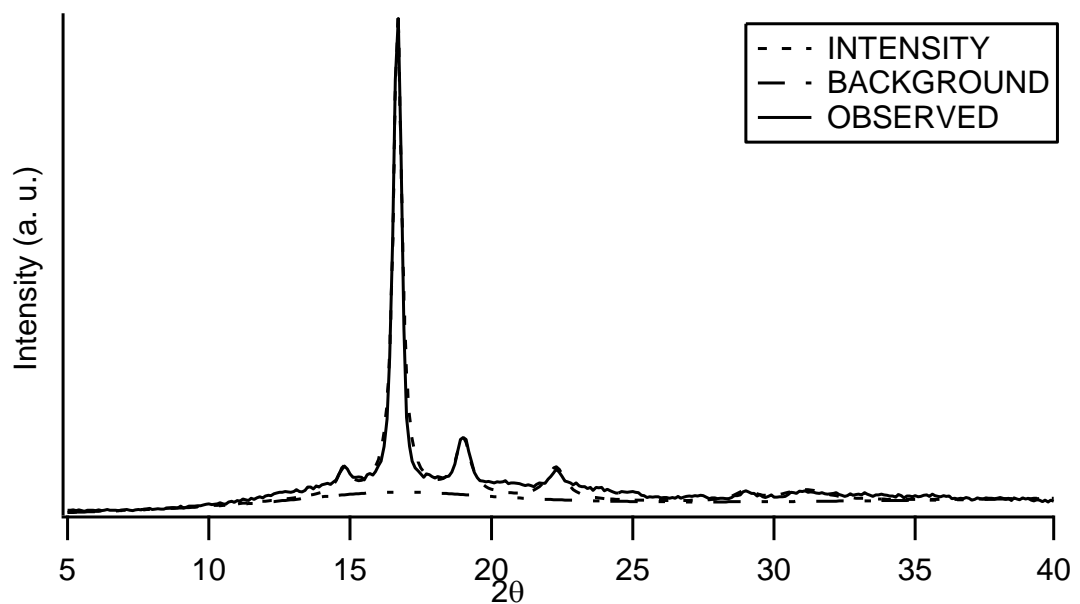


Fig.5.3.4. WAXD pattern (solid line) of PLA4 sample, dotted line shows the fitting for the peaks and solid line with dots line shows fitting for amorphous region

The degree of crystallinity (Φ_{WAXD}) was evaluated by fitting the amorphous and crystalline contributions in obtained diffractograms. Results are tabulated in Table 5.3.2. An example of peak fitting for WAXD is shown in Figure 5.3.4 of sample PLA4. The same kind of fittings was carried out for the other samples. In all compositions the addition of Hildegardia fabric to PLA matrix is increasing the Φ_{WAXD} . The largest increase in crystallinity was obtained when just one layer of fibrous fabric was used, whereas, no considerable changes in Φ_{WAXD} were observed, as a function of the preparation method when two layers were added.

Table 5.3.2: Φ_{WAXD} of PLA and of its composites

Sample	Φ_{WAXD} (%)
PLA	57
PLA1	65
PLA2	61
PLA3	63
PLA4	61

The TGA curves of untreated Hildegardia (UTHG), and alkali treated Hildegardia (THG) are shown in Figure 5.3.5. It can be seen that THG has more thermal stability than UNTHG as it is reported in the literature. In fact, THG starts degradation at higher temperatures than UTHG and leave a larger residue at the end of the TGA experiment. The thermograms of neat PLA and of its composites with Hildegardia fabric are shown in Figure 5.3.6.

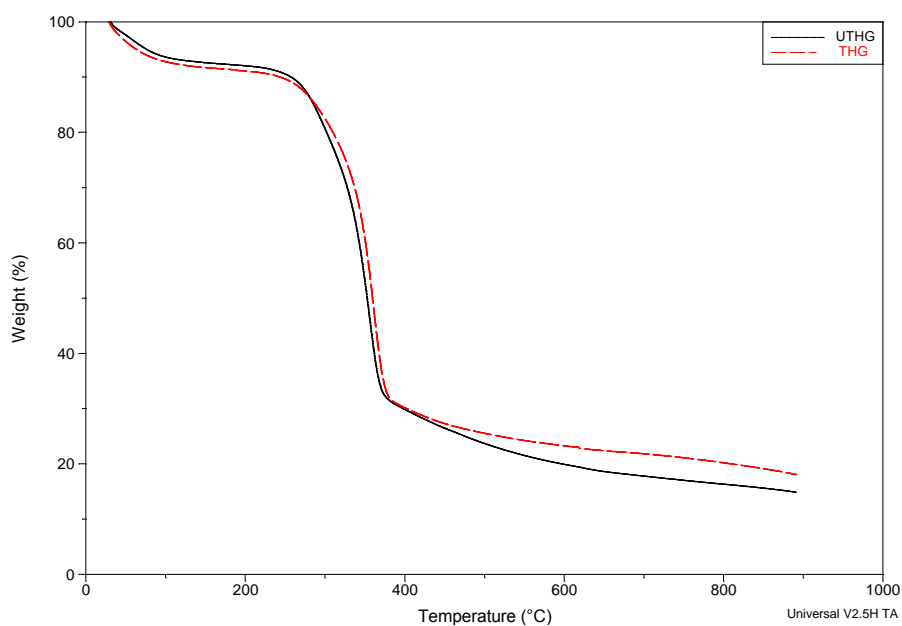


Fig.5.3.5. TGA thermograms of untreated Hildegardia (UTHG) and alkali treated Hildegardia (THG)

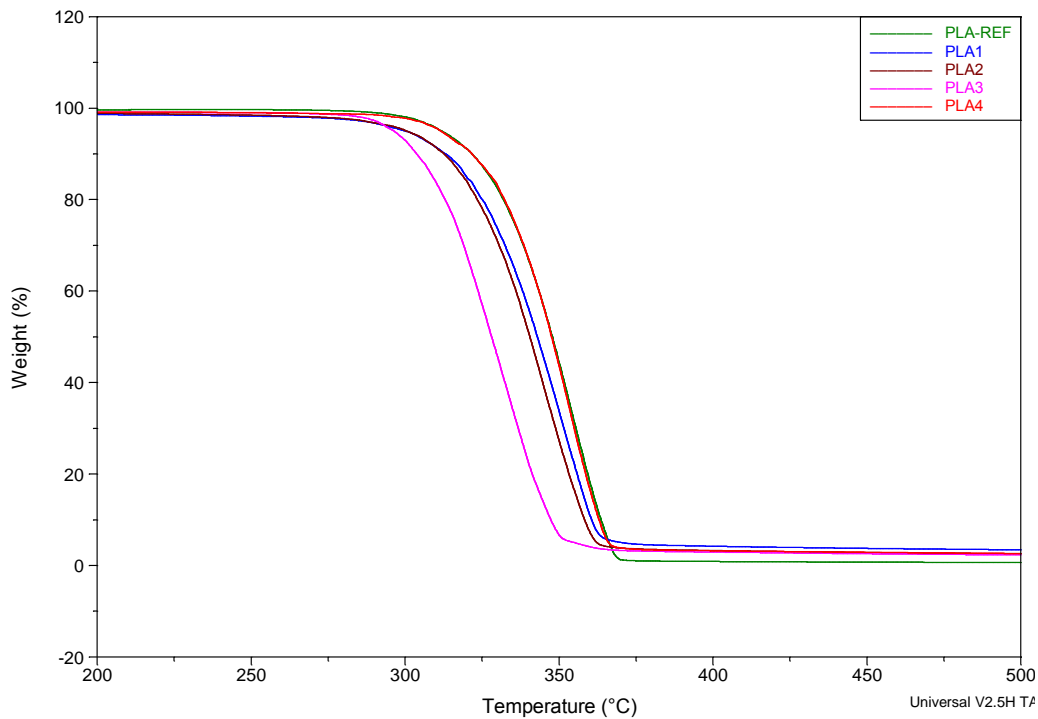


Fig.5.3.6. TGA thermograms of neat PLA and of its composites with Hildegardia fabric

The onset thermal decomposition temperature of neat PLA is 330°C, so the matrix polymer degrades at higher temperature than neat Hildegardia and alkali treated Hildegardia fabric. The thermal stability of prepared composites has also been studied using TGA. Using Hildegardia fabric as reinforcement for PLA reduces the thermal stability of PLA; it is not a surprise to observe the decrease in thermal stability. It is already known that the addition of natural fibers to the polymers reduces the thermal stability of polymers. Lee et.al [150] reported that the addition of Kenaf fibers to PLA reduced the thermal stability of the composites compare to the pristine matrix.

Table 5.3.3: Tensile mechanical properties

Sample	Modulus (MPa)	Stress @ break (MPa)	Strain @ break (%)
PLA-REF	210	68	0.4
PLA1	340	96	0.36
PLA2	220	79	0.53
PLA3	200	46	0.3
PLA4	200	64	0.47

The tensile testing was performed on Instron. At least 5 specimens were tested for every composition. Table 5.3.3 shows the tensile modulus and stress at break of the tested materials. The pure PLA has a tensile modulus of 210 MPa. Increase in tensile modulus was observed with the addition of Hildegardia fabric to PLA matrix. We observed 62 % of increase in tensile modulus of PLA when only one layer of fabric was used as reinforcement, i.e. for the sample PLA1. This is may be mainly because of two reasons, one is the orientation of fabric in composites, and the other reason is good interfacial adhesion between matrix and the fabric. As it is already known that Hildegardia fabric has good tensile mechanical properties in one direction, and the orientation of the fabric in composite is the same as the direction of applied tensile stress, it was possible to obtain increase in tensile modulus. This allowed us to think to prepare composites keeping Hildegardia fabric in multiple directions in the composites. Surprisingly we observed decrease in tensile modulus for the composites in which fabric was oriented in multiple directions. This is may be due to the higher fabric content in the composites. In a work by K. Oksman et.al [206], it is reported that the addition of flax will increase the modulus but the higher fiber content will not improve the modulus in the PLA composites. The explanation they had given for this is orientation of fibers. Composites were prepared in twin screw extruder, then the test samples were compression molded and thus fibers can be oriented differently from one sample to another. However, in our study, orientation might not be the reason, because as we already mentioned, we could preserve the shape of the fabric even after preparation of the composites, so all the fabric was in same direction in which they were melt pressed. The possible reason might be the nature of the fabric which is naturally oriented i.e. Hildegardia has good tensile properties in one direction, but in another direction it has very poor tensile mechanical properties.

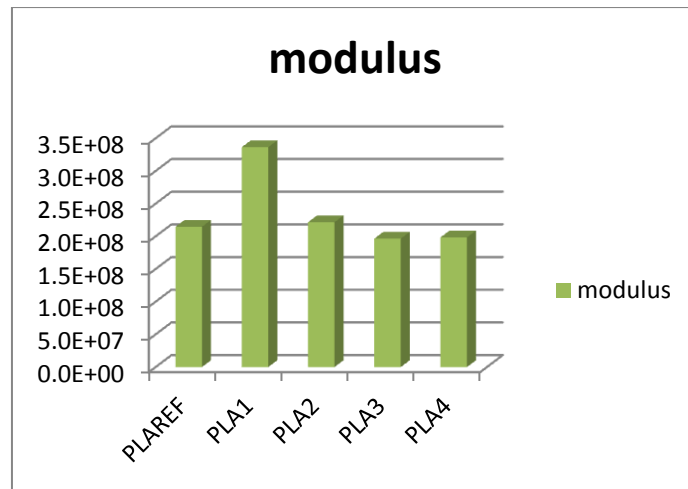


Fig.5.3.7. Tensile modulus of neat PLA and of its composites

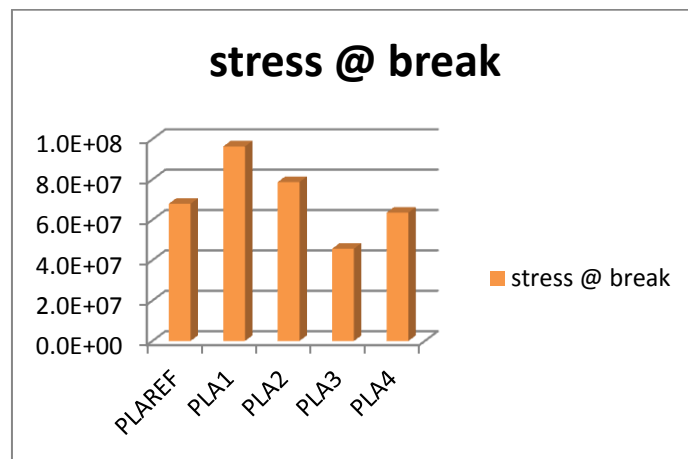


Fig.5.3.8. Tensile strength at break of neat PLA and of its composites

Not surprisingly, within the samples with a larger fiber content, PLA2 was the one which best performed, with a slight increase in modulus, but a significant increase in stress at break with respect to neat PLA. PLA2 has both fiber layer oriented in the same direction. The fact that a double quantity of fibers turns out to be detrimental for modulus increase is due to the hindering effect of the presence of fibers toward an ordered formation of a regular semicrystalline framework. In fact, PLA2 has crystallinity much lower than that of PLA1. It is known that modulus and crystallinity are very closely correlated.[117] PLA2 is the only sample which is showing more strain at break among all composites compared to pristine matrix.

To probe this further, the SEM micrograph of fractured surface of the composite i.e. PLA is presented in [Figure 5.3.9](#). As one can see, when sample was fractured, one layer of the fabric is not broken and well embedded in matrix. Whereas, in the other layer, the fabric is broken and came out of the polymer matrix, this clearly indicates that the layer aligned in the same direction to the tensile stress applied could bear the stress but the other layer in other direction could not withstand the force applied and broke. As we already mentioned, in that direction Hildegardia has poor tensile properties, so the fabric was broken easily and hence the sample also. Similar kind of trend was observed in tensile strength, i.e. increase in tensile strength was observed when a single layer of fabric was used. In other composites, the tensile strength is decreasing may be because of higher content of fabric in composites. Park and Balatinecz [263] reported that the ultimate strain decreased as the wood fiber content increased because of the decreased deformability of the matrix, which was restricted by the rigid particles.

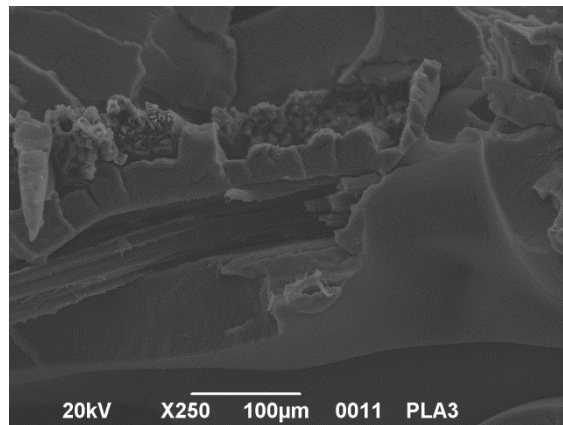
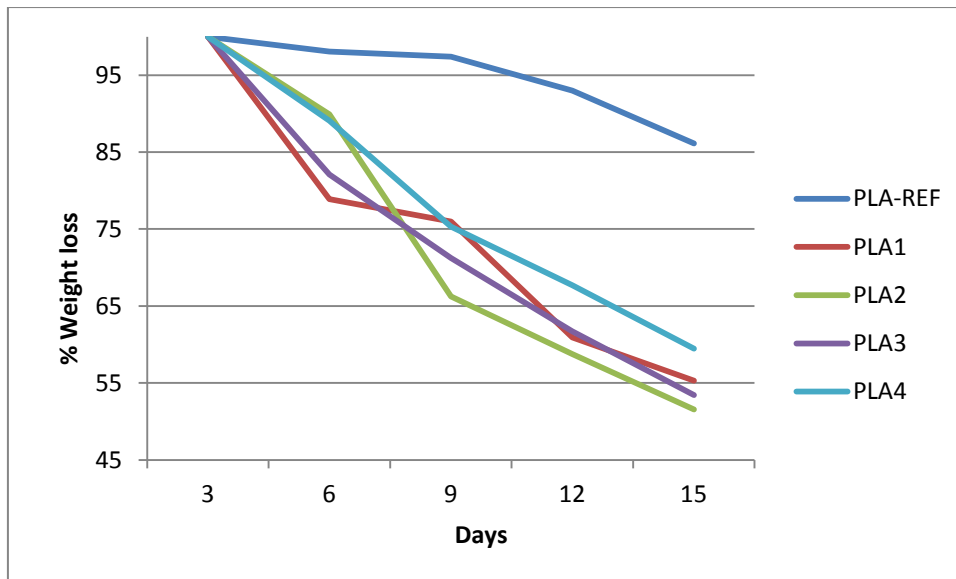


Fig.5.3.9. SEM micrograph of the composite PLA3

Degradation studies of all prepared samples were performed in compost environment. Weight losses of samples were obtained from the differences between the initial weight and the sample weight after aging for two months in compost. We observed almost no weight loss in all samples including pristine polymer. Later on, we studied the degradation studies in alkali as a medium. The obtained results are shown in [Figure 5.3.10 and 11](#).



5.3.10. % weight loss of the samples in NaOH solution



(a)



(b)

5.3.11. Images of the samples before (a), and after (b) degradation studies

From the [Figure 5.3.11\(b\)](#), it is clearly evident that pristine PLA is just started to degrade in alkali media after 15 days, whereas in case of composites, they are degrading faster than that of neat PLA.

Conclusions

In this work, we prepared biocomposites from PLA reinforced with Hildegardia Fabric which is obtained from the plants. According to our knowledge, this is the first attempt to prepare biocomposites by a simple melt pressing technique to reinforce PLA with Hildegardia fabric. Such kind of preparation method allowed us to attain good interfacial adhesion between continuous long natural fabric and PLA matrix. We also observed increase in the tensile modulus when only one layer of fabric was using with retained ductility. However, when we used two layers of fabric in same direction we obtained increase in the ductility without magnificent increase in the tensile modulus. This is shedding more interesting results, i.e in this way we can tune the properties of the final composites by choosing the preparation method. The good interfacial adhesion did not allow samples to degrade samples in compost even after two months. However, same samples are degrading faster when NaOH used as a media.

Chapter 6

PBSA BASED NANOCOMPOSITES

6. Nanofibers with multi-compositions as reinforcement for Poly (butylene succinate-co-adipate) (PBSA): study on structure, morphology and properties

Introduction

Recently, nano-scaled materials have been investigated with amazing increased interest. Among different nano-scaled materials, nanofibers, especially polymeric nanofibers, are promising for diverse applications, such as in drug delivery, tissue engineering and wound healing,[264-266] due to a very large surface area to volume ratio, flexibility in surface functionalities, and superior mechanical performance. Electrospinning has attracted much attention both in academic research and industry applications because electrospinning

(1) can fabricate continuous fibers with diameters down to a few nanometers,

(2) is applicable to a wide range of materials such as synthetic and natural polymers, metals as well as ceramics and composite systems,

(3) can prepare nanofibers with low cost and high yielding.[267-270]

The use of nanofibers as the reinforcing and conductive filler in polymers to improve their mechanical and electrical properties is generally encountered in polymer technology. Nanofibers, such as carbon and glass fibers, are routinely used in composites of a range of different polymers. As it described in previous chapters, in recent years, nanofibers based on polymeric materials are attaining more interest in fiber reinforced polymer composites.

Functional nanofibers or nanofibers with multi-compositions can be prepared by electrospinning of polymers blended with additional compounds like nanoparticles, carbon nanotubes, catalysts, and enzymes, ceramics and so on.[271-274] Functional nanofibers or the nanofibers with multi-compositions are used for various applications ranging from biotechnology to advanced microelectronics.

Poly ((butylene succinate)-*co*-adipate) (PBSA) is a synthetic aliphatic polyester and is synthesized by the polycondensation of butane-1,4-diol in the presence of succinic and adipic acids with relatively low production cost and satisfactory mechanical properties equivalent to that of polyolefins.[275] PBSA, compared with poly(butylene succinate) (PBS), is more

susceptible to biodegradation because of its lower crystallinity and more flexible polymer chains.[276] It also has excellent processibility, so that it can be processed in the field of textiles into melt blow, multifilament, monofilament, flat, and split yarn, and also in the field of plastics into injection-molded products. It is, thus, a promising polymer for various applications. However, mechanical and other properties of PBSA, such as softness, gas-barrier, and thermal stability of the neat polymer are often not sufficient for wide-range of end-use applications.

Till date, very few studies exist on the structure, morphology and properties of PBSA based nanocomposites. So far, PBSA was reinforced with different types of fillers like layered silicates (mostly montmorillonite) and carbon nanotubes.[277-279] In this work we employed polymer nanofibers with additional nanoparticles in them as reinforcing agents for the preparation of nanocomposites based on PBSA. The aim of this work is to understand the effect of particle filled electrospun nanofibers on structure, morphology and properties of PBSA matrix, and also to co-relate changes in structure and morphology brought about by these kinds of fibers to PBSA properties such as mechanical properties and degradation behavior. It is noteworthy to understand the effect of this kind of fibers on polymer matrices. According to authors knowledge, so far, a very few works are reported on using electrospun fibers as reinforcement for thermoplastic polymers, but in none of them it was attempted to use electrospun polymer nanofibers as reinforcement in which already nanoparticles are dispersed. This is the first time that we are reporting such kind of nanofibers as reinforcement for PBSA to improve the performance.

Experimental

Materials

PBSA used in this study is commercial product from Showa Denko (Japan), with the designation BIONOLLE # 3001, which according to the supplier, has a weight-average molecular weight, $\overline{M}_w = 190$ kg/mol. PBSA was dried under vacuum at 50 8C for 36 h prior to use. Two different kinds of electrospun nanofibers were used as reinforcement, i.e. 1) polystyrene (PS) fibers in which titanium dioxide (TiO₂) nanoparticles were already dispersed and 2) polyvinylidene fluoride nanofibers in which organically modified organoclay (Cloisite 20A) was dispersed.

This work was studied in two parts; first we evaluated the effect of PS nanofibers on PBSA structure, morphology, mechanical properties and degradation and in second part, the effect of PVDF nanofibers was explored.

The degradability of the samples was studied by evaluating weight loss of the samples over time in soil. Samples of 50 mm x 50 mm x 0.5 mm were weighed and then buried in boxes containing commercial compost for gardening purpose. The soil was maintained at 100% moisture in weight, and the samples were buried at a depth of 10 cm. The buried samples were dug out once a month, washed in distilled water, and wiped with tissue paper, and the samples were then weighed before returning them to soil.

Tensile mechanical properties of rectangular-shaped samples (30 mm × 10 mm × 0.5 mm) were measured using an Instron model 3345 mechanical tester at room temperature and 50% humidity. The strain rate was 5 mm. min⁻¹. At least five measurements were performed for each sample.

6.1 PBSA/PS electrospun nanofiber nanocomposites

Four types of composites were prepared using PS fibers as reinforcement with different amounts of TiO₂ content in them. All composites were prepared by a simple melt press technique as like in our previous works.[191,223] The composites were prepared by keeping the fiber mat placed between two PBSA films, subsequently pressure and heat were applied in a press (Alfredo Carrea, Genova, Italy) at 130°C, PBSA was melted and percolated between the voids in the mat, constituting a continuous phase in which the fibers were dispersed. Such operating temperature is in fact higher than the melting temperature of PBSA, but not high enough for melting the nylon constituting the fibers. All other composites were prepared in same method, but the amount of nanoparticles in PS fibers was varied. The sample codes are given based on matrix polymer followed by type of nanofibers used and at the end number indicates the quantity of nanoparticles present in fibers. [Table 6.1.1](#) describes the sample codes and the amount of nanoparticles present in fibers.

Table 6.1.1: Formulation and codes of the samples

Sample	TiO ₂ content (%) W/W
PBSA	-
PBSAPS	-
PBSAPS5	5
PBSAPS15	15
PBSAPS25	25

Results and discussion

The effect of particles filled PS nanofibers on structure and morphology of PBSA was explored by WAXD. Obtained WAXD diffractograms were shown in [Figure 6.1.1](#). Three major crystalline peaks were observed at 2 Theta ~ 19.45, 22.55 and 28.75°. In the case of nanocomposites, the position of the peaks corresponding to the crystalline structure of PBSA is not altered. This indicates that the crystalline lattice parameters were not changed after introducing the fibers. Moreover, increasing the TiO₂ within the fibers did not bring about any changes to crystalline structure of PBSA. Similarly S. S. Ray et.al [280] reported similar kind of observations when PBSA nanocomposites were prepared with Cloisite 30B (C30B) organo clay. The presence of C30B did not significantly change the crystalline structure of matrix polymer i.e. PBSA.

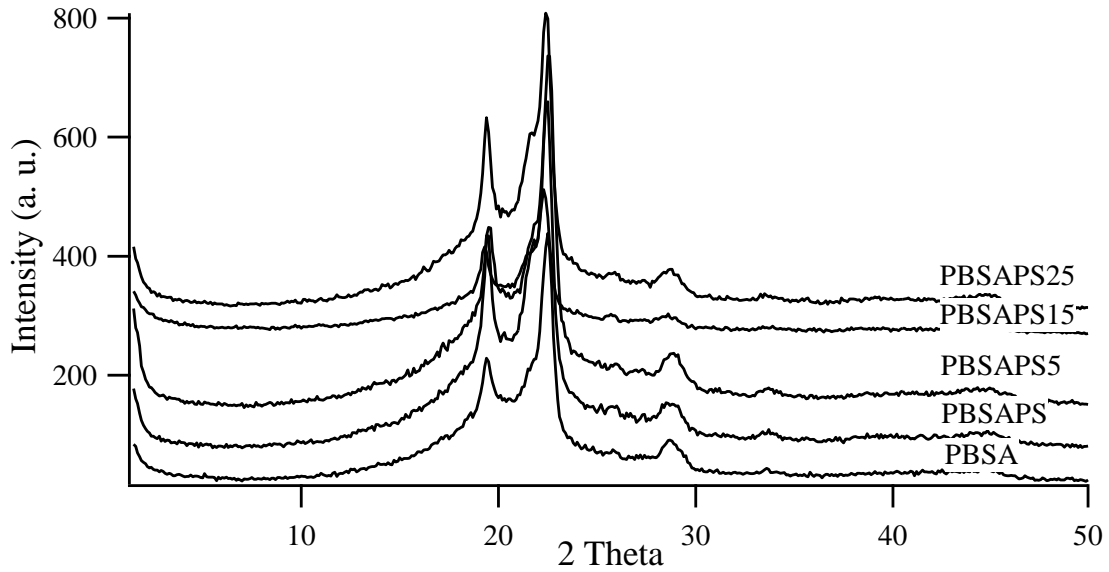


Fig.6.1.1. WAXD diffractograms of PBSA and of its composites with PS electrospun nanofibers with TiO_2 in fibers

The trend of the degree of crystallinity (Φ_{WAXD}) was measured (Table 6.1.2) by fitting the diffractograms, results showed no increase in the degree of crystallinity assessed by WAXD. In a work by our group, a small increase in Φ_{WAXD} was observed when nylon (Ny) electrospun fibers were added to poly caprolactone (PCL). On the other hand, when polyvinyl pyrrolidone electrospun fibers were used as reinforcement for PCL, no considerable changes in Φ_{WAXD} was observed. In other work by our group, Ny electrospun fibers were used as reinforcement for PLA, and a very small increase in Φ_{WAXD} was observed but almost negligible. S. S. Ray et.al [280] reported that, due to the addition of C30B to PBSA, the intensity of the peaks was significantly diminished and hence decrease in Φ_{WAXD} occurred. So, the effect of reinforcing filler on Φ_{WAXD} varies from filler to filler depending on the nature and type of filler. In this study, the addition of PS fibers in which TiO_2 particles already dispersed doesn't show any effect on PBSA crystalline structure.

The lamellar morphology was studied by SAXS and the obtained traces were fitted.[73,96] Data from fittings were tabulated in Table 6.1.2.

Table 6.1.2: Degree of crystallinity obtained by WAXD (Φ_{WAXD}) and morphological parameters of the lamellar stacks obtained by SAXS analysis of considered samples. The thickness of the crystalline (C) and amorphous layer (A), the long period (D), and the crystallinity (Φ_{SAXS}), along with their relative distributions ($\sigma_{\text{C/C}}$, $\sigma_{\text{A/A}}$, $\sigma_{\text{D/D}}$ and $\sigma_{\Phi/\Phi_{\text{SAXS}}}$)

Sample	C (Å)	A (Å)	D (Å)	Φ_{WAXD} (%)	Φ_{SAXS} (%)	$\sigma_{\text{C/C}}$	$\sigma_{\text{A/A}}$	$\sigma_{\text{D/D}}$	$\sigma_{\Phi/\Phi_{\text{SAXS}}}$
PBSA	52	26	78	30	67	0.3	0.3	0.2	0.1
PBSAPS	53	27	80	32	67	0.34	0.2	0.3	0.1
PBSAPS5	65	35	101	32	65	0.34	0.2	0.2	0.4
PBSAPS15	56	26	83	32	68	0.4	0.2	0.3	0.1
PBSAPS25	38	32	70	31	54	0.55	0.5	0.4	0.2

When only PS fibers without TiO_2 were used, the long period was unaltered, whereas, when fibers with minimum amount of TiO_2 nanoparticles were used, increase in the thickness of crystalline layer, C (Å) was observed and hence increase in the long period was observed. Increasing the quantity of TiO_2 content in fibers again decreases the thickness of crystalline layer and hence decreases in the long period. Though the long period was decreasing with increasing the nanoparticles content in composites, the resulting long period is still more in composites than that of pristine matrix except in the case of PBSAPS25. Increasing the quantity of TiO_2 in the fibers also produced a broadening of distribution of the lamellar features. This is associated to a disordering effect of the inorganic filler, confirmed by the fact that higher amounts of nanoparticles are not only decreasing the thickness of crystalline layer but also simultaneously increasing the thickness of amorphous layer. The trend of the semicrystalline features which shows a maximum for TiO_2 contents between 5 and 15% is due to a conflicting behavior of TiO_2 . On one hand, this inorganic species tends to nucleate the formation of crystals, but on the other hand a too large TiO_2 content hinders a smooth motion of the macromolecular chains, eventually hampering the formation of a regular semicrystalline framework.

The thermal behavior of neat PBSA and of its composites was analyzed by DSC, and the relative scans are shown in [Figure 6.1.2](#).

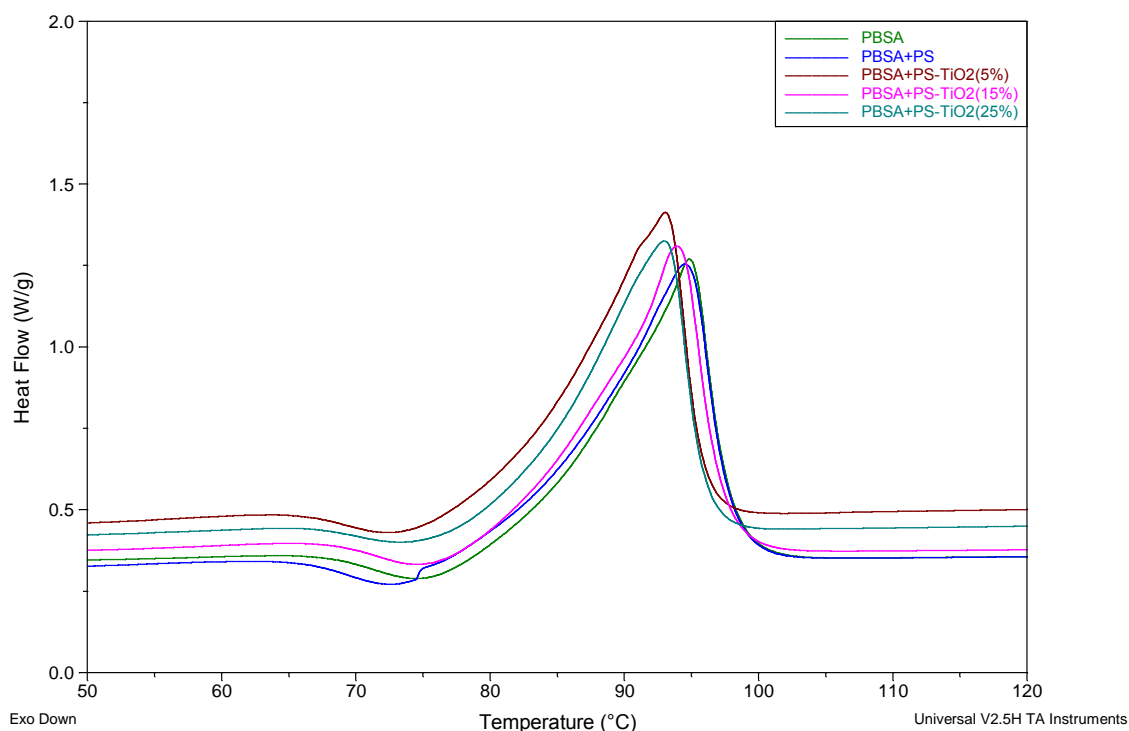


Fig.6.1.2. DSC thermograms of neat PBSA and of its composites

Reported data were taken after erasure of all previous thermal history and to ensure reproducible thermograms. In all cases, we found a single melting peak around 95°C, and no considerable changes in melting temperature was observed with the addition of PS nanofibers to PBSA matrix. Unlike in a report by S. S. Ray [280], we observed only a single melting peak, indicating that PS fibers are not nucleating an additional population of crystallites like C30B in their work. Cooling thermograms allowed us to study the crystallization behavior of all prepared samples. It was observed that the crystallization temperature (T_c) is larger for the pristine matrix (39°C), compared to the composites (35°C) except PBSAPS25 (45°C) which is higher than that of neat PBSA. T_c is useful for evaluating nucleation behavior: if nucleation occurs, the polymer crystallizes at a higher temperature (and the contrary occurs for inhibition of crystallization). So, based on T_c values, nucleation effect were observed in sample i.e. PBSAPS25. This nucleation behavior in this sample is probably not due to fibers but due to the presence of high amount of inorganic particles. Generally fibers show an inhibiting because they tend to hinder the polymer motion for small filler quantities, and nucleation was observed only with high filler contents.[126,191] These results are supporting the data obtained by WAXD.

The interfacial morphology between matrix polymer and reinforcement fibers was studied by SEM and obtained micrographs for the fractured surfaces are shown in [Figure 6.1.3](#).

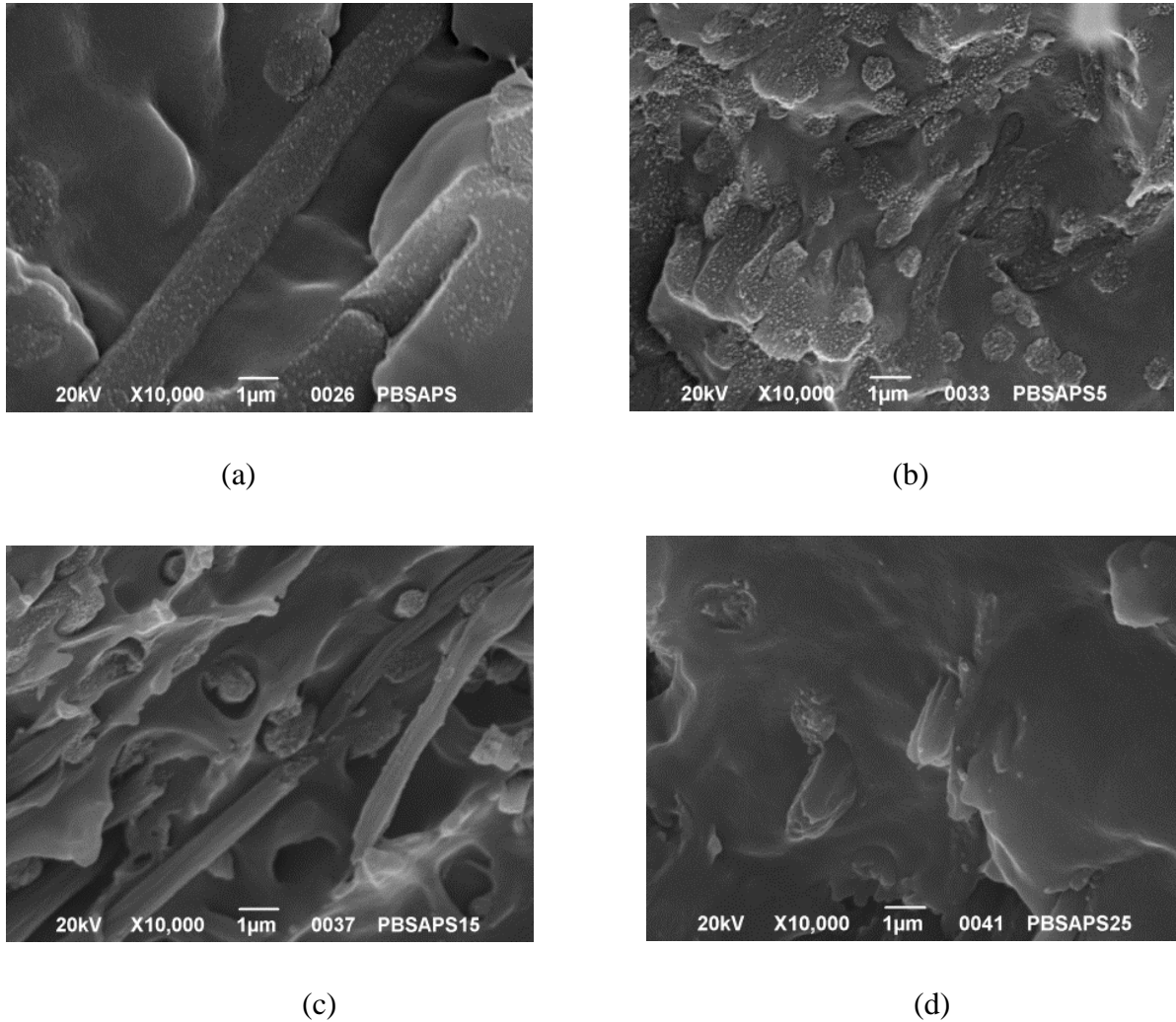
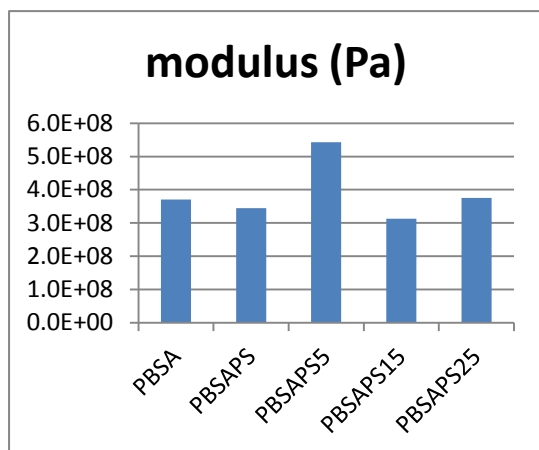


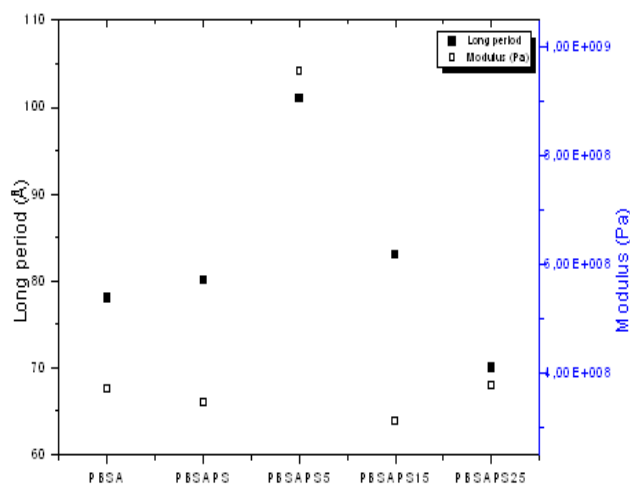
Fig.6.1.3. SEM images of PBSA composites; a) PBSAPS, b)PBSAPS5, c) PBSAPS15, d) PBSAPS25

It seems that in all composites we attained good interfacial adhesion between fibers and matrix polymer. This was possible due to the small diameter of the fibers which were used.

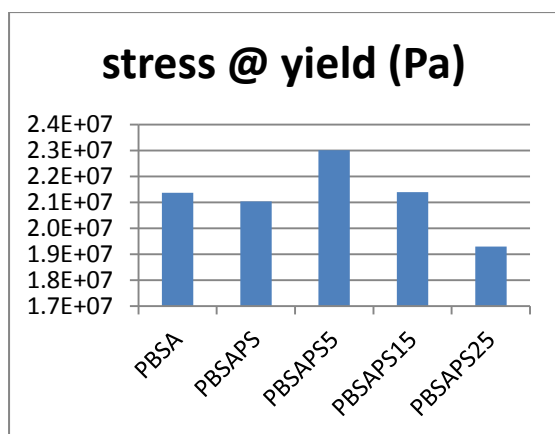
Differences in the semicrystalline framework and in interfacial adhesion between matrix and filler were reflected by tensile mechanical properties shown in [Figure 4](#).



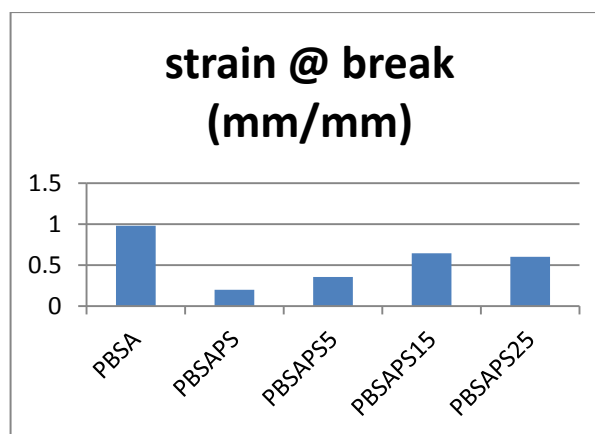
(a)



(b)



(c)



(d)

Fig.6.1.4. Tensile mechanical properties of PBSA and of its composites (a) tensile modulus (b) correlation between modulus and long period (c) tensile strength (d) elongation at break

Compared to that of neat PBSA (370 Pa), the tensile modulus is not changing much in composites except in PBSAPS5 (542 Pa). The main reason for such improved tensile modulus is the stronger interfacial adhesion between filler and matrix, also dispersion of TiO₂ nanoparticles. In PBSAPS5, due to less quantity, nanoparticles might have dispersed thoroughly all over the matrix and increase the interfacial area. This helps transfer of applied load from the main matrix to the dispersed phase. PBSAPS15 has the thickest lamellae and the largest long period and modulus is correlated with lamellae thickness. Similarly, S. S. Ray [280] reported, that increase in tensile modulus was observed with full dispersion of C30B in PBSA matrix. However, in their study they obtain increase in tensile modulus with the increase in filler content in composites. Also, modulus is known to depend on the lamellar

thickness and crystallinity. In this case lamellar thickness was the preponderant factor which is influencing the modulus.

Similar trend to tensile modulus was noted for tensile strength in our study. The highest value was obtained with fibers with low quantity of nanoparticles and the lowest value was with fibers with highest nanoparticles. The elongation at break gradually decreased with the addition of electrospun PS nanofibers to PBSA. The neat PBSA has still better elongation at break than composites. Comparing the results within composites, elongation at break increases with increasing the nanoparticles content in fibers, similar kind of results was observed by S. S. Ray [280], where they observed increase in the elongation at break with increasing the C30B content in composites. In Ray's work, the elongation at break was greater than neat PBSA in all cases, whereas in our study, in all composites, the elongation at break is less than neat PBSA irrespective to the content of nanoparticles in PS fibers. These results are contrary to the results observed by our group in our previous works, where the addition of electrospun nylon fibers to PCL increased the elongation at break. This is probably due to the nature of electrospun fibers, because PS is a brittle polymer, which does not have the high modulus and the high strength of nylon fibers which yielded so promising results when mixed with PCL and PLA.

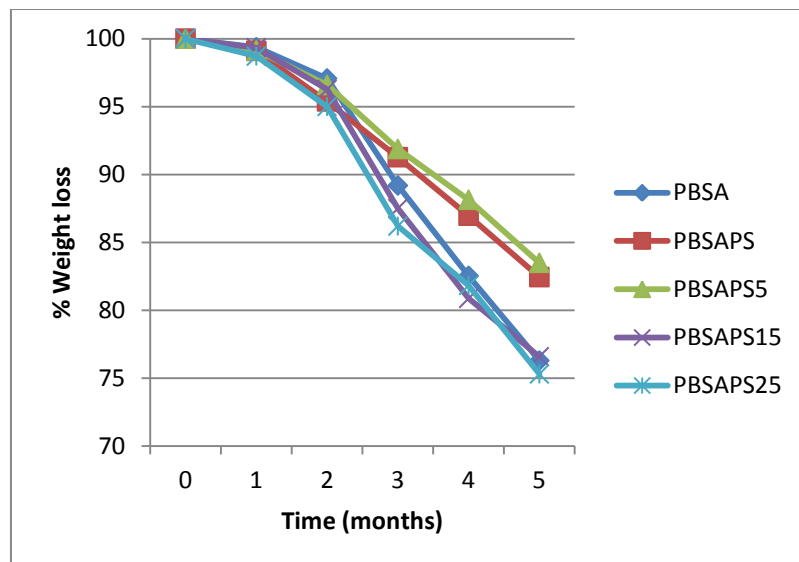


Fig.6.1.5. Mass residue of the samples as a function of time, obtained during biodegradation in compost

Good results could be obtained on the degradation behavior. The degradability of PBSA/PS electrospun fiber composites was evaluated by burying the specimens in compost for gardening purpose. The tests were carried out at 100% relative humidity. PS fibers without TiO₂ nanoparticles and with very low quantities showed slower degradation rate than neat PBSA, which means they are suppressing the degradation behavior of PBSA matrix. On the other hand, when TiO₂ content increased in fibers, the degradation rate gradually increased. Especially, sample PBSAPS25 degraded faster than neat PBSA. In fact PBSAPS25 was the only composite less crystalline than neat PBSA, which is compatible with the hypothesis that degradation happened preferentially in the ordered portion of the sample.

6.2. PBSA/PVDF electrospun fiber nanocomposites

Composites were prepared using PVDF fibers as reinforcement with different amounts of cloisite 20A (C20A) content in them. Composites were prepared by a simple melt press technique as described in the previous chapter. The composites were prepared by keeping the fiber mat between two PBSA films, and applying pressure and heat in a press (Alfredo Carrea, Genova, Italy) at 130°C. At this temperature, the PBSA was melted and percolated between the voids in the mat, constituting a continuous phase in which the fibers were dispersed. At 130°C, in fact, the PVDF mat remained unaltered because PVDF melts just at 160°C. The sample codes are given based on the matrix polymer followed by the type of nanofibers used and at the end a number indicates the quantity of nanoparticles present in fibers. [Table 6.2.1](#) describes the sample codes and the amount of nanoparticles present in fibers.

Table 6.2.1: Formulation and codes of the samples

Sample	TiO ₂ content (%) W/W
PBSA	-
PBSAPVDF3	3
PBSAPVDF5	5

Results and discussion

The effect of particles filled PVDF nanofibers on structure and morphology of PBSA was explored by WAXD. Obtained WAXD diffractograms were shown in [Figure 6.2.1](#). Three major crystalline peaks were observed at 2 Theta \sim 19.45, 22.55 and 28.75°. In the case of nanocomposites, the position of the peaks corresponding to the crystalline structure of PBSA is not altered like in composites with PS nanofibers. As it is discussed in previous chapter, S. S. Ray et.al [280] reported that clay particles did not change the crystalline structure of PBSA, in our study also fibers with clay nanoparticles did not change the crystalline structure of neat PBSA in composites.

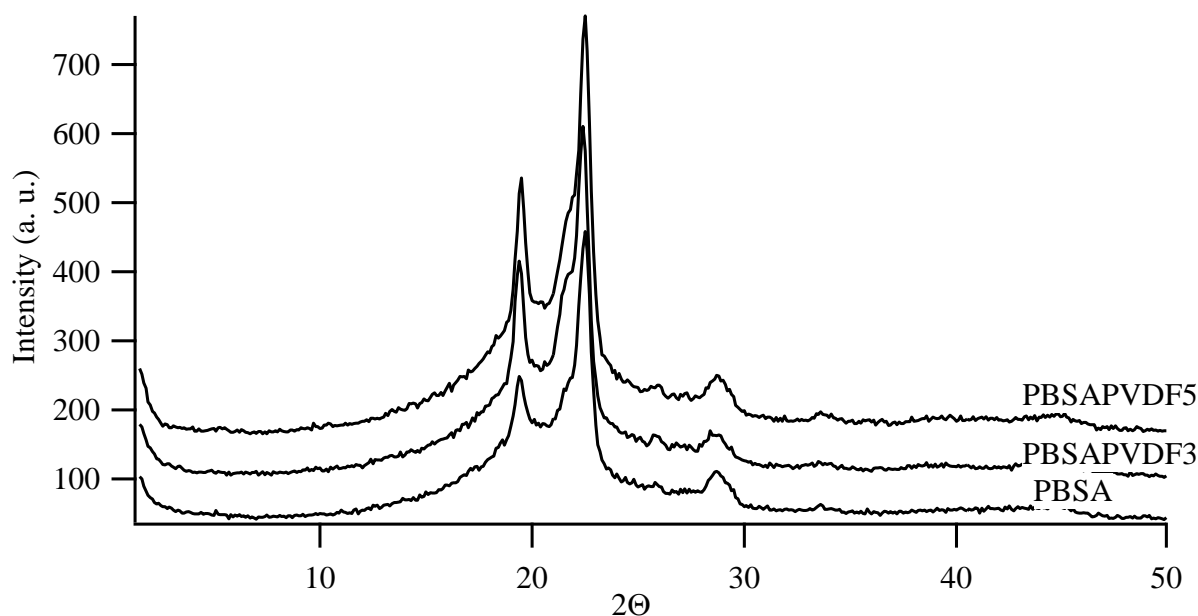


Fig.6.2.1. WAXD diffractograms of PBSA and of its composites with PVDF fibers

The trend of the degree of crystallinity (Φ_{WAXD}) was measured ([Table 6.2.2](#)) by fitting the diffractograms. Results showed a small increase in the degree of crystallinity assessed by WAXD, whereas, by comparison, PS fibers did not show any effect on the degree of crystallinity.

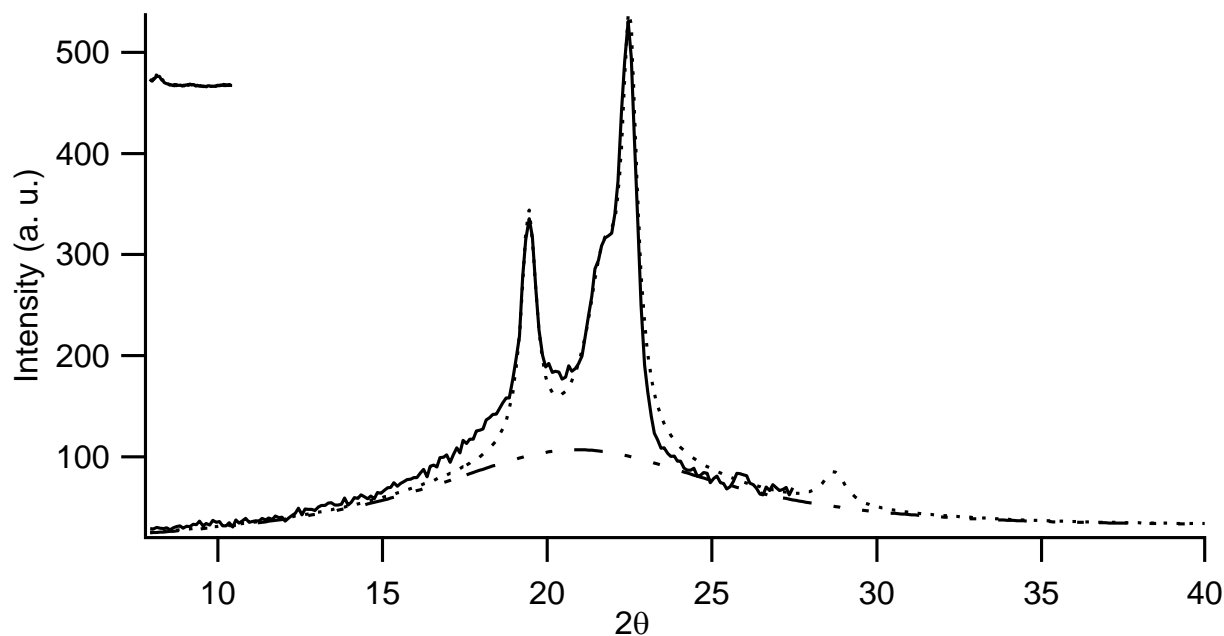


Fig.6.2.2. WAXD pattern (solid line of the) of the sample PBSAPVDF3. Dotted line shows the fitting for the peaks and semi solid line shows fitting for amorphous region

This may be due to fibers, not due to clay particles in fibers, as it is already known that electrospun fibers can increase the degree of crystallinity.[126,191] S. S. Ray[280] also reported that C30B hinders the crystalline structure, resulting in a decrease in degree of crystallinity, thus we assume that in our study, a small increase in the degree of crystallinity is because of fibers but not due to clay particles in fibers.

The lamellar morphology was studied by SAXS and the obtained traces fitted like in previous chapter, obtained data from fittings are tabulated in [Table 6.2.2](#). In the case of composite with PVDF fibers with low amount of clay particles, showed no significant changes in lamellar morphology. Whereas, when the amount of clay was increased, i.e. in the case PBSAPVDF5, disordered lamellae were observed, as reflected by a decrease in thickness of crystalline lamellae by an increase in the thickness of the amorphous layer, by a broadening the distribution and thus by a decrease in degree of crystallinity (Φ_{SAXS}).

Table 6.2.2: Degree of crystallinity obtained by WAXD (Φ_{WAXD}) and morphological parameters of the lamellar stacks obtained by SAXS analysis of considered samples. The thickness of the crystalline (C) and amorphous layer (A), the long period (D), and the crystallinity (Φ_{SAXS}), along with their relative distributions ($\sigma_{\text{C}}/\text{C}$, $\sigma_{\text{A}}/\text{A}$, $\sigma_{\text{D}}/\text{D}$ and $\sigma_{\phi}/\Phi_{\text{SAXS}}$)

Sample	C (Å)	A (Å)	D (Å)	Φ_{WAXD} (%)	Φ_{SAXS} (%)	$\sigma_{\text{C}}/\text{C}$	$\sigma_{\text{A}}/\text{A}$	$\sigma_{\text{D}}/\text{D}$	$\sigma_{\phi}/\Phi_{\text{SAXS}}$
PBSA	52	26	78	30	67	0.3	0.3	0.2	0.1
PBSAPVDF3	52	27	79	36	66	0.3	0.2	0.2	0.1
PBSAPVDF5	32	35	67	34	48	0.5	0.6	0.4	0.4

The thermal behavior is not altered when PBSA was reinforced with PVDF fibers in which C20A clay particles were already dispersed. Like in previous study with PS fibers, in this study also we observed a single melting peak and no considerable effects on crystallization.

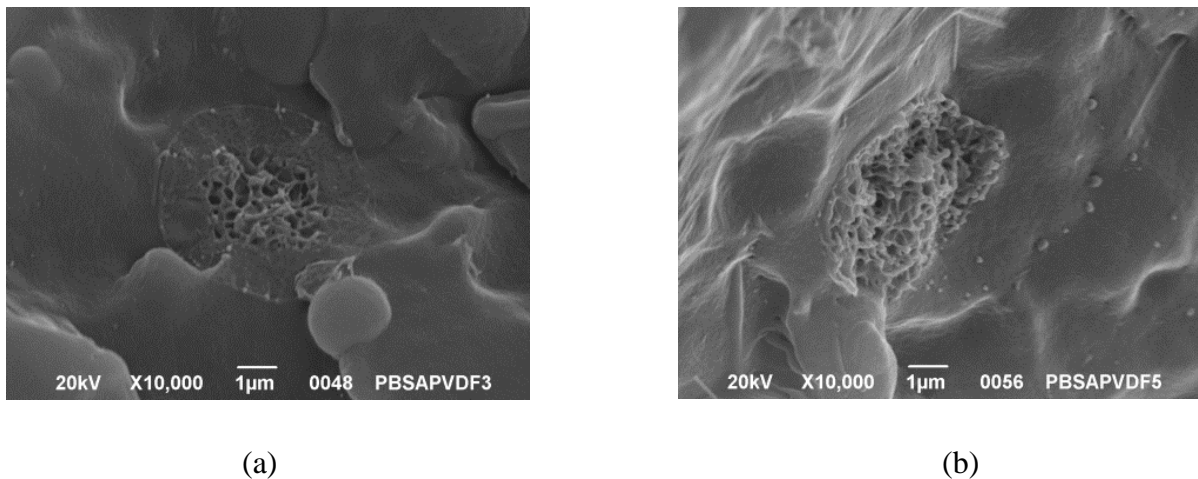


Fig.6.2.3. SEM images of PBSA composites; a) PBSAPVDF3, b) PBSAPVDF5

The interfacial adhesion between filler and matrix was analyzed by SEM at fractured surfaces; [Figure 6.2.3](#) shows the SEM images of a) PBSAPVDF3 and b) PBSAPVDF5. PVDF-based fibers attained very good adhesion ([fig 6.2.3a and b](#)). Surprisingly, some spider web kind of structures was observed in PVDF fiber reinforced composites probably due to solvent evaporation during spinning the fibers. Arkadii Arinstein et.al [281] reported that sometimes solvent is trapped in fibers and will be evaporated slowly results in porous structures.

The tensile properties of neat PBSA and of the two composite samples are reported in [Table 6.2.3](#). Tensile modulus, stress at yield, strain at yield, stress at break and strain at break were measured for all samples.

Table 6.2.3: Tensile mechanical properties of prepared samples

Sample	Modulus (MPa)	Stress @ yield (MPa)	Strain @ yield (mm/mm)	Stress @ break (Pa)	Strain @ break (mm/mm)
PBSA	370	21	0.12	19	1.0
PBSAPVDF3	437	21	0.1	19	0.49
PBSAPVDF5	435	22	0.13	20	0.34

From the results, it was observed that tensile modulus of neat PBSA was increased after nanocomposite preparation with PVDF fibers. The increase in tensile modulus for PBSAPVDF3 is about 18% compared to the neat PBSA. With increasing clay content in fibers, we did not observe any further increase in tensile modulus. This is may be due to electrospun nanofibers and as well as to dispersion of clay particles in fibers. As we already know, a better dispersion of clay particles in nanocomposites will result in better mechanical properties. Other properties such as stress at yield, strain at yield and stress at break are not altered compared to neat PBSA except strain at break which is decreasing in the composites. Increasing the clay content in fibers, resulted in further decrease in strain at break, which is opposing the results reported by S. S. Ray.[280] In their study they observed increase in the elongation a break with increasing the clay content in nanocomposites. The results we observed in this work are commonly observed in polymer/clay nanocomposites, and it is often reported that the addition of high amount of clay can decrease the mechanical properties.

The degradation behavior was studied in compost; images of samples after degradation are shown in [Figure 6.2.4](#). Addition of particle filled fibers to the PBSA matrix is not enhancing the degradation rate because the good adhesion between matrix and fibers hinders the penetration of water in the matrix. This is corroborated by the fact that almost no degradation (only 3% weight loss) was observed in sample PBSAPVDF3, which is characterized by a very good adhesion between matrix and filler. As we can see in [Figure 6.2.3a](#) (PBSAPVDF3)

all fibers were well embedded in polymer matrix and hence water molecules did not find sufficient channels to penetrate inside.

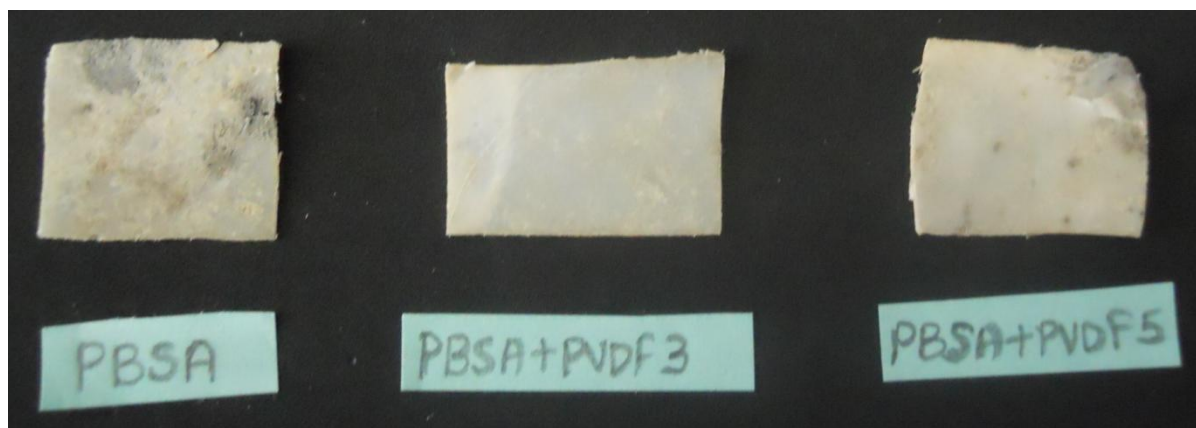


Fig.6.2.4. Images of samples after degradation in compost for 5 months

Conclusion

For this work, composites based on biodegradable polymer i.e. PBSA reinforced with nanoparticles electrospun nanofibers were prepared. These kinds of fibers are showing different effects on the structure and morphology of the polymer depending on the type of fibers used, thus it is possible to control the structure and morphology of PBSA according to the need. Due to the small diameters, it was possible to attain very good interfacial adhesion between filler and matrix, which is also a parameter which affects the mechanical properties. PBSA composites with PVDF fibers showed good tensile modulus compared to the composites with PS fibers. Both kinds of fibers did not show any effect on crystallization behavior of PBSA matrix. Both kinds of fibers are slowing down the degradation of PBSA matrix. Only PBSAPS25 is showing the degradation rate similar to that of neat PBSA, it is may be due to the higher amount of inorganic content in fibers.

Chapter 7

Conclusions

7. Conclusions

As we mentioned in our scope and objectives, we prepared nanocomposites based on some bio degradable polymers such as PCL, PLA and PBSA. We used different inorganic and organic nano fillers as reinforcement. All prepared composites were thoroughly characterized in order to understand the effect of used nanofillers on the structure and morphology of the polymer matrix, and thus on physical-mechanical properties and degradation behavior. The following observations were noticed.

Firstly, PCL was reinforced with inorganic clay nanoparticles. In this work we successfully prepared intercalated PCL/organoclay nanocomposites by solution mixing method using THF as solvent. It was observed that organoclay has some significant effect on crystalline lamellae of lower molecular weight PCL samples. Addition of clay nanoparticles inhibited the crystallization behavior of PCL, which is opposite to what often reported in the literature for polymer/clay nanocomposites. The modulus of the prepared nanocomposites was unaltered, but their ductility increased which is unusual in polymer/clay nanocomposites. It was also observed that the addition of C15A to PCL, reduced the degradation rate of PCL.

On the other hand, reinforcing PCL with electrospun nylon fibers, it was possible to obtain not only improved stiffness and strength, but also increased ductility. PCL was also reinforced with a mixture of electrospun nanofibers to improve the physical mechanical properties and to modify the degradation behavior of PCL-based composites. Nylon 6 fibers were chosen as the reinforcement, whereas PVP fibers were selected to tune the degradation behavior. It was observed that electrospun fibers of different chemical nature and with different sizes could cooperate in improving the physical mechanical properties of PCL matrix; at the same time tuning its degradation behavior.

PLA was another matrix used in this work. This polymer has been reinforced with different types of fillers. Even though a similar degree of dispersion could be achieved in cationic and anionic clays, these two kinds of fillers exerted different effects on the structure and morphology. The anionic perkalite clay induced higher crystallinity, a faster crystallization rate and also a modification of the crystallization mechanism.

PLA also reinforced with electrospun nylon fibers. They showed an interesting potential for the property improvement of biodegradable polymeric matrices because they were able on one hand to shape the semicrystalline framework at a lamellar level, therefore influencing the mechanical properties of the material, and on the other hand to tune the degradation behavior. In this work, a large quantity of fibers allowed to increase the modulus by 50%, while retaining the same elongation at break of the pristine matrix.

We also prepared biocomposites based on PLA using *Hildegardia* natural fabric as reinforcement. Using this kind of fibers it was possible to tune the mechanical properties by altering the preparation method i.e. changing the orientation of fabric and the number of layers of fabric in composites.

As a part of this work, we prepared nanocomposites based on PBSA using different particles filled electrospun nanofibers as reinforcement. The fibers we used in this work are showing different effects on structure and morphology of neat polymer, thus it is possible to control the structure and morphology of PBSA, on which mainly mechanical properties are dependant.

Finally, according to our knowledge, we were the first to prepare biodegradable polymer nanocomposites using different types of electrospun nanofibers as reinforcement by a simple melt pressing approach. Since these fibers are showing significant effects on their pristine matrix semicrystalline framework, thus on physical-mechanical properties, this shows the potential of the addition of this kind of nanofillers for tuning the properties of PLA, in order to widen the application range of this promising polymer.

References:

1. Mikitaev AK, Ligidov MK, Zaikov GE. Polymer, Polymer Blends, Polymer Composites and Filled Polymers: Synthesis, Properties and Applications. 2006.
2. Peters ST. Hand Book Of Composites. 1998.
3. Thomas S, Stephen R. Rubber Nanocomposites: Preparation, Properties, and Applications. 2010.
4. Okada A, Fukushima Y, Inagaki S. Composite material and process for manufacturing same. 1988(US Patent 4.739.007).
5. Mark JE. Polym Eng Sci 1996;36:2905.
6. Reynaud E, Gauthier C, Perez J. Rev Metall /Cah Inf Tech 1999;96:169.
7. Herron N, Thorn DL. Adv Mater 1998;10:1173.
8. Calvert P. Potential applications of nanotubes. In: Ebbesen TW, editor. Carbon Nanotubes. Boca Raton: CRC Press, 1997.
9. Favier V, Canova GR, Shrivastava SC, Cavaille JY. Polym Eng Sci 1997;37:1732.
10. Chazeau L, Cavaille JY, Canova G, Dendievel R, Bouterin B. J Appl Polym Sci 1999;71:1797.
11. Mohanty AK, Misra M, Drzal LT. Natural Fibers, Biopolymers, and Biocomposites. 2005.
12. Bhatnagar N, Sain M. Journal of Reinforced Plastics and Composites 2005;24:1259.
13. Angellier H, Molina-Boisseau S, Dufresne A. Macromolecules 2005;38:9161.
14. Angellier H, Molina-Boisseau S, Lebrun L, Dufresne A. Macromolecules 2005;38:3783.
15. Putaux JL, Molina-Boisseau S, Momaur T, Dufresne A. Biomacromolecules 2003;4(1198).
16. Lapa, V. L. da C., de Oliveira PD, Visconte LLY, Nunes RCR. Polymer Bulletin 2008;60:281.
17. Theng BKG. Formation and Properties of Clay-Polymer Complexes, 1979.
18. <http://www.nanoclay.com>.
19. <http://www.rheox.com>.
20. Blumstein A. J Polym Sci , Part A: Polym Chem 1965;3:2665.

21. Okada A, Kawasumi M, Usuki A, Kojima Y, Kurauchi T, Kamigaito O. In: Schaefer DW, Mark JE, editors. Polymer based molecular composites, vol. 171. Pittsburgh: MRS Symposium Proceedings, 1990.
22. Ogawa M, Kuroda KB. Chem Soc Jpn 1997;70:2593.
23. Pinnavaia TJ, Beall GW. Polymer clay nanocomposites. 2000.
24. Koo JH. Polymer Nanocomposites: Processing, Characterization and Applications. 2006.
25. Mai Y-, Yu Z-. Polymer Nanocomposites. Woodhead Publishing in Materials, CRC 2006.
26. LeBaron PC, Wang Z, Pinnavaia T. J Appl Clay Science 1999;15:11.
27. Alexandre M, Dubois P. Mater Sci Engg R: Reports 2000;28:1.
28. Ray SS, Okamoto M. Prog Polym Sci 2003;28:1539.
29. Viswanathan V, Laha T, Balani K, Agarwal A, Seal S. Mater Sci Engg R: Reports 2006;54:121.
30. Nguyen QT, Baird DG. Adv Polym Tech 2006;25:270.
31. Leszynska A, Njuguna J, Pielichowski K, Banerjee JR. Thermochim Acta 2007;453:75.
32. Leszynska A, Njuguna J, Pielichowski K, Banerjee JR. Thermochim Acta 2007;454:1.
33. Vaia RA, Maguire JF. Chem Mater 2007;19:2736.
34. Chen B, Evans JRG, Greenwell HC, Boulet P, Coveney PV, Bowden AA, Whiting A. Chem Soc Rev 2008;37:568.
35. Esfandiari A, Nazokdast H, Rashidi A-, Yazdanshenas M-. J Appl Polym Sci 2008;80:545.
36. Yeh J-, Chang K-. J Ind & Eng Chem 2008;14:275.
37. Ciardelli F, Coiai S, Passaglia E, Pucci A, Ruggeri G. Polym Int 2008;57:805.
38. Paul DR, Robson LM. Polymer 2008;49:3187.
39. Leroux F, Taviot-Guého C. J Mater Chem 2005;15:3628.
40. Williams GR, O'Hare D. J Mater Chem 2006;16:3065.
41. Rives V, Ulibarri MA. Coord Chem Rev 1999;181:61.
42. <http://www.ptsuk.com/perkalite.html>.

43. Marega C, Causin V, Marigo A, Ferrara G, Tonnaer H. *J Nanosci Nanotechnol* 2009;9:2704.
44. Vaia RA, Ishii H, Giannelis EP. *Chem Mater* 1993;5:1694.
45. Sanchez C, Julian B, Belleville P, Popall M. *J Mater Chem* 2005;15:3559.
46. Zeng QH, Yu AB, Lu GQ, Paul DR. *J Nanosci Nanotech* 2005;5:1574.
47. Subbiah T, Bhat GS, Tock RW, Parameswaran S, Ramkumar SS. *J Appl Polym Sci* 2005;96:557.
48. Huang ZM, Zhang YZ, Kotakic M, Ramakrishna S. *Compos Sci Technol* 2003;63:2223.
49. Bose GM. *Recherches sur la cause et sur la veritable theorie del'electricite.* 1745.
50. Formhals A. 1934(1,975,504).
51. Reneker DH, Chun I. *Nanotechnology* 1996;7:216.
52. Doshi J, Reneker DH. *J Electrostat* 1995;35:151.
53. Greiner A, Wendorff JH. *Angew Chem Int Ed* 2007;46:5670.
54. Lannutti J, Reneker D, Ma T, Tomasko D, Farson D. *Mater Sci Eng (Biomim Supramol Sys)* 2007;27:504.
55. Li WJ, Laurencin CT, Catterson EJ, Tuan RS, Ko FK. *J Biomed Mater Res* 2002;60:613.
56. Shields KJ, Beckman MJ, Bowlin GL. *Tiss Eng* 2004;10:1510.
57. Chen F, Peng X, Li T, Chen S, Wu XF, Reneker DH, Hou H. *J Phys D: Appl Phys* 2008;41:025308.
58. Wang YZ, Blasioli DJ, Kim HJ, Kim HS, Kaplan DL. *Biomaterials* 2006;27:4434.
59. Moroni L, Licht R, de Boer J, de Wijn JR, van Blitterswijk CA. *Biomaterials* 2006;27:4911.
60. Fong H. *Polymer* 2004;453:2427.
61. Tian M, Gao Y, Liu Y. *Polymer* 2007;48:2720.
62. Kim JS, Reneker DH. *Polym Compos* 1999;20:124.
63. Bergshoef MM, Vancso GJ. *Adv Mater* 1999;11:1362.
64. Joseph HK. *Polymer nanocomposites- processing, characterization, and applications.* McGraw-Hill Nanoscience and Technology Series, 2006.

65. Ruiz-Hitzky E, Aranda P, Casal B, Galvan JC. *Adv Mater* 1995;7:180.
66. Aranda P, Galvan JC, Casal B, Ruiz-Hitzky E. *Electrochim Acta* 1992;37:1573.
67. Peter CL, Wang Z, Pinnavaia T. *J Applied Clay Science* 1999;15:11.
68. Causin V, Marega C, Marigo A, Ferrara G. *Polymer* 2005;46:9533.
69. Hindeleh AM, Johnson DJ. *J Phys D: Appl Phys* 1971;4:259.
70. Vonk, C. G. in *Small angle X-ray scattering*, Glatter, O., Kratky O. Academic press, London 1982.
71. Blundell D. *Polymer* 1978;19:1258.
72. Marega C, Marigo A, Causin V. *J Appl Polym Sci* 2003;90:2400.
73. Marega C, Causin V, Marigo A. *J Appl Polym Sci* 2008;109:32.
74. Hosemann R, Bagchi SN. *Direct Analysis of diffraction by matter*, North Holland, Amsterdam. 1962.
75. Ruland W. *J Appl Crystallogr* 1971;4:70.
76. Chen BQ, Evans JRG. *Macromolecules* 2006;39:747.
77. Krzaczkowska J, Fojud Z, Kozak M, Jurga S. *Acta Physica Polonica* 2005;108:187.
78. Chrissafis K, Antoniadis G, Paraskevopoulos KM, Vassiliou A, Bikiaris DN. *Composites Science and Technology* 2007;67:2165.
79. Di Maio E, Iannace S, Sorrentino L, Nicolais L. *Polymer* 2004;45:8893.
80. Gain O, Espuche E, Pollet E, Alexandre M, Dubois P. *Journal of Polymer Science Part B-Polymer Physics* 2005;43:205.
81. Gorrasi G, Tortora M, Vittoria V, Galli G, Chiellini E. *J Polym Sci B* 2002;40:1118.
82. Gorrasi G, Tortora M, Vittoria V, Pollet E, Alexandre M, Dubois P. *Journal of Polymer Science Part B-Polymer Physics* 2004;42:1466.
83. Homminga D, Goderis B, Dolbnya I, Groeninckx G. *Polymer* 2006;47:1620.
84. Kim HB, Lee CH, Choi JS, Park BJ, Lim ST, Choi HJ. *Journal of Industrial and Engineering Chemistry* 2005;11:769.
85. Kiersnowski A, Dabrowski P, Budde H, Kressler J, Piglowski J. *Eur Polym J* 2004;40:2591.
86. Kiersnowski A, Kozak M, Jurga S, Piglowski J. *Polym Compos* 2004;12:727.

87. Kiersnowski A, Gutmann JS, Pigtowski J. *Journal of Polymer Science Part B-Polymer Physics* 2007;45:2350.
88. Kiersnowski A, Piglowski J. *European Polymer Journal* 2004;40:1199.
89. Lepoittevin B, Devalckenaere M, Pantoustier N, Alexandre M, Kubies D, Calberg C, Jerome RD, P. *Polymer* 2002;43:4017.
90. Lee SK, Seong DG, Youn JR. *Fibres polym* 2005;6:289.
91. Marras SI, Kladi KP, Tsvintzelis L, Zuburtikudis I, Panayiotou C. *Acta Biomaterialia* 2008;4:756.
92. Pantoustier N, Lepoittevin B, Alexandre M, Kubies D, Calberg C, Jerome Rea. *Polym Eng Sci* 2002;42:1928.
93. Pucciariello R, Villani V, Belviso S, Gorrasi G, Tortora M, Vittoria V. *Journal of Polymer Science Part B-Polymer Physics* 2004;42:1321.
94. Shibata M, Teramoto N, Someya Y, Tsukao R. *J Appl Polym Sci* 2007;104:3112.
95. Wu K, Wu C, Chang J. *Process Biochemistry* 2007;42:669.
96. Marega C, Marigo A, Causin V. *J Appl Polym Sci* 2003;90:2400.
97. Lincoln DM, Vaia RA, Wang ZG, Hsiao BS, Krishnamoorti R. *Polymer* 2001;42:9975.
98. Lincoln DM, Vaia RA, Wang ZG, Hsiao BS. *Polymer* 2001;42:1621.
99. Lincoln DM, Vaia RA, Krishnamoorti R. *Macromolecules* 2004;37:4554.
100. Homminga D, Goderis B, Dolbnya I, Reynaers H, Groeninckx G. *Polymer* 2005;46:11359.
101. Marega C, Causin V, Marigo A, Ferrara G, Tonnaer H. *J Nanosci Nanotech* 2009;9:2704.
102. Causin V, Yang BX, Marega C, Goh SH, Marigo A. *J Nanosci Nanotech* 2008;8:1790.
103. Causin V, Yang BX, Marega C, Goh SH, Marigo A. *Eur Polym J* 2009;45:2155.
104. Jimenez G, Ogata N, Kawai H, Ogihara T. *J Appl Polym Sci* 1997;64:2211.
105. Tarkin-Tas E, Goswami SK, Nayak B. R., Mathias LJ. *J Appl Polym Sci* 2008;107:976.
106. Osman MA, Rupp JEP, Suter UW. *Polymer* 2005;46:8202.
107. Truss RW, Yeow TK. *J Appl Polym Sci* 2006;100:3044.
108. Marega C, Causin V, Marigo A, Ferrara G. *J Appl Polym Sci* 2009;113:3920.

109. Funck A, Kaminsky W. *Compos Sci Technol* 2007;67:906.
110. Karaman VM, Privalko EG, Privalkoa VP, Kubies D, Puffr R, Jerome R. *Polymer* 2005;46:1943.
111. Ray SS, Bousmina. M. *Progress Mater. Sci.* 2005, 50, 962. *Progress Mater Sci* 2005;50:962.
112. Gao Y, Sagi S, Zhang L, Liao Y, Cowles DM, Sun Y. *J Appl Polym Sci* 2008;110:2063.
113. Blundell D. *Polymer* 1978;19:1258.
114. Marega C, Marigo A, Cingano G, Zannetti R, Paganetto G. *Polymer* 1996;37:5549.
115. Marega C, Causin V, Marigo A. *J Appl Polym Sci* 2008;109:32.
116. Maiti P, Nam PH, Okamoto M, Hasegawa N, Usuki A. *Macromolecules* 2002;35:2042.
117. Pukanszky B, Mudra I, Staniek P. *J Vinyl Add Tech* 1997;3:53.
118. Zhou Z, Wang S, Zhang Y, Zhang Y. *J Appl Polym Sci* 2006;102:4823.
119. Xia H, Wang Q, Li K, Hu GH. *J Appl Polym Sci* 2004;93:378.
120. Moore EM, Ortiz DL, Marla VT, Shambaugh RL, Grady BP. *J Appl Polym Sci* 2004;93:2926.
121. Koval'chuk AA, Shchegolikhin AN, Shevchenko VG, Nedorezova PM, Klyamkina AN, Aladyshev AM. *Macromolecules* 2008;41:3149.
122. Bikiaris D, Vassiliou A, Chrissafis K, Paraskevopoulos KM, Jannakoudakis A, Docoslis A. *Polym Degrad Stabil* 2008;93:952.
123. van der Meer, D. W., Pukanszky B, Vancso GJ. *J Macromol Sci Phys* 2002;B41:1105.
124. Causin V, Yang BX, Marega C, Goh SH, Marigo A. *Eur Polym J* 2009;45:2155.
125. Lepoittevin B, Pantoustier N, Devalckenaere M, Alexandre M, Calberg C, Jerome R, Henrist C, Rulmont A, Dubois P. *Polymer* 2003;44:2033.
126. Neppalli R, Marega C, Marigo A, Bajgai MP, Kim HY, Causin V. *European Polymer Journal* 2010;46:968.
127. Neppalli R, Causin V, Marega C, Saini R, Mba M, Marigo A. *Polymer Engineering and Science* 2011;51:1489.
128. Woodruff MA, Hutmacher DW. *progr polym sci* 2010;35:1217.
129. Armentano I, Dottori M, Fortunati E, Mattioli S, Kenny JM. *Polym Degrad Stab* 2010;95:2126.

130. Fejido JL, Cabedo L, Gimenez E, Lagaron JM, Saura JJ. *Journal of Materials Science* 2005;40:1785.
131. Oksmana K, Skrifvarsb M, Selinc J. *Composites Science and Technology* 2003;63(1317).
132. Ray SS, Okamoto M. *Macromol Rapid Commun* 2003;24:815.
133. Wu T-, Chiang M. *Polymer Engineering and Science* DOI 10.1002/pen.20370, 2005:1615.
134. Tsuji H, Ikada Y. *J Appl Polym Sci* 1998;67:405.
135. Urayama H, Kanamori T, Kimura Y. *Macromol Mater Eng* 2002;287:116.
136. Taylor MS, Daniels AU, Andriano KP, Heller J. *J Appl Biomater* 1994;5:151.
137. Jain RA. *Biomaterials* 2000;21:2475.
138. Mikos AG, Lyman MD, Freed LE, Langer R. *Biomaterials* 1994;15:55.
139. Park TG, Cohen S, Langer R. *Macromolecules* 1992;25:116.
140. Kamath KR, Park K. *Adv Drug Deliv Rev* 1993;11:59.
141. Davis SS, Illum L, Stolnik S. *Curr Opin Colloid Interface Sci* 1996;1(660).
142. Edlund U, Albertsson AC. *Adv Polym Sci* 2002;157(67).
143. Garlotta D. *Journal of Polymers and the Environment* 2002;9:63.
144. Zhang J-, Sun X. *Journal of Applied Polymer Science* 2007;106:3058.
145. Petersson L, Oksman K. *Composites Science and Technology* 2006;66:2187.
146. Suryanegara L, Nakagaito AN, Yano H. *Composites Science and Technology* 2009;69:1187.
147. Wang L-, Chen H-, Xiong Z-, Pang X-, Xiong C. *Macromol Mater Eng* 2010;295:381.
148. Avella M, Bogoeva-Gaceva G, Buzarovska A, Errico ME, Gentile G, Grozdanov A. *Journal of Applied Polymer Science* 2008;108:3542.
149. Dobрева T, Perena JM, Perez E, Benavente R, Garcia M. *Polymer Composites* DOI 10.1002/pc.20882:974.
150. Lee B-, Kim H-, Lee S, Kim H-, Dorgan JR. *Composites Science and Technology* 2009;69:2573.

151. Huda MS, Drzal LT, Misra M, Mohanty AK. *Journal of Applied Polymer Science*, Vol 102, 4856–4869 (2006) 2006;102:4856.
152. Ogata N, Jimenez G, Kawai H, Ogihara T. *J Polym Sci Part B: Polym Phys* 1997;35:389.
153. Bandyopadhyay S, Chen R, Giannelis EP. *Polym Mater Sci Eng* 1999;81:159.
154. Ray SS, Maiti P, Okamoto M, Yamada K, Ueda K. *Macromolecules* 2002;35:3104.
155. Paul M-, Alexandre M, Degee P, Calberg C, Jerome R, Dubois P. *Macromol Rapid Commun* 2003;24:561.
156. Chang J-, An YU, Sur GS. *J Polym Sci Part B: Polym Phys* 2003;41:94.
157. Paul M-, Alexandre M, Degee P, Henrist C, Rulmont A, Dubois P. *Polymer* 2003;44:443.
158. Hasook A, Muramatsu H, Tanoue A, Iemoto Y, Unryu T. *Polym Compos* 2008;29:1.
159. Jollands M, Gupta RK. *Journal of Applied Polymer Science* 2010;118:1489.
160. Ray SS, Yamada K, Okamoto M, Ueda K. *Nano Lett* 2002;2:1093.
161. Ray SS, Yamada K, Okamoto M, Ueda K. *Polymer* 2003;43:857.
162. Katiyar V, Gerds N, Koch CB, Risbo J, Hansen HCB, Plackett D. *Polymer Degradation and Stability* 2010;95:2563.
163. Dagnon KL, Ambadapadi S, Shaito A, Ogbomo SM, DeLeon V, Golden TD, Rahimi M, Nguyen K, Braterman PS, D'Souza NA. *Journal of Applied Polymer Science* 2009;113:1905.
164. PAN P, ZHU B, DONG T, INOUE Y. *Journal of Polymer Science: Part B: Polymer Physics* 2008;46:2222.
165. Kontou E, Niaounakis M, Georgiopoulos P. *Journal of Applied Polymer Science* 2011;122:1519.
166. Avrami M. *J Chem Phys* 1941;9:177.
167. Benetti EM, Causin V, Marega C, Marigo A, Ferrara G, Ferraro A, Consalvi M, Fantinel F. *Polymer* 2005;46:8275.
168. Causin V, Marega C, Marigo A, Ferrara G. *Polymer* 2005;46(23):9533.
169. Costa FR, Abdel-Goad M, Wagenknecht U, Heinrich G. *Polymer* 2005;46:4447.
170. Vaia RA, Liu W. *J Polym Sci Phys* 2002;40:1590.

171. Causin V. "Wide-Angle X-ray Diffraction and Small-Angle X-ray Scattering Studies of Rubber Nanocomposites." And references therein. In: Thomas S, Stephen R, editors. Rubber Nanocomposites: Preparation, Properties and Applications. Singapore: Wiley, 2010.
172. Zhang Z, Zhang L, Li Y, Xu H. *Polymer* 2005;46:129.
173. Mehta S, Mirabella FM, Rufener K, Bafna A. *J Appl Polym Sci* 2004;92:928.
174. Fasulo PD, Rodgers WR, Ottaviani RA, Hunter DL. *Polym Eng Sci* 2004;44:1036.
175. Causin V, Marega C, Marigo A, Ferrara G, Idiyatullina G, Fantinel F. *Polymer* 2006;47(4773).
176. Causin V, Marega C, Marigo A, Ferrara G, Ferraro A, Selleri R. *J Nanosci Nanotech* (in press).
177. Bourbigot S, Fontaine G, Bellayer S, Delobel R. *Polym Test* 2008;27:2.
178. Nam PH, Fujimori A, Masuko T. *Journal of Applied Polymer Science* 2004;93:2711.
179. Causin V, Marega C, Saini R, Neppalli R, Ferrara G, Adhikari R, Marigo A. *J Nano Sci and Nano Techno* (in press).
180. Li M, Hu D, Wang Y, Shen C. *Polymer Engineering and Science* DOI 10.1002/pen.21755:2298.
181. Day M, Nawaby AV, Liao X. *Journal of Thermal Analysis and Calorimetry* 2006;86(3):623.
182. Huang SM, Hwang JJ, Liu HJ, Lin LH. *Journal of Applied Polymer Science* 2010;117:434.
183. Li X, Yin J, Yu Z, Yan S, Lu X, Wang Y, Cao B, Chen X. *Polymer Composites* DOI 10.1002/pc.20721.
184. Caskey TC, Lesser AJ, McCarthy TJ. *Polym Compos* 2003;24:545.
185. Goitisoló I, Eguiazábal JI, Nazabal J. *Compos Sci Tech* 2010;70:873.
186. Goitisoló I, Eguiazábal JI, Nazabal J. *Macromol Mater Eng* 2010;295:233.
187. Rajesh C, Unnikrishnan G, Purushothaman E, Thomas S. *J Appl Polym Sci* 2004;92:1023.
188. Seema A, Kutty SKN. *J Appl Polym Sci* 2006;99:532.
189. Romo-Urbe A, Arizmendi L, Romero-Guzman ME, Sepulveda-Guzman S, Cruz-Silva R. *ACS Appl Mater Interfaces* 2009;1:2502.

190. Chen LS, Huang ZM, Dong GH, He CL, Liu L, Hu YY, Li Y. *Polym Compos* 2009;30:239.
191. Neppalli R, Marega C, Marigo A, Bajgai MP, Kim HY, Causin V. *Polymer* 2011;52:4054.
192. Bayley GM, Hedenqvist M, Mallon PE. *Polymer* 2011;52:4061.
193. Hosemann R, Bagchi SN. *Direct Analysis of diffraction by matter*. 1962.
194. Causin V, Marega C, Saini R, Marigo A, Ferrara G. *J Therm Anal Calorimetry* 2007;90:849.
195. Hambir S, Bulakh N, Jog JP. *Polym Eng Sci* 2002;42:1800.
196. Ma J, Zhang S, Qi Z, Li L, Hu Y. *J Appl Polym Sci* 2002;83:1978.
197. Causin V, Marega C, Marigo A, Ferrara G, Ferraro A. *Eur Polym J* 2006;42:3153.
198. Wu D, Wu L, Zhou W, Zhang M, Yang T. *Polym Eng Sci* 2010;50:1721.
199. Haggmueller R, Fischer JE, Winey KI. *Macromolecules* 2006;39:2964.
200. SU Z, LI Q, LIU Y, HU G, WU C. *Journal of Polymer Science: Part B: Polymer Physics* 2009;47:1971.
201. Li M, Hu D, Wang Y, Shen C. *Polym Eng Sci* 2010;50:2298.
202. Zhou WY, Duan B, Wang M, Cheung WL. *Journal of Applied Polymer Science* 2009;113:4100.
203. Dobрева T, Perena JM, Pérez E, Benavente R, García M. *Polym Composites* 2010;31:974.
204. Shieh YT, Twu TK, Su CC, Lin RH, Liu GL. *J Polym Sci Polym Phys* 2010;48:983.
205. Su Z, Guo W, Liu Y, Li Q, Wu C. *Polym Bull* 2009;62:629.
206. Oksman K, Skrifvars MS, Eli JF. *Compos Sci Technol* 2003;63:1317.
207. Mat Taib R, Ramarad S, Mohd Ishak ZA, Todo M. *Polym Compos* 2010;31:1213.
208. Meng QK, Hetzer M, De Kee D. *J Compos Mater* 2010;45:1145.
209. Graupner N, Herrmann AS, Müssig J. *Composites A* 2009;40:810.
210. Chiu WM, Chang YA, Kuo HY, Lin MH, Wen HC. *J Appl Polym Sci* 2008;108:3024.
211. Di Y, Iannace S, Maio E, Nicolais L. *J Polym Sci Part B: Polym Phys* 2005;43:689.

212. Causin V, Yang BX, Marega C, Goh SH, Marigo A. *Eur Polym J* 2009;45:2155.
213. Zhou Q, Xanthos M. *Polym Degrad Stab* 2008;93:1450.
214. Ray SS, Yamada K, Okamoto M, Ueda K. *Macromol Mater Eng* 2003;288:203.
215. Paul M-, Delcourt C, Alexandre M, Degee P, Monteverde F, Rulmont A, Dubois P. *Macromol Chem Phys* 2005;206:484.
216. Mei F, Zhong JS, Yang XP, Ouyang XY, Zhang S, Hu XY, Ma Q, Lu JG, Ryu SK, Deng XL. *Biomacromolecules* 2007;8:3729.
217. Kim JS, Reneker DH. *Polym Compos* 1999;20:124.
218. Bergshoef MM, Vancso GJ. *Adv Mater* 1999;11:1362.
219. Zucchellia A, Focareteb ML, Gualandib C, Ramakrishna S. *Polym Adv Technol* 2011;22:339.
220. Neppalli R, Marega C, Marigo A, Bajgai MP, Kim H, Causin V. *Eur Polym J* 2010;46:968.
221. Swart M, Olsson RT, Hedenqvist MS, Mallon PE. *Polym Eng Sci* 2010;50:2143.
222. Romo-Uribe A, Arizmendi L, Romero-Guzman ME, Sepulveda-Guzman S, Cruz-Silvan R. *ACS Appl Mater Interf* 2009;1:2502.
223. Neppalli R, Marega C, Marigo A, Bajgai MP, Kim HY, Causin V. *Eur Polym J* 2010;46:968.
224. Fong H. *Polymer* 2004;45:2427.
225. Tian M, Gao Y, Liu Y, Liao Y, Xu R, Hedin NE, Fong H. *Polymer* 2007;48:2720.
226. Mock JA. *Mater Eng* 1979;89:60.
227. Kulakarni AG, Satyanarayana KG, Sukumaran KG, Rohatgi PK. *J Mater Sci* 1981;16:905.
228. Mansur MA, Aziz MA. *Int J Chem Compos Light Weight Concrete* 1982;4:75.
229. Beimares H, Berrera A, Castillo E, Veheugen E, Monjaras M, Patfoort GA, Bucqueye MEN. *Ind Eng Chem Prod Res Dev* 1981;20:555.
230. Satyanarayana KG, Kulkarni AG, Rohatgi PK. *J Sci Ind Res Dev* 1981;40:222.
231. Kulakarni AG, Satyanarayana KG, Rohatgi PK, Vijayan K. *J Mater Sci* 1983;18:2290.
232. Jindal UC. *J Compos Mater* 1986;20:19.

233. Varada Rajulu A, Ramachandra Reddy G, Narasimha Chary K. *Ind J Fiber Textile Res* 1996;21:223.
234. Varada Rajulu A, Ramachandra Reddy G, Narasimha Chary K. *Ind J Fiber Textile Res* 1998;23:49.
235. Varada Rajulu A, Allah Baksh S, Ramachandra Reddy G, Narasimha Chary K. *J Reinforced Plast Comp* 1998;17:1507.
236. Rajulu AV, Guduri BR, Rao BRP, Reddy AMS, He J, Zhang J. *Journal of Applied Polymer Science* 2002;84:2216.
237. Jagadeesh D, Reddy JPD, Rajulu AV, Li R. *Polymer Composites* 2011:399.
238. Li X, Zhang J, He J, Reddy JPD, Rajulu AV. *Journal of Composite Materials* 2010;44:1681.
239. Jagadeesh D, Rajulu AV, Guduri BR. *Journal of Natural Fibers* 2010;7(2):93.
240. Guduri BR, Rajulu AV, Luyt AS. *Journal of Applied Polymer Science* 2006;102:1297.
241. Rajulu AV, Guduri BR, Devi LG. *Polymer Composites* 2004;6:563.
242. Li XH, Meng YZ, Wang SJ, Rajulu AV, Tjong SC. *Journal of Polymer Science: Part B: Polymer Physics* 2004;42:666.
243. Wong S, Shanks RA, Hodzic A. 2003. *Polym Eng Sci* 2003;43:1566.
244. Shanks RA, Hodzic A, Ridderhof D. *J Appl Polym Sci* 2006;101:3620.
245. Shanks RA, Hodzic A, Ridderhof D. *J Appl Polym Sci* 2006;99:2305.
246. Plackett D, Andersen TL, Pedersen WB, Nielsen L. *Compos Sci Technol* 2003;63:1287.
247. Nishino T, Hirao K, Kotera M, Nakamae K, Inagaki H. *Compos Sci Technol* 2003;63:1281.
248. Seriwzawa S, Inoue K, Iji M. *J Appl Polym Sci* 2006;100:618.
249. Shibata M, Ozawa K, Teramoto N, Yosomiya R, Takeishi H. *Macromol Mater Eng* 2003;288:35.
250. Teramoto N, Urata K, Ozawa K, Shibata M. *Polym Degrad Stab* 2004;86:401.
251. Lee SH, Ohkita T. Eco-composite from poly(lactic acid) and bamboo fiber *Holzforschung* 2004;58:529.
252. Lee SH, Wang S. *Composites Part A* 2006;37:80.
253. Plackett D. *J Polym Environ* 2004;12:131.

254. Mathew AP, Oksman K, Sain M. *J Appl Polym Sci* 2005;97:2014.
255. Mathew AP, Oksman K, Sain M. *J Appl Polym Sci* 2006;101:300.
256. Gamstedt EK, Bogren KM, Neagu RC, Akerho LMM, Lindstrom M. *J Thermoplast Compos Mater* 2006;19:613.
257. Yu L, Petinakis S, Dean K, Bilyk A, Wu D2. *Macromol Symp* 2007;249/250:535.
258. Oksman K, Mathew AP, Bondeson D, Kivien I. *Compos Sci Technol* 2006;66:2776.
259. Petersson L, Oksman K. *Compos Sci Technol* 2006;66:2187.
260. Fink HP, Ganster J. *Macromol Symp* 2006;244:107.
261. Shibata M, Oyamada S, Kobayashi S, Yaginuma D. *J Appl Polym Sci* 2004;92:3857.
262. Avella M, Bogoeva-Gaceva G, Arovska AB, Errico ME, Gentile G, Grozdanov A. *Journal of Applied Polymer Science* 2008;108:3542.
263. Park BD, Balatinez JJ. *Polym Compos* 1997;18:79.
264. Boundriot U, Dersch R, Greiner A, Wendorff JH. *Artif Organs* 2006;30:779.
265. Katti DS, Robinson KW, Ko FK, Laurencin CT. *J Biomed Mater Res B* 2004;70:286.
266. Li S, Hashi C, Huang NF, Kurpinski K. WO07090102A2 2007.
267. Zong X, Kim KS, Fang D, Ran S, Hsiao BS, Chu B. *Polymer* 2002;43:4403.
268. Ma K, Chan CK, Liao, S. W. Y. K., Feng Q, Ramakrishna S. *Biomaterials* 2008;29:2906.
269. Chong EJ, Lim CT, Makrishna S, Phan TT, Lim I. WO06036130A1 2006.
270. Renuga G, Satinderpal K, Chao YF, Casey C, Seeram R. *J Memb Sci* 2007;289:210.
271. Kim GM, Wutzler A, Radosch HJ. *Chem Mater* 2005;17:4949.
272. Edror Y, Salalha W, Khalfin RL, Cohen Y, Yarin AL, Zussman E. *Langmuir* 2003;19:7012.
273. Jun Z, Aigner A, Czubayko F, Kissel T, Wendorff JH, Greiner A. *Biomacromolecules* 2005;6:1484.
274. Demir MM, Gulgun MA, Menciloglu YZ. *Macromolecules* 2004;37:1787.
275. Ishioka D. *Biopolymers, polyesters III. Applications and commercial products.* 2002;4.
276. Fujimaki T. *Polym Degrad Stab* 1998;59:209.

277. Bandyopadhyay J, Ray SS. *Polymer* 2010;51:4860.
278. Chen G, Yoon J. *Polym Int* 2005;54:939.
279. Zhaobin Q, Siyu Z, Wantai Y. *Journal of Nanoscience and Nanotechnology* 2009;9:4961.
280. Ray SS, Bousmina M, Okamoto K. *Macromol Mater Eng* 2005;290:759.
281. Arinstein A, Zussman E. *Jornal of Polymer Science PartB: Polymer Physics* 2011;49(691).

List of Publications

1. **“Electrospun nylon fibers for the improvement of mechanical properties and for the control of biodegradation rate of poly (lactic acid)-based composites”**. Ramesh Neppalli, Roberta Saini, Carla Marega, Antonio Marigo, Valerio Causin. (*Journal of Materials Research: in press*)
2. **“Structure-Property Relationships in Heterophasic Thermoplastic Elastomers Filled with Montmorillonite”**. Valerio Causin, Carla Marega, Roberta Saini, **Ramesh Neppalli**, Giuseppe Ferrara, Rameshwar Adhikari, Antonio Marigo. *Journal of Nanoscience and Nanotechnology (in press)*
3. **“Improvement of tensile properties and tuning of the biodegradation behavior of polycaprolactone by addition of electrospun fibers”**. **Ramesh Neppalli**, Carla Marega, Antonio Marigo, Madhab Prasad Bajgai, Hak Yong Kim, Valerio Causin. *Polymer* 52, 4054 (2011)
http://www.sciencedirect.com/science?_ob=MiamiImageURL&_cid=271607&_user=607988&_pii=S0032386111005246&_check=y&_origin=search&_zone=rslt_list_item&_coverDate=2011-08-18&_wchp=dGLbVlt-zSkzV&_md5=46ecb8989786b324984af499ff451ea4/1-s2.0-S0032386111005246-main.pdf
4. **“Structure, Morphology, and Biodegradability of Poly (ε-caprolactone)-Based Nanocomposites”**. **Ramesh Neppalli**, Valerio Causin, Carla Marega, Roberta Saini, Miriam Mba, Antonio Marigo. *Polymer Engineering and Science* 51, 1489 (2011)
<http://onlinelibrary.wiley.com/doi/10.1002/pen.21948/pdf>
5. **“The effect of a synthetic double layer hydroxide on the rate of II→I phase transformation of poly (1-butene)”**. C. Marega, V. Causin, **R. Neppalli**, R. Saini, G. Ferrara, A. Marigo. *Express Polymer Letters* 5, 1050 (2011)
<http://www.expresspolymlett.com/>

6. **“Conductivity, XRD, and FTIR Studies of New Mg²⁺-ion-conducting Solid Polymer Electrolytes: [PEG: Mg(CH₃COO)₂]”**. Anji Reddy Polu and Ranveer Kumar, Valerio Causin and Ramesh Neppalli. *Journal of the Korean Physical Society*, 59, 114, (2011)
http://www.kps.or.kr/jkps/abstract_view.asp?articleid=399E2268-35AB-4CF6-923B-6251B2D25452&globalmenu=3&localmenu=10

7. **"Poly (ε-caprolactone) filled with electrospun nylon fibres: A model for a facile composite fabrication"**. Ramesh Neppalli , Carla Marega , Antonio Marigo , Madhab Prasad Bajgai , Hak Yong Kim, Valerio Causin. *European Polymer Journal* 46 (2010) 968–976
http://www.sciencedirect.com/science?_ob=MiamiImageURL&_cid=271558&_user=607988&_pii=S0014305710000340&_check=y&_origin=&_coverDate=31-May-2010&_view=c&_wchp=dGLbVlk-zSkzV&_md5=d3e8c0551fd03824c94192f2570573f9/1-s2.0-S0014305710000340-main.pdf

8. **“Nanocomposites improve performance of biodegradable polymers”**. Valerio Causin, Carla Marega, Ramesh Neppalli, Roberta Saini, and Antonio Marigo. *Society of Plastics Engineers Plastic research online* **10.1002/spepro.003638**
<http://www.4spepro.org/view.php?source=003638-2011-04-12>

9. **“Consequences of different clays on Poly (lactic acid) morphology and properties”**. Ramesh Neppalli, Roberta Saini, Carla Marega, Antonio Marigo, Valerio Causin. (*Manuscript submitted*)

10. **“The effect of nanoparticles filled electrospun nanofibers on PBSA matrix: structure, morphology, mechanical properties and bio degradation”**. Ramesh Neppalli, Roberta Saini, Carla Marega, Antonio Marigo, Valerio Causin. (*Manuscript under preparation*)

11. **“Biodegradable composites: natural fabric reinforced PLA”**. Ramesh Neppalli, Roberta Saini, Carla Marega, Antonio Marigo, Valerio Causin. (*manuscript under preparation*)

Conferences Attended

1. poster presented at an international conference POLYCHAR-19 (20th -24th March, 2011) entitled **“STUDY ON POLYLACTIC ACID REINFORCED WITH ELECTROSPUN NYLON FIBRES”**
Ramesh Neppalli, Valerio Causin, Carla Marega, Roberta Saini, Antonio Marigo, Madhab Prasad Bajgai, Hak Yong Kim
2. poster presented at an international conference POLYCHAR-18 (6th -10th April,2010) entitled **“STRUCTURE, MORPHOLOGY AND BIODEGRADABILITY OF POLY(ϵ -CAPROLACTONE) BASED NANOCOMPOSITES”**
Ramesh Neppalli, Valerio Causin, Carla Marega, Roberta Saini, Antonio Marigo
3. Work presented as invited talk at second **international conference on polymer processing and characterization**, Kottayam, India (14-17 January 2009).
Ramesh Neppalli, Carla Marega, Antonio Marigo, Madhab Prasad Bajgai, Hak Yong Kim, Valerio Causin
4. Poster presented entitled **“PRELIMINARY STUDIES ON STRUCTURE, MORPHOLOGY AND BIODEGRADABILITY OF POLY (ϵ -CAPROLACTONE) BASED NANOCOMPOSITES”**. **Ramesh Neppalli**, Valerio Causin, Carla Marega, Roberta Saini, Antonio Marigo at INTERNATIONAL CONGRESS **“THE CENTENARY”** 100th Anniversary of the Italian Chemical Society, Padova, August 31-September 4, 2009.